Volume: 6 Issue: 1 2025

Eurasian Journal of Science Engineering & Technology

Eurasian Journal of Science Engineering and Technology

Editors

Editorial Board

Eurasian Journal of Science Engineering and Technology

Eurasian Journal of Science Engineering and Technology

Correspondence Address

Niğde Ömer Halisdemir University
Eurasian Journal of Science Engineering and Technology Publishing Coordinatorship, 51240
Niğde/Türkiye

***E-mail*:** recep.zan@ohu.edu.tr
mbarut@ohu.edu.tr
eyavuzer@ohu.edu.tr

***Web page*:** https://dergipark.org.tr/tr/pub/ejset

Publication information

The objective of Eurasian Journal of Science Engineering and Technology (EJSET) is to provide an academic environment for researchers in various fields of science and engineering and for the publication and dissemination of high-quality research results in the fields of science, applied science, engineering, architecture, agricultural science and technology.

Eurasian Journal of Science Engineering and Technology

CONTENTS/*İÇİNDEKİLER*

Eurasian J. Sci. Eng. Tech., 2025; 6(1): 001-035

Eurasian Journal of Science Engineering and Technology

Research article

www.dergipark.org.tr/tr/pub/ejset / www.dergipark.org.tr/en/pub/ejset

Re-examining the law of energy conservation-A Euclidean geometric proof

Alex Mwololo Kimuya [1,*]

[1] *Department of Physical Sciences (Physics), Meru University of Science and Technology, Kenya*

Abstract

The law of energy conservation is a cornerstone of physics, limiting energy use and dictating the efficiency of thermodynamic processes. The primary objective of this paper is to challenge the traditional acceptance of the law of energy conservation as an unprovable axiom by presenting a novel, provable, and purely geometric approach within the framework of Euclidean geometry, thereby re-evaluating its theoretical and empirical foundations. Driven by the ongoing pursuit of solutions to energy crises, the paper critically examines attempts to disprove the law and the search for alternative energy sources. Contrary to prevailing beliefs, it posits two key viewpoints: the lack of rigorous proof establishing the law's validity and the obscured motivations driving the invention of new energy sources. Highlighting the gap between theoretical acceptance and empirical evidence, the paper introduces a geometric framework to elucidate the empirical limitations and precision of energy conservation. Through this lens, it challenges the law's universal applicability, particularly debunking the notion of perpetual motion machines as proof of its validity. The findings include a geometric and practical redefinition of isolated systems, a proof of Newton's laws of motion, a geometric derivation of the Newtonian kinetic energy equation, and the demonstration of these geometric concepts' practicality independent of experiments. These insights call for a re-evaluation of the traditional understanding of energy conservation and offer transformative implications for future energy exploration and innovation.

Keywords: Energy conservation; Thermodynamics; Energy; Perpetual motion; Descartes; Spinoza; Leibniz; Euclid; Inverse points; Euclidean geometry

1 Introduction

The concepts of matter, motion, and energy have enthralled the best minds in philosophy and science for more than a century. The principle of conservation of energy is one of the most fundamental ideas relating these concepts in classical physics (Newton, 1687) [1,2]. Henri Poincaré, a prominent mathematician and physicist, argued that experiments cannot definitively prove foundational concepts like the uniformity of time, the law of inertia, and the principle of energy conservation [3]. He pointed out that experiments themselves rely on conventions, such as the definition of time units, which can be chosen differently (Poincaré, 1904) [3,4]. Despite this, the correctness of the underlying principles is not compromised (Einstein, 1916) [5]. From various perspectives, the principle of energy conservation has been viewed as an unprovable axiom due to the lack of a direct, empirical verification (Mach, 1883 [6]), [7,8]. The primary objective of this paper is to challenge this assumption by presenting a novel, provable, and purely geometric approach for the principle within the framework of Euclidean geometry. Considerably, it is important to remember that while experiments play a crucial role in physics, the ultimate goal of scientific theories is to establish their consistency with the observed world [9,10]. This geometric proof serves as a formal demonstration of the principle's internal coherence, independent of specific measurement conventions. This paper specifically addresses two key gaps in existing literature: the lack of a rigorous, formal proof for the principle of energy conservation and the disconnection between theoretical frameworks and practical applications. First, it develops a purely geometric proof of energy conservation, drawing upon Euclidean axioms to establish a theoretical foundation that is both universal and logically irrefutable. Second, the paper redefines the relationship between isolated systems and material particles to clarify energy redistribution across various forms, including kinetic and potential energy. These contributions not only fill existing theoretical voids but also provide a robust platform for re-evaluating the empirical limitations and precision of energy-related laws, offering fresh perspectives on their validity and applicability. While a defining characteristic of scientific theories is their provisional nature and openness to revision [11,12], the principle of energy conservation has held a remarkably rigid position for centuries, seemingly defying this very principle. This enduring quality of the principle motivates us to explore why, despite the lack of a rigorous proof, it has remained universally accepted. It is intriguing to consider that a serious attempt at proving energy conservation could lead to unexpected discoveries about our current understanding of physics. This novel "physics-geometry" review hinges on the distinction between "energy/matter" and "energy system/matter system". A pivotal aspect of this work is its integration of philosophical discourse into the geometric proof framework. Philosophical debates on the nature of foundational principles—ranging from Poincaré's views on the provisional nature of physical laws to Kant's emphasis on inherent understanding—serve as a backdrop for re-examining energy conservation. By bridging philosophical reflections with rigorous geometric methodologies, this

* Corresponding author, e-mail: alexkimuya23@gmail.com (A. M. Kimuya)
Recieved: 01.10.2024 Accepted: 09.01.2025 Published: 30.01.2025
doi: 10.55696/ejset.1559047

paper highlights the relationship between abstract reasoning and empirical insights. This synthesis not only contextualizes the geometric proof within a broader intellectual tradition but also challenges entrenched assumptions about the unprovability of energy conservation, advocating for a deeper alignment between philosophical principles and scientific practice. The primary aim here is to characterize the fundamental unity between these concepts. Specifically, the foundation of this review lies in the relationship between a thermodynamically isolated energy system and how particulate systems interact within this hypothetical framework. Considerably, the paper acknowledge that physics itself does not operate on the concept of "proof" in the strict sense. Unlike mathematics, which is a deductive science [13-15], physics is inherently inductive, relying on observations to build theories (Karl Popper, 1959 [16]), [17]. The closest equivalent to proof in physics involves creating a mathematical model of a classical system, deriving mathematical consequences within that model, and then interpreting those consequences back into the physical world [12,18]. Therefore, the concept of absolute proofs for physical principles is more relevant to the domain of pure mathematics and has limited applicability to scientific disciplines. This paper advocates for the establishment of scientific norms that enable rigorous proofs in physics, extending beyond mere mathematical consequences within physical models. A central premise is that the absence of such proofs fosters misconceptions about fundamental physics concepts, such as energy and the principle of energy conservation in physical systems. Consequently, this paper presents a novel type of proof – a geometric demonstration of energy conservation – that departs from the usual approach in physics by deriving the principle from fundamental geometrical truths, mirroring Euclid's axiomatic approach in geometry. The paper argues that the lack of well-defined methods for rigorous proofs in physics is not an intrinsic limitation of scientific reasoning itself. The strong link between physics and mathematics presents a significant opportunity to establish verifiable scientific concepts that are both theoretically robust and experimentally independent. Accordingly, this paper calls for a shift from justifications based solely on observation and experimentation within physical models towards a more rigorous "proof-oriented" approach for scientific concepts. The current paradigm often relies on an inherent understanding of the fundamental nature of things based on our everyday experiences (Immanuel Kant, 1781 [19]), [20]. This paper challenges the notion that the principle of energy conservation is unprovable by establishing a geometric proof analogous to Euclid's demonstrations in geometry. Building upon Newton's Laws of Motion and the concept of energy redistribution across particulate structures in all material systems, this paper offers a geometric perspective on certain physical and philosophical concepts. The principle of mechanical energy is extended to encompass various energy forms by leveraging the particulate nature of material systems. Crucially, material systems are fundamentally composed of interacting particles, ranging from elementary particles to those classically understood and relevant to our understanding of the world [21].

2 Literature review

The concept of proof in physics, particularly in the context of energy conservation, differs significantly from its mathematical counterpart [12,18]. While mathematics seeks absolute certainty, physics often relies on the construction of mathematical models that approximate real-world phenomena. These models, when subjected to rigorous analysis, can provide compelling evidence for the conservation of energy. This section will delve into the key mathematical frameworks used to demonstrate energy conservation in classical systems, such as the Lagrangian formalism [22,23], Noether's theorem [24,25], and the Hamiltonian framework [26]. While these methods offer powerful insights, it is essential to acknowledge their limitations, especially when dealing with anomalous cases such as the electrical short circuits modeled in this paper. The applicability of these methods is subject to certain limitations, including the assumption of idealized systems [22,25], the distinction between discrete and continuous systems, the presence of non-conservative forces [1], and the emergence of energy conservation as a property of complex systems [1,2,27]. For instance, many mathematical proofs of energy conservation assume idealized conditions, such as frictionless surfaces or point masses, which may not accurately reflect real-world scenarios. Additionally, while these methods primarily focus on continuous systems, real-world systems often involve discrete elements or quantum phenomena, which can introduce complexities not fully captured by classical models. Non-conservative forces, such as friction or air resistance, can also introduce energy dissipation, making the conservation of total mechanical energy less straightforward. Moreover, in complex systems, energy conservation may be a property that emerges from the interactions of many individual components, making it challenging to derive the conservation law directly from the fundamental properties of the system.

2.1 The Lagrangian approach to energy conservation

In classical mechanics, the principle of energy conservation is most commonly derived from the Lagrangian formulation [1,22,28]. The Lagrangian function, denoted by L, is defined as the difference between the system's kinetic energy T and potential energy V: $L = T - V$. Using the Euler-Lagrange equation, the equations of motion for the system can be expresses as: $\frac{d}{dt}\left(\frac{\partial L}{\partial \dot{q}_i}\right) - \frac{\partial L}{\partial q_i} = 0$; where q_i are the generalized coordinates of the system and $\dot{q}_i$ are their velocities. If the Lagrangian does not explicitly depend on time, the system is time-independent, leading to the conservation of energy. The energy is expressed through the Hamiltonian H, which is derived from the Lagrangian as: $H = \sum_i \dot{q}_i \frac{\partial L}{\partial \dot{q}_i} - L$. The Hamiltonian corresponds to the total energy of the system and remains constant if the system's dynamics are time-invariant. This process—constructing a model using the Lagrangian, deriving the equations of motion, and interpreting the Hamiltonian as a conserved

quantity-serves as the closest analog to proof in physics for energy conservation. However, while the Lagrangian formalism is mathematically rigorous, its assumptions often fail to hold in practical physical scenarios. The model assumes a closed system where all forces are conservative [22,29,30], and it breaks down in systems that involve non-conservative forces such as friction or electrical resistance. For example, in the case of an electrical short circuit (modeled in Figure 8), the rapid dissipation of energy as heat due to minimal resistance introduces non-conservative effects that are not accounted for by this framework. The inability to describe energy dissipation means that the derived model does not fully capture the physical behavior of systems with irreversible processes, highlighting the limitations of applying the Lagrangian approach universally.

2.2 Noether's theorem and conservation laws

Noether's theorem is another mathematical framework that models physical systems and derives conservation laws [24,25]. The theorem states that for every continuous symmetry of the action (integral of the Lagrangian), there is a corresponding conserved quantity. In the case of time-translation symmetry, Noether's theorem leads to the conservation of energy. If the Lagrangian L is invariant under time translations $t \to t + \epsilon$, the energy, expressed by the Hamiltonian H, is conserved according to: $\frac{dH}{dt} = 0$. This result provides a profound connection between symmetries in the mathematical model and the physical conservation of energy. The application of Noether's theorem involves constructing a model of the system based on its symmetries and interpreting the mathematical consequences of these symmetries as physical conservation laws. While this approach is robust and elegant, it assumes ideal conditions where system symmetries are perfect. However, physical systems often exhibit deviations from these idealizations. For instance, in standard circuit theory, an electrical short circuit exemplifies an anomalous event where energy is rapidly dissipated as heat. Such events disrupt the time-translation symmetry upon which Noether's theorem relies, leading to observable deviations from energy conservation. These disruptions highlight the limitations of the theorem in describing non-ideal, dissipative systems. The detailed empirical and theoretical proof of how an electrical short circuit violates the law of energy conservation, including the specific mechanisms through which time-translation symmetry is broken, is a complex topic requiring comprehensive mathematical and physical analysis. This specific investigation is thoroughly addressed in a separate article dedicated to the subject. For this discussion, the focus remains on the theoretical foundation provided by Noether's theorem and its limitations under idealized conditions.

2.3 Modeling energy conservation with Hamiltonians

Hamiltonian mechanics is another framework that models classical systems and derives energy conservation laws. The Hamiltonian H, which represents the total energy of the system, evolves according to Hamilton's equations: $\dot{q}_i = \frac{\partial H}{\partial p_i}$, $\dot{p}_i = \frac{\partial H}{\partial q_i}$; where q_i are the generalized coordinates and p_i are the conjugate momenta [1,31]. In time-independent systems, the Hamiltonian is conserved, representing the total energy as a constant of motion. This approach is often used to model isolated systems where energy transformations are fully reversible. While Hamiltonian mechanics provides a rigorous mathematical model for energy conservation, it assumes that all energy transformations are reversible and that no energy is lost to non-conservative processes. Again, in the case of electrical short circuits, where energy is rapidly dissipated as heat due to minimal resistance, the Hamiltonian framework cannot capture the irreversible nature of energy loss. The model's assumptions break down, as it is unable to account for the non-conservative forces at play in real-world systems. Thus, while Hamiltonian mechanics models energy conservation effectively in idealized settings, it is limited in scope when applied to systems with significant dissipative effects.

2.4 Conservation of energy in non-conservative systems

In systems that involve non-conservative forces, such as friction or electrical resistance, the traditional proofs of energy conservation derived from Lagrangian or Hamiltonian mechanics fail [32,33]. The work-energy theorem, which accounts for both conservative and non-conservative forces, provides a more accurate model for these systems. The total mechanical energy is no longer conserved, as energy is dissipated. This can be expressed mathematically as: $\Delta T = W_{nc} + W_c$; where ΔT is the change in kinetic energy, W_{nc} is the work done by non-conservative forces, and W_c is the work done by conservative forces. In the context of electrical short circuits, W_{nc} represents the energy dissipated as heat (the chaos expanded in Equation (45)), illustrating that the total mechanical energy decreases over time. This dissipation is a physical consequence that cannot be derived from the traditional models discussed earlier, further demonstrating their limitations. In such cases, these models, while mathematically consistent, fail to fully capture the complexities of non-ideal, real-world systems.

2.5 A geometric perspective on energy conservation in complex systems

As discussed, in modern physics, the law of energy conservation has primarily been approached through advanced mathematical frameworks such as the Lagrangian and Hamiltonian formulations, and Noether's theorem. These methods are highly effective within the context of ordered systems and scenarios governed by well-defined constraints. However, they often lose clarity when dealing with chaotic, disordered, or complex systems, where the behavior of energy is less predictable [33,34]. The reliance on abstract mathematical representations, while powerful, can obscure the intuitive physical interpretations of the systems they model. This creates a gap, particularly when attempting to reconcile energy conservation in chaotic or less-structured classical systems, thus opening a need for alternative approaches that offer both rigor and clarity. One such alternative approach lies in the principles of Euclidean geometry [35], which provide a constructive and physically interpretable foundation for addressing the conservation of

energy in both ordered and chaotic systems. Euclidean geometry not only allows for the geometric construction of fundamental operations but also provides tools for proving solutions to polynomial problems, such as those explored by Descartes in his geometric operations [36,37]. This imperial geometric approach emphasizes a tangible, visual form of reasoning, grounded in constructability, which contrasts with the abstract symbolic manipulation found in modern physics and non-Euclidean methods [38-40].

2.5.1 Theoretical rigor and physical limitations in energy conservation

The Lagrangian, Hamiltonian, and Noether's theorem models, while providing a rigorous mathematical approach to energy conservation in classical systems, are ultimately limited by their characteristic assumptions of isolated, reversible, and symmetric systems [1,25]. These methods, designed for ordered and well-defined systems, struggle to capture the complexity of chaotic or disordered systems, where energy dissipation and non-conservative forces are prevalent [34,41]. Lagrangian mechanics, based on the principle of least action, offers a powerful framework for systems with smooth energy distribution and conservation. However, its reliance on differential equations can hinder its ability to interpret chaotic systems, where energy flows unpredictably. Similarly, Hamiltonian mechanics, while effective for simplifying certain dynamical problems, relies heavily on mathematical abstraction and provides little insight into the practical and geometric nature of energy in classical physics. Both Hamiltonian and Lagrangian methods are tailored for smooth, deterministic systems, limiting their use in chaotic or discontinuous systems. Noether's theorem, which links symmetries of a physical system to conservation laws, provides profound insight into the nature of energy conservation [25]. However, this method requires the existence of continuous symmetries, which may not be present in disordered or chaotic systems. Furthermore, Noether's theorem, while elegant, offers a highly formal mathematical explanation that can lose sight of the tangible, constructive essence of physical laws. These methods, though immensely valuable, demonstrate a clear disconnect between the abstract mathematical domain and the physical, tangible reality that geometric methods address more directly.

2.5.2 Euclidean geometry-A constructive foundation for energy conservation

Euclidean geometry, in contrast to modern mathematical frameworks, offers a constructive framework for understanding the physical properties of energy conservation. Geometric principles emphasize the creation of shapes, lines, and figures through definable operations, which can be directly visualized and understood [42-44]. In classical systems, where chaotic dynamics or complex polynomials emerge, Euclidean geometry offers a practical and concrete method for exploring how energy distributes and conserves within the system (this notion is elaborated in Theorem 2). For instance, Descartes' geometric solutions to polynomials demonstrate how physical principles, such as equilibrium points or energy distribution, can be explored using constructible operations [44]. Geometric proofs based on Euclidean principles can ensure that solutions are not merely abstract but grounded in operations that can be performed with basic tools like a straightedge and compass [40,43]. This physicality aligns with the classical interpretations of energy, where forces and motions can be visualized and constructed geometrically. In this light, the conservation of energy can be understood as a geometric construct: energy conservation in a system implies that no matter the transformation or configuration, the geometric properties of the system-such as its area or volume-remain constant. This geometric invariance echoes the physical invariance of energy in a closed system, providing a clearer, more intuitive model for understanding the law of energy conservation.

2.5.3 Applicability to chaotic and classical systems

In chaotic systems, where the smooth predictability of modern physics methods breaks down, geometric principles can offer an alternative interpretation. By understanding the system through geometric constructions, we can establish models that track how energy flows and redistributes in ways that are physically realizable. For instance, a chaotic pendulum or turbulent fluid can be described in terms of its geometrically conserved properties, such as rotational symmetry or volume in phase space. Euclidean geometry allows us to visualize how energy moves through such systems in a concrete way that Lagrangian or Hamiltonian methods might only approximate abstractly. Moreover, Euclidean geometric operations offer a rigorous model for solving polynomial equations or modeling systems where energy flows through non-linear interactions [44]. In classical systems, the trajectory of energy flow can be constructed geometrically, allowing for a physical interpretation of conservation laws that transcends mere symbolic representation.

Physical interpretation of energy conservation through geometry.

The constructive nature of Euclidean geometry directly maps onto the physical interpretation of energy conservation. In classical physics, energy conservation is often represented as a principle that holds across all transformations of a system. Geometrically, this can be understood as the invariance of certain properties-such as area or distance-under transformations like rotation, translation, or scaling. For example, the area of a triangle remains constant under rotation or reflection, just as the total energy in a system remains constant, even as it transforms from kinetic to potential forms. By grounding energy conservation in imperial geometric operations, we move away from abstract, mathematically complex descriptions and towards a physical interpretation that is intuitive, constructive, and visually realizable. As demonstrated in Definition 10, this approach provides a direct, physical model for energy conservation, one that applies not only in well-ordered systems but also in chaotic and disordered systems where energy distribution may be harder to capture with modern physics methods.

2.6 Analyzing energy conservation

This paper explores the principle of energy conservation from two complementary perspectives. First, it analyzes the interaction between material particles using Newton's Laws of Motion (Newton, 1687) [45]. This analysis demonstrates that during any interaction, energy transfers between the particles in equal amounts, thus conserving the total energy. Conversely, when particles do not interact, their individual energies remain constant, again leading to overall energy conservation. This concept provides a foundation for extending the reasoning behind energy conservation to any system. Second, the paper introduces the Euclidean geometric system as a practical framework for translating the quantities "*geometric points*" into physical systems composed of particles (*point-particle* (Definition 1)). This perspective allows for viewing energy conservation through a geometric lens. Euclidean geometric models are established within this paper to represent the relationships between material structures on a Newtonian scale.

2.7 Natural forces and geometric equivalence

The principle of energy conservation itself is remarkably simple, yet it manifests in a vast array of forms. This universality and unity between simplicity and complexity can make it challenging to recognize the underlying simplicity within intricate phenomena. Classically, the existence of any structure in nature (material system) is definitively described by its inertial mass and the "*structural*" interacting forces between its components (Ernst Mach, 1883), [46]. These forces can be understood as a form of "*natural symmetry*" or "*forceful competition*" that allows the structure to exist in spacetime. If these forces are unbalanced, the structure becomes unstable and may collapse (refer to Section 4 for a detailed analysis using Newton's Laws). Following this principle, the net action forces acting on a system must be balanced by the sum of the net reaction forces and the net inertial forces [47,48]. Through the succeeding sections of the paper, these natural physical relationships between forces in equilibrium states will be observed and preserved by translating the interactions between material systems to geometric quantities while invoking the concept of equality, as presented in [49]. The employed translation involves establishing geometric constructs that directly correspond to our physical understanding. These constructs are based on the concept of a "*Point-Particle*" (Definition 1) within a in a "*Euclidean-Plane*" (Definition 2). This approach ensures a perfect comparison between the physical and geometric domains.

3 Contextual background

This section lays the groundwork for understanding the newly presented proof of the Law of Energy Conservation (LEC). It delves into three key areas-Section 3.1 (Foundational Philosophical Concepts) explores the core philosophical principles that serve as the bedrock for the proof. Section 3.2 (Historical Narrative) traces the historical evolution of LEC understanding, providing crucial context for appreciating the significance of the new proof. Section 3.3 (Re-evaluating Efforts to Challenge the Law) analyzes the persistent, yet unsuccessful, attempts to defy the LEC. By examining these historical efforts, this section establish a strong foundation on which the new proof is built, highlighting the need for a more rigorous framework.

3.1 Foundational philosophical concepts

Despite its fundamental role in physics, the exact nature of energy remains a subject of philosophical debate [50,51]. While most scientists define energy as the capacity to do work, a more precise understanding may be required. In the domain of physics, the concept of energy is tightly linked to experiments that measure various quantities assumed to be driven by energy. However, the term "*energy*" can sometimes be used loosely as a catch-all explanation for phenomena that are not fully understood through established physical relationships. Due to the inherent complexity of the energy concept, some scientists attempt to bridge the gap by focusing on the relationship between energy and matter [52-54]. This approach leverages the well-defined properties of matter to gain a better grasp of the underlying principles governing energy. At the very least, it allows us to work with measurable aspects of matter and then translate those observations back to the concept of energy. Historical writings often described matter as possessing a mysterious essence [50,51,55], which this paper identifies as energy. Scientific discoveries have revealed the interchangeability of energy and matter under specific physical conditions [50,56]. This paper leverages the unifying principle that all known forms of energy can transform into matter and vice versa. Within this context, a material particle is treated as an energy carrier or equivalent. Throughout history, philosophers have debated the infinite divisibility of matter [57-59]. However, this paper focuses on a scientific approach grounded in evidence. To maintain focus on the proof, we posit the existence of a fundamental particle within Euclidean space, the smallest possible unit describable. This particle will possess characteristics of both Euclidean geometry and mathematical analysis. Furthermore, we assume the existence of a "*Euclidean space (a geometric plane)*" (Definition 2) where, for an arbitrary "*point-particle*" A accessible about a point O, the arithmetic operations of geometric multiplication (denoted as $G_m \Longrightarrow A \otimes B$ (Definition 8)) and geometric division (Denoted as $G_d \Longrightarrow A \oslash B$) can be performed using straightedge and compass constructions. Building on this framework, we define the physical quantity "*point-particle*" as follows.

Definition 1 (Point-Particle as a fundamental unit).

Let S be an infinite set of particles in Euclidean space (written otherwise, imagine an infinite set of particles in a flat, geometric space). According to the power set axiom, we assume that S can be scaled to a set $P_p(S) = \exists x \left(\forall_y (y \in x \Leftrightarrow y \subseteq S)\right)$, where $\forall_y$ is a geometric arithmetic quantification (either G_m or G_d) over the entirety of all sets and $P_p(S)$ is a member of that totality. Thus, we call the member $P_p(S)$, a ***point-particle***.

A simple notion of energy as an interchangeable quantity is explicitly established by [50] through logical operations

similar to those used in Definition 1 to equate concrete (material) entities.

A unifying perspective on matter and energy.

Definition 1 combines logic with a physical perspective that resonates with ancient ideas about the nature of matter. It inherently implies the construction of fundamental quantities on a plane, encompassing both relativistic and ordinary (Newtonian) scales. Crucially, this definition applies specifically to a Euclidean geometric system, emphasizing the arrangement of objects within a Euclidean plane, not simply their projection using real numbers. As outlined, the Euclidean geometric system prohibits the direct use of real numbers to represent geometric quantities [39,40,60]. However, this paper also acknowledge that Euclid allowed for the inclusion of special types of numbers arising from geometric operations, like ratios [39]. This paper assumes the existence of both real numbers and geometric magnitudes, considering them not as direct substitutes for but, as representations of analogous quantities (objects) within the Euclidean framework. This is based on the understanding that Euclidean geometry lacks a formal definition for magnitude, and contextually disallows negative numbers and zero, suggesting geometric magnitudes cannot measure such ratios. Furthermore, the modern view on numbers does not necessarily imply their inherent existence in physical systems. Therefore, it is crucial to differentiate between using real numbers within geometry and using them in physics. This distinction creates challenges, but by strictly limiting how we interpret real numbers, we can integrate them with geometric magnitudes within the same physical context. In this context, this section posits that a set of point-particles, denoted as $P_p(S)$ establishes a distinct relationship between the Euclidean geometric system and the physical description of matter. Consequently, when considering $P_p(S)$ within a Euclidean space and utilizing solely positive real numbers as representations for $P_p(S)$, Definition 1 logically embodies both intuitionistic and analytical characteristics for any instance of $P_p(S)$. This definition serves as a cornerstone for the subsequent sections of the proof.

3.2 Historical narrative (Perspectives on the LEC)

The law of energy conservation (LEC) has a rich historical background. Early formulations focused on the concept of mechanical energy within a conservative force field. The notion of mechanical work itself emerged alongside the development of mechanics principles. The terms "*mechanical work*" (travail mécanique) and "*quantity of motion*" are credited to Gaspard-Gustave Coriolis (1792-1843), [61] and René Descartes (1596-1650) [18,62,63], respectively. The modern understanding simplifies the concept by comparing the gains in kinetic energy and losses in potential energy for objects falling in a gravitational field, and vice versa for objects ascending. This paper utilizes the axiomatic Euclidean geometric model (for the established geometric rigor see [63-65]) as a foundation for a unique proof. This model leverages the strengths of logic to construct a proof that bridges the gap between the Euclidean geometric system and analytical models. However, a key challenge arises when attempting to integrate a Euclidean plane with the modern mathematical structure reliant on coordinate systems. The coordinates system designates an arbitrary point O in the Euclidean plane as the "*origin*". It has two perpendicular lines through O called the "$x-axis$" and "$y-axis$". Any other point is describable on this plane by two real numbers (x, y), which are thought of as the side lengths of a rectangle whose sides are perpendicular to the $x-axis$ and $y-axis$. By recalling the earlier established restriction to the origin (x, y); where $x \neq 0$ and $y \neq 0$, the translation from a Euclidean plane to coordinate plane allows us to identify the Euclid's plane with the set $\mathbb{R}^2$ of pairs of real numbers. In this context, the $\mathbb{R}^2$ plane becomes a model of Euclid's axioms (a mathematical structure that satisfies a specific interpretation of those axioms). This translation is the hurdle to overcome when establishing a physics proof analogous to geometric proofs within the Euclidean system.

Motion and energy.

In Cartesian physics, the concept of motion is central. Descartes, in his work Principia Philosophiae [66], proposed that God was the primary cause of motion and maintained a constant quantity of motion within the universe. Energy, on the other hand, remains a concept beyond direct experience. While its existence is widely accepted, its exact nature is still debated [67]. This paper builds upon the concept of particulate structures as equivalent to energy models. However, this paper avoids delving into the historical debates surrounding energy that often carry religious undertones. While the core focus of this paper is the theoretical foundation of motion, energy, and matter, it recognizes the importance of understanding their historical development. This broader perspective enriches the understanding of these concepts by tracing their evolution and appreciating the intellectual journey that led to our current understanding. René Descartes, for instance, argued that both motion and inertia are universally constant, though their distribution can vary depending on location and time within the cosmos [68]. He viewed the universe as an extension of matter and motion. Building on Descartes' ideas, Baruch Spinoza (1632-1677) adopted a propositional and proof-based approach in his work (as described by [69]). Similar to Descartes, Spinoza established a law of motion conservation, again relying on theological reasoning. He believed that God predetermined everything, including the nature of motion. Considerably, perspectives on these concepts can vary greatly. As a result, this paper remains focused on the theoretical framework, avoiding religious interpretations of energy. Gottfried Wilhelm Leibniz (1646-1716) challenged Descartes' notion of absolute motion conservation [70]. Leibniz argued that while the total amount of motion in nature might not be constant, motion in any specific direction is conserved. While Descartes believed in a constant total amount of motion, Leibniz's ideas on motion largely align with the geometric experiment established in Definition 1 of this paper. This paper builds upon the concept of a "*point-particle*" to unify ideas analogous to the views of Descartes and Leibniz on motion and energy. The proofs

throughout this paper are fundamentally based on the models defined; *ETIS* (Definition 3) and *TIS* (Definition 5).

3.3 Re-evaluating efforts to challenge the law of energy conservation

The history of attempts to challenge the law of energy conservation reveals a fascinating, yet often misguided, trajectory. Early efforts, fueled by genuine scientific curiosity, aimed to explore the frontiers of energy generation. However, over time, these endeavors have become increasingly plagued by scientific misconceptions and a lack of rigorous frameworks [71-75]. This section delves into these issues and proposes a novel approach for establishing the law's validity.

Flawed use of perpetual motion machines (PMMs).

A common misconception among those who doubt the law of energy conservation is the belief in the possibility of perpetual motion machines (PMMs). These devices are often envisioned as mechanisms that can produce energy indefinitely without an external energy input [74-76]. This misunderstands the fundamental nature of energy – it is not a substance that can be created or destroyed. Instead, it is a fundamental property of matter and its interactions. The law of energy conservation, also known as the first law of thermodynamics, states that the total energy within a closed system remains constant. This means that energy can neither be created from nothing nor disappear without a trace. While energy can be transformed from one form to another, in the ordered states, the total amount of energy within the system always remains the same [77]. The second law of thermodynamics, a cornerstone of physics, provides further clarity on this matter. It states that in any isolated system, the entropy, or disorder, always tends to increase over time. This means that any process that appears to generate energy from nothing would inevitably violate the second law. As a result, the concept of a perpetual motion machine, while appealing, is fundamentally impossible.

The need for rigorous frameworks and a shift in perspective.

The historical lack of success in defying the Law of Energy Conservation (LEC) through traditional methods suggests the need for a fresh perspective. While the core principles of the LEC remain widely accepted, the frameworks used to establish its validity might require re-evaluation. This re-examination aims to address the concerns of skeptics and provide a clearer understanding of the conditions under which the LEC could potentially be violated. The historical reliance on experiments, while valuable (as championed by Descartes' view on the accessibility of experiments through logic, even without physical execution [78-80]), needs to be complemented by more robust theoretical frameworks. A rigorous mathematical proof, grounded in established physical principles, would provide a more solid foundation for understanding and applying the law. This paper addresses this critical need by presenting the first-ever proof of the law of energy conservation at the interface of Euclidean geometry and physics. This unique approach leverages the well-defined principles of Euclidean geometry to construct a framework within which the law's validity can be demonstrably established. By translating geometric operations into a physical context, the paper offers a new lens for reasoning about energy conservation, one that surpasses the limitations of relying solely on the concept of perpetual motion.

The need for proof and its implications for sustainability.

The law of energy conservation has served as a cornerstone of physics for centuries, guiding our understanding of energy transformations and resource limitations. However, the historical lack of a rigorous proof has left room for misinterpretations and misguided attempts to defy the law. The sheer number of unsuccessful endeavors aimed at breaking the law underscores the importance of establishing a definitive proof beyond simple observation. While the law's practical applications have been evident for centuries, a provable foundation strengthens our understanding and paves the way for innovative solutions. In the face of the ever-growing energy crisis [81-83], a robust foundation for energy conservation becomes paramount for developing sustainable solutions. Through providing a rigorous proof, this paper aims to bridge the gap between theoretical understanding and practical application, ultimately leading to a more sustainable future.

The logic of proof.

The existence of a rigorous proof fosters trust in the law's validity, encouraging further scientific exploration. Without a solid foundation, skepticism and misunderstandings can hold back progress. A proof establishes a clear point of reference, allowing scientists to build upon established knowledge and explore new avenues for energy generation and utilization within the framework of the law. Scientific understanding is a continuous process [79,80], constantly evolving through new discoveries and reinterpretations of existing knowledge. This paper's contribution lies in its introduction of a novel proof within the unique context of Euclidean geometry and physics. Recognizing the limitations of past frameworks allows us to refine our understanding and develop more robust approaches to fundamental principles like energy conservation.

Breaking free from misconceptions.

Through addressing scientific misconceptions and presenting a novel proof, this paper opens the door to a new era of energy exploration. With a deeper grasp of the law of energy conservation, scientists can confidently explore alternative energy sources and devise innovative solutions to the global energy crisis. Moving beyond the constraints of perpetual motion machines and relying on rigorous frameworks heralds a future where energy production and utilization are anchored in sound scientific principles, ultimately fostering a more sustainable world.

4 Geometric characterization of the proof

This section aims to establish a geometric configuration characterization of the proof within a *Euclidean-*

Thermodynamic Isolated System (ETIS) (Definition 3). Traditionally, a gap exists between rigorous Euclidean geometric proofs and the more characteristic, less rigorous proofs found in physics. The prevailing view often considers the Euclidean geometric system incompatible with physics, as exemplified in studies of general relativity [84]. However, this paper argues against such a definitive conclusion. The Euclidean geometric system inherently offers a robust framework for proofs that build upon the specifics of a problem, rather than imposing a pre-existing structure. This allows for both deductive and inductive proofs within the Euclidean framework, potentially extending its applicability to scientific reasoning. While physics traditionally relies on inductive approaches based on established practices [18,79], ongoing research highlights the limitations of proofs solely reliant on experimental observations and experiences for validation. This paper questions the necessity of always adhering to purely inductive methods in physics, which will be further elaborated upon later. Therefore, this paper challenges the assumed incompatibility between rigorous Euclidean geometric proofs and characteristic physics proofs. While the Euclidean geometric system leaves concepts like "*Magnitude*", "*Plane*", and "*Equality*" undefined, their corresponding terms, "*Quantity*", "*Space*", and "*Equality*" – often possess more concrete and tangible scientific interpretations. However, the challenge in this section lies in establishing a consistent mnemonic to bridge this gap throughout the analysis.

4.1 Important terminologies

Definition 2 (*Euclidean Plane [Plane used interchangeably for Space]*).

In Euclid's Elements, the term "*plane*" is employed contextually without a precise definition [35]. It appears that Euclid regarded a geometric plane as the inherent existence (here, carefully avoiding the philosophical notion of existence) of a geometric structure, representing the potential for a geometric quantity or magnitude, or the consideration upon which these geometric concepts can be conceived. This paper adopts a similar approach, defining a geometric plane as the $Euclidean\ Plane\ (or\ Space)$ based on its intuitive and contextual understanding. This means that a plane is simply the underlying framework or space in which geometric figures and relationships can be defined and studied.

Definition 3 (*Euclidean-Thermodynamic Isolated System* ($\boldsymbol{ETIS}$)).

Building upon Definitions 1 and 2, an *ETIS* is arbitrarily defined as a system comprising a minimum of two "*point-particles"*, each corresponding to distinct geometric objects referred to as points within a Euclidean plane.

Remark 1.

In many physical contexts, point-particles are commonly assumed to be identical. In the context of an *ETIS*, we interpret the similarity feature among point-particles geometrically, relying on the concept of equality within the system's geometries. This equality between geometric points holds a unique significance, as it does not describe the geometric configurations per se but provides an account of the relationships between geometric magnitudes (refer to *lemma 1*).

To proceed, we position point-particles at points A, B, O, U, and Z, with points O and U characterizing the geometries of the *ETIS*, and points A, B and Z constituting matter interactions within and outside the *ETIS*. Using straightedge and compass operations, and inverting point A in a Euclidean plane to basepoints O and U, the resulting inverse points A and B create a geometric singularity on a locus centered at the point of inversion (point O). The subsequent proof demonstrates that Definition 3 describes a geometric configuration equivalent to the scientific understanding of an isolated thermodynamic system. As per empirical definitions, an isolated thermodynamic system is rigid, immovable, non-conductive of heat, perfectly reflective of all radiation, and impervious to all types of matter and forces [85,86].

4.2 Formalizing Definition 3

This section rigorously establishes Definition 3 using the principles of Euclidean geometric constructions, specifically those achievable with straightedge and compass. The proof centers around demonstrating the geometric inversion of a point relative to a pair of distinct base points within a Euclidean plane. We begin by introducing the concept of "invasion" (defined precisely later), followed by the formal proof itself. For clarity, this section temporarily departs from the established concept of a point-particle. Instead, it utilizes the pure language of Euclidean geometry to build a solid geometric foundation. The concept of a "*point-particle*" will be reintroduced later when interpreting and translating the established geometric proof into the context of physics. For the conclusive steps of this proof, consider the following geometric experiment.

4.2.1 A geometric experiment within an ETIS

The goal of this experiment is to illustrate the characteristics of a thermodynamically isolated system (*ETIS*) within a Euclidean Plane through a geometric approach. Employing Euclidean inversion techniques relative to distinct basepoints, the experiment showcases the behavior of point-particles within the *ETIS* under the influence of external forces originating from nearby particles. The geometric construction involves establishing circles, lines, and intersection points to demonstrate the motion and interaction of these particles within the system.

Definition 4 (*Euclidean inversion of a point A relative to a pair of basepoints O and U*).

The Euclidean inversion of point A concerning distinct basepoints O and U is characterized by the geometric relation $((OM_1)^2 = OB \times OA)$, where OM_1, OB, and OA represent valid geometric magnitudes subjected to a G_m operation. This inversion, designated as A^{-1}, is established through a construction involving the points $\{O, U, A\}$.

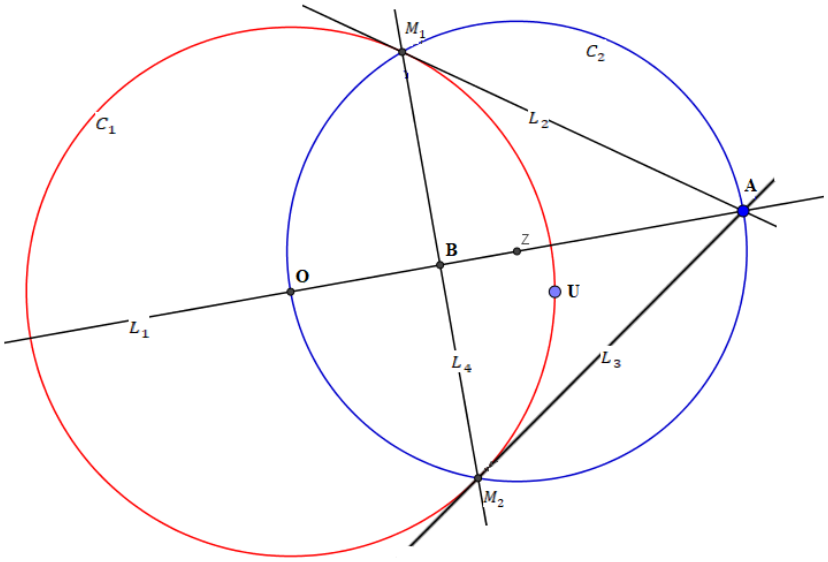

Figure 1. Geometric characterization of Euclidean-thermodynamic isolated system (***ETIS***) in a Euclidean Plane. (This figure articulates the Euclidean inversion process of point ***A*** relative to distinct basepoints ***O*** and ***U***. This geometric characterization provides a detailed representation of the Euclidean-Thermodynamic Isolated System (***ETIS***) within a Euclidean Plane).

1. If $U \cong O$, construct the point O. Otherwise, proceed to step (2).
2. Construct circle C_1 centered at the point O though point U.
3. Construct line L_1 passing points O and A.
4. Construct the point Z, a bisection of L_1.
5. Construct circle C_2 centered at the point Z though point O.
6. Let the points M_1 and M_2 denote the intersection points of the circle C_2 and circle C_1.
7. Construct line L_2 passing through the points A and M_1.
8. Construct line L_3 passing through the points A and M_2.
9. Construct line L_4 passing through the points M_1 and M_2.
10. Construct point B, the intersection points of L_4 and L_1.

Figure 1 illustrates the points O and U, delineating the geometric configuration of a circular plane, which we refer to as the Euclidean-Thermodynamic Isolated System (*ETIS*) in subsequent discussions. In this experiment, let the point B symbolize matter within the *ETIS*, denoted as a "*point-particle*" labeled as n. The objective is to show that the point B experiences motion solely under the influence of a force originating from another nearby "*point-particle*" in the vicinity C_1. This principle extends to any other particle (n) subjected to external forces, presumed to originate from the point A. For illustrative purposes, we propose that the circumference created by C_1 acts as a permeable isolation wall, allowing the force from the point A to affect the point B. This implies that even if the isolated system defined by C_1 is closely surrounded by other systems, its contents could still be influenced by external interactions. While somewhat aligning with the physics definition of an isolated system, this notion diverges significantly. In standard physics, a truly isolated system remains impervious to external interactions, encompassing both matter and energy exchanges [85,86].

Distinct characteristics of the thermodynamically isolated system.

Furthermore, we conceive of this wall as naturally occurring, embodying the environmentally independent characteristic of a truly isolated system. This establishes a unique relationship between the interior of the system and its external environment. Within this thermodynamically isolated system, we assert two primary properties;

- **Physical Isolation.** The system operates independently from other systems, maintaining its internal characteristics without exporting its contents.

- **Information Preservation.** The system's information structure remains intact, even upon the entry of foreign material.

Revelations from the geometric experiment.

The geometric experiment reveals that as the point A moves towards the circumference of C_1, the point B shifts towards the curvature of C_1, ultimately converging at the circumference. Further movement of the point A within C_1 results in the dissolution of the geometric form of the circular plane, erasing information pertaining to the points B, M_1 and M_2, along with the connecting lines L_2, L_3, L_4, and C_2. Notably, as the point B approaches the circumference C_1, point Z moves in the opposite direction.

Challenging traditional definitions of isolated systems.

This illustrative geometric experiment challenges the validity of commonly assumed physics definitions for a

thermodynamically isolated system. Traditional definitions typically fall into two categories.

- ***Defn 1 (Infinite Separation).*** The system is located infinitely far from surrounding systems, precluding any exchange of matter and energy (Figure 3 provided by [85]).

- ***Defn 2 (Rigid Barrier).*** The system is equipped with a rigid isolation wall obstructing matter and energy exchange with the surroundings [87].

This geometric experiment suggests that a truly isolated system might necessitate a different conceptualization, potentially amalgamating elements of both these traditional definitions while emphasizing the preservation of information within the system.

Proposition 1.

In physical settings, an isolated thermodynamic system maintains balance in its contents (matter-energy), signifying it as a self-sustaining model. The assertion of the physical relation $E_s = 0$ (with E_s as the total energy within the isolated system) [77,88,89] challenges the assumed characteristics of thermodynamic isolated systems (*Defn 1* and *Defn 2*), revealing them as a significant misconstruction of matter-energy content in such systems.

Remark 2

Expanding upon proposition 1, the proposition that the energy relationship $E_s = 0$ is universally applicable [77,89] prompts consideration of the entire universe as a thermodynamically isolated system. In defining this isolation (*Defn 2*), it is suggested that the universe, in its physical essence, possesses an intrinsic boundary, mirroring an isolation wall, representing a perfect thermodynamically isolated system. However, the unknown size of the universe challenges this assertion, with projections indicating its indeterminability. The indeterminate size of the universe contradicts (*Defn 2*), as the isolation wall remains undefined. Consequently, assuming the validity of the relation $E_s = 0$ for the entire universe renders (*Defn 1*) incorrect, as it implies isolation from other systems that cannot be part of the entire universe-an untenable scientific notion. Proposition 1 necessitates the rejection of conflicting definitions of a thermodynamically isolated system, leading to the introduction of a more rational definition (Definition 5) aligned with the constructed $ETIS$ at the interface between the Euclidean geometric system and physics.

Definition 5 (*Thermodynamics isolated system-TIS*).

The Euclidean plane defined by the relationship $(E_s \leftrightarrow M_s) \cong 0$ signifies a balanced interchangeability between total energy (E_s) and matter (M_s) within a system exhibiting the following characteristics:

- It is a Euclidean plane that is inherently geometrically extensible, in accordance with Euclid's postulate on straight line extensibility [42].
- The system's configuration establishes a rigid arbitrary structure, naturally preventing the exchange of E_s and M_s from both external sources into the system and from the system to the external environment.

In the subsequent sections, we will denote this system as *Thermodynamics Isolated System (TIS)*. Specifically, when implemented on a Euclidean plane, it will be denoted as *ETIS*.

Consider Theorem (1), facilitating the translation of this geometric proof into a more comprehensive scientific framework.

Theorem 1. *For any given circle of inversion (C_{inv}) with a center of inversion O and the radius $\overline{OM_1}$, the point A is an inversion of the point B outside the C_{inv} such that in its square, the magnitude $\overline{OM_1}$ corresponds to the G_m of the magnitudes $\overline{OB}$ and $\overline{OA}$ where $\overline{OA} > \overline{OB}$ and A is the point of intersections between the tangents to the C_{inv}.*

Consider Figure 2 (an extended result of Figure 1) obtained by a construction from the points $\{O, U, A\}$ as follows.

1. Construct a straight line segment L_5 passing through the points O and M_1.
2. Construct a straight line segment L_6 passing through the points O and M_2.

Through this construction, we derive two geometrically symmetrical triangles; OAM_1 and OAM_2 in Figure 2. Applying the theory of similar triangles to Figure 2 facilitates the proof of Theorem (1), subsequently establishing Definition 3. By considering the congruence property (Side-Angle-Side-(SAS)) for the similar triangles OM_1A and OBM_1, we deduce the relation $\frac{OM_1}{OB} \cong \frac{OA}{OM_1}$. This leads to the following geometric deduction.

$$\frac{OM_1}{OB} \cong \frac{OA}{OM_1} = (OM_1)^2 \cong OB \otimes OA \tag{1}$$

Equation (1) shows that the point B and the point A are geometric inverse points and the inversion is expressible in the form $B = A^{-1}$.

4.2.2 Interpretation and translation of the proof

Equation (1) represents a critical juncture in this paper. It translates geometric relationships with the precision of the Euclidean geometric system, specifically adhering to the principles outlined in the first six books of Euclid's Elements [42]. The equation can also be interpreted scientifically using coordinate geometry (analytical geometry) within a physical context.

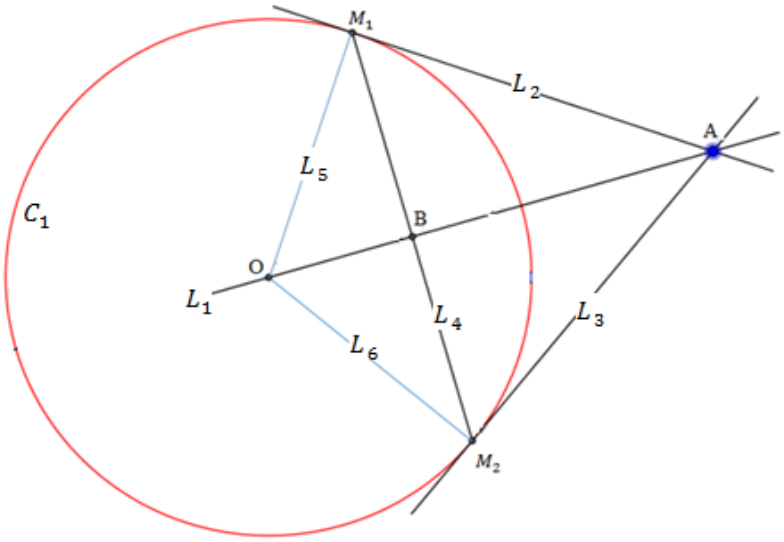

Figure 2. Geometric inversion of a point inside the circle of inversion to a point outside the same circle (The Geometric Characterization of a ***ETIS***). (The figure demonstrates the construction from points $\{\boldsymbol{O}, \boldsymbol{U}, \boldsymbol{A}\}$, leading to the creation of triangles $\boldsymbol{OAM_1}$ and $\boldsymbol{OAM_2}$. The resulting geometric relationships, guided by the theory of similar triangles, provide evidence for Theorem (1) and contribute to the establishment of Definition 3).

From a Euclidean geometric perspective.

From a Euclidean standpoint, Equation (1) naturally involves operations between geometric magnitudes of the same kind, exemplified by magnitudes OM_1, OB and OA in Figure 2. Applying Euclid's theory of proportions based on magnitudes of similar kinds to the geometric ratio $\frac{OM_1}{OB} \cong \frac{OA}{OM_1} \cong \aleph$ (where $\aleph$ is a positive real integer), the ratio $\aleph$, according to Euclid's geometric scheme, possesses essential characteristics; it is a positive real number and non-zero [39,42]. Under these conditions, Equation (1) can be carefully translated into an equivalent analytical geometric interpretation.

Translation to analytical geometry.

With systematic consideration for points in the Cartesian coordinate system, we arbitrarily designate a point of origin as (x, y) where $x \neq 0$ and $y \neq 0$. We adhere to the conditions of the Cartesian coordinate system, acknowledging that no geometric magnitude can be zero in the Euclidean system. This disregards the analytic notion that the Cartesian origin (often denoted as $(0,0)$) serves as a point of reference. The focus here is on geometric magnitudes, leading us to set conditions that $OM_1 \ncong 0$, $OB \ncong 0$, $OA \ncong 0$, and that OM_1, OB and OA are non-negative. This confines operations to real positive integers, allowing for their use as both geometric objects and descriptive language. Euclid's Proposition 10 in Book 1 affirms the possibility of bisecting any straight line segment through straightedge and compass operations [90,91]. This paper posits that any straight line segment can be infinitely bisected using these procedures. In analytical systems, a straight line segment is perceived with a material essence expressible on the coordinate system. Considering Definition 1 and aligning with scientific understanding, atoms are known to be theoretically infinitely divisible [92,93]. To complete the proof, we assume the existence of an infinitesimally short line segment in the *ETIS*, corresponding to a perceptibly infinitesimal point-particle in the *TIS* perspective. Referring to Figure 2, let the geometric magnitudes OM_1, OB and OA represent the infinitesimally small interacting point-particles within the *ETIS*. This allows for quantifying the inherent properties (whether matter or energy) of these point-particles as objects using real numbers. This contrasts with the traditional Euclidean geometric system, which worries about the application of real numbers as representation of geometric magnitudes, and not as abstract expressions for the inherent properties of objects. Thus, the approach is within the inherent territory set up earlier in the paper.

Physical interpretation.

In a physics context, Equation (1) can be interpreted for *ETIS* with the center of inversion O and the radius of inversion ($\overline{\mathrm{OM}_1}$) given that point-particle A is the inverse of point-particle B outside the $ETIS$ of inversion. In this interpretation, within its square, the particle system $(OM_1)^2$ corresponds to a G_m on the point-particles A and B expressed as $OB \otimes OA$.

Remark 3.

The statement of Theorem (1) omits consideration of (*Defn 1*) and (*Defn 2*) as crucial components of an ideal *TIS*. This results in a naturally free system resilient to gains or losses of content similar to its structure and genetic contents. This scenario also applies when point-particle B is outside the inversion circle and point-particle A is inside it. Thus, Definition 3 is established for a naturally existing *ETIS*.

Remark 4.

In the modern perspective, with the aid of a *TIS*, Definition 3 is established in a spherical model denoted by $\mathbb{C}^3$ (extending beyond a Euclidean plane). Due to a lack of comprehensive understanding regarding the appropriate geometric models for describing the entire physical universe, it is prudent to characterize the properties of the universe from a Euclidean plane, as these properties remain independent of the system's geometries. Here, we associate the universe's infinitude with the indeterminate concept of infinity in the Euclidean context.

Rethinking isolated systems

Remark 5 (A Consequences of Definition 3).

According to traditional physics definitions (*Defn 1*), a thermodynamically isolated system is either incredibly distant from other systems or enclosed by rigid, impenetrable walls (*Defn 2*). However, proving Definition 3 using the described geometric experiment suggests these traditional definitions might be incomplete. In Figure 1, point B is closer to the assumed isolation wall (C_1) compared to point A. yet the interaction between points B and A demonstrates an even meeting on the circumference C_1. This demonstrates that the distance between a system and its isolation wall is not the sole factor in isolation. Therefore, we propose a new way to understand a Thermodynamically Isolated System (*TIS*). A *TIS* inherently prevents the transfer of matter and energy in or out, potentially representing a self-sustaining system. While Equation (1) applies at any scale in our geometric model, the existence of observable Extremely Thermodynamically Isolated Systems (*ETIS*) in the physical world is beyond the scope of this paper. To ensure adherence to the Law of Energy Conservation, all geometric operations in this paper will be confined within an *ETIS*, aligning with the physics concept of a thermodynamically isolated system.

4.3 Proving Newton's laws of motion

A thorough examination of energy conservation theory underscores the necessity of involving Newtonian physics to rigorously prove LEC, particularly when considering the concept of motion between interacting bodies. To ensure balance, this paper significantly engages in providing geometric treatments for Newton's laws of motion. Emphasizing the law of inertia as a central component in two of Newton's three laws, this section focuses on proving Newton's first law (N^{1st}) and the third law (N^{3rd}), illustrating their integration in the second law (N^{2nd}). The proof demonstrates how analogous models can be applied to establish LEC. A special case of N^{2nd} emerges naturally when the inertial force is zero, signifying balanced action and reaction forces. This leads to two crucial consequences: (1) balanced forces on any boundary interface surface (N^{3rd}), and (2) non-accelerated systems (N^{1st}). Fundamentally, all three Newton Laws of motion derive from N^{2nd}, making N^{1st} and N^{3rd} special cases when acceleration or mass is zero, respectively.

4.3.1 A geometric model of the Newton's First Law (N^{1st})

The goal of this section is to show that all points of the parallel straight lines constructed from a chosen point $O(x, y)$ through a distinct point $A(x_1, y_1)$ in a Euclidean plane where $O \ncong A$; are the same.

Lemma* 1 *(The empirical identity property for addition).

For any point A, $A \oplus O \ncong A$.

Consider two distinct points such that $B \cong O$ and $A \cong C$ in naturally constructed geometric configuration. We extend the addition property operation ($\oplus$) via the following straightedge and compass construction.

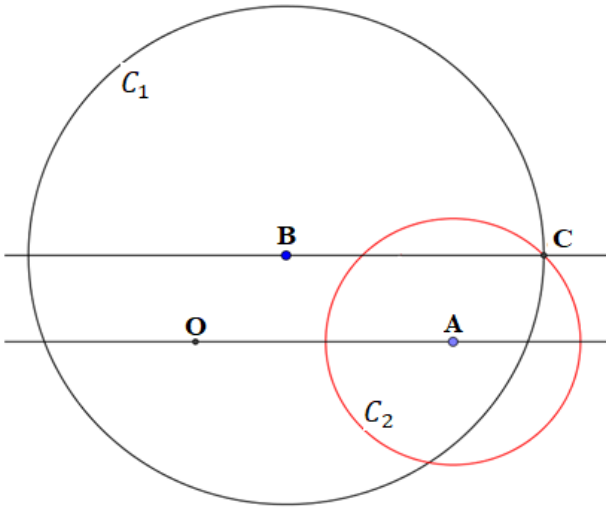

Figure 3. Geometric Identity Property of Addition. (Illustrating a geometric model of Newton's First Law ($\boldsymbol{N^{1st}}$), this figure demonstrates the empirical identity property for addition lemma (**1**). The construction involves distinct points $\boldsymbol{B}$ and $\boldsymbol{C}$, with $\boldsymbol{B \cong O}$ and $\boldsymbol{A \cong C}$, and employs the addition operation ($\oplus$) through a stepwise geometric process.)

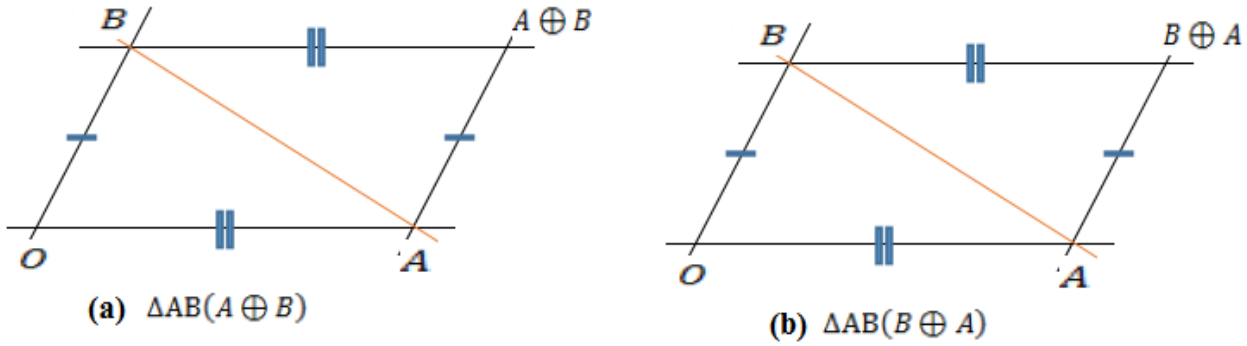

Figure 4. Geometric proof for Lemma **1**.

1. If $A \cong O$, construct the point O. Otherwise, proceed through step (2).
2. Construct line L_1 passing the points O and A.
3. Construct line L_2 parallel to line L_1 though point B.
4. Construct circle C_1 of radius L_1 cantered at the point B.
5. Construct a point C, the intersection of the line L_2 and circle C_1.
6. Construct circle C_2 of radius $\overline{OB}$ cantered at the point A.

Figure 3 offers an extended fashion of lemma (1). In the essence of the described construction, it is assumed that both the lines L_1 and L_2 are constructed through the points O and A. The figure, therefore, provides a simplified geometric characteristic illustration for showing that when traced on each other, the lines L_1 and L_2 are geometrically equal (the same).

Claim 1.

The circle C_2 intersects L_2 through the point C, implying that the lines $\overline{OB} \cong \overline{AC}$ and, $O \cong B$ and $A \cong C$ when the construction is not stretched.

Proof for Claim 1.

We redefine Figure 3 so that the inherently constructed point C corresponds to the point $A \oplus B$ in the diagram (a) of Figure 4 and in a distinct view, the point C correspond to the point $B \oplus A$ according in the diagram (b) of Figure 4.

Consider a congruent relation deduced from the diagram (a) of Figure 4 and diagram (b) of Figure 4 expressed as $\Delta AB(A \oplus B) \cong \Delta AB(B \oplus A)$, respectively. Further, based on Figure 3 we note that since $\overline{OA} \parallel \overline{BC}$, then $\overline{OB} \parallel \overline{AC}$. This corresponds to the schemes in the diagram (a) of Figure 4, $\overline{OB} \parallel \overline{A(A \oplus B)}$ and in the diagram (b) of Figure 4, $\overline{OB} \parallel \overline{A(B \oplus A)}$.

Remark 6.

In Figure 4, the congruent triangles ($\Delta AB(A \oplus B)$ and $\Delta AB(B \oplus A)$) share points A and B, with their third points situated on the side $\overline{AB}$. The equality of these third points can be demonstrated through the following deductions.

Starting with ΔAOB, we set the angles;

$$\angle OAB = \alpha \text{ and } \angle OBA = \theta \quad (2)$$

It follows that $\angle AOB = \pi - (\alpha + \theta)$ (Angles sum in a triangle) (3)

We focus on $\Delta AB(A \oplus B)$, from the diagram (a) of Figure 4.

The $\angle BA(A \oplus B) = \theta$, and the $\angle AB(A \oplus B) = \alpha$ (alternate angles to $\angle OBA$ and $\angle OAB$ respectively). (4)

Therefore, $\angle A(A \oplus B)B = \pi - (\alpha + \theta)$, (Angles sum in a triangle) (5)

Similarly, consider $\Delta AB(B \oplus A)$ in the diagram (b) of Figure 4.

$\angle BA(B \oplus A) = \theta$ and the $\angle AB(B \oplus A) = \alpha$ (alternate angles to $\angle OBA$ and $\angle OAB$ respectively). (6)

Therefore, $\angle A(B \oplus A)B = \pi - (\alpha + \theta)$, (Angles sum in a triangle) (7)

Since $\overline{OB} \parallel \overline{A(A \oplus B)}$ and $\overline{OB} \parallel \overline{A(B \oplus A)}$, and, $\angle A(A \oplus B)B = \angle A(B \oplus A)B$, then $\overline{OB} = \overline{A(A \oplus B)}$. Thus, $\Delta AB(A \oplus B)$ is similar to $\Delta AB(B \oplus A)$ by the property; SAS. Equation (5) and Equation (7) show that $A \oplus B = B \oplus A$, and this proves lemma (1).

Translation of Lemma 1 to it physics equivalence.

Lemma 1, when translated into its physics equivalence, establishes a geometric framework limited to rectilinear forms of motion. This aligns with Descartes' early conceptualization of motion systems; wherein non-rectilinear motions were reduced to rectilinear motions. Descartes proposed that a body's tendency to move instantaneously is rectilinear, as only such motion can be clearly identified. According to Descartes, the conservation of motion occurs except during collisions, where the total motion is conserved but may be redistributed among the colliding bodies. To comprehend motion in a circle or within any other trajectory, it is essential to consider "*at least two of its distinct instants, or rather two of its parts that are*

distinct and the relations between them" [44,80,94]. Here, we reflect on the idea that a point-particle launched between two points in a Euclidean plane naturally seeks to continue moving in a straight line. This perspective is illustrated in the motion between points B and Z in the earlier-established *ETIS*. In Figure 1, it was observed that the causal effect of motion between the point-particles from points B and Z ensured that both particles followed a common straight line pathway. We affirm that Definition 4 and Lemma (1) offer reliable geometric frameworks for explaining concepts corresponding to physical situations in physics. The N^{1st} statement in physics involves rectilinear forms of uniform motions and motions influenced by external forces (non-rectilinear). Applying Descartes' perspective on motion to a point-particle, this section contends that Descartes' understanding is adequate to explain any motion executed by a point-particle in the *EITS*. Reducing circular motion to instantaneous limits of rectilinear motion aligns with geometric principles, given the understanding that a straight line connects any two points in a Euclidean plane [95]. This implies that the N^{1st} is always rectilinear from a Euclidean geometric viewpoint.

4.3.2 Formulating the N^{1st} from the N^{2nd}

As mentioned earlier, the N^{1st} and N^{3rd} are pivotal to the N^{2nd}, being constructible from it. The genetic form of the N^{2nd}, rooted in the concept of force, is not explicitly known but is experienced in a physical system. This genetic form is characterized by the effect of force in nature, devoid of a tangible sense of the force itself. At elementary levels, the N^{2nd} can be expressed mathematically as follows.

$$F = ma \tag{8}$$

Equation (8) can be broken down to the N^{1st} statement as follows.

$$F = m\left(\frac{v-u}{t}\right) \Rightarrow Ft = mv - mu \tag{9}$$

Where;

$v = final\ motion\ velocity,$
$u = initial\ motion\ velocity,$
$m = mass\ of\ the\ point - particle,$ and the Ft leads to the experience of a force due to the point-particle, through a time event.

We can construct two perspectives of the N^{1st} from Equation (9).

a. When $F = 0$, and $u = 0$, then $v = 0$, implying that an object (the point-particle in this case) will remain at rest unless a force acts on it.
b. When $F = 0$, then $v = u$, and this is a statement of a fraction of the N^{1st} that in the absence of external forces, an object (say the point-particle) will continue moving with the same velocity.

The N^{1st} is subject to force based on the N^{2nd}. Comparing both perspectives to the geometric algorithm in Lemma (1), if the basepoints are the same ($A \cong O$), no construction is possible, as at least two distinct basepoints are needed to initiate the construction. This aligns with the understanding that, in reality, a point-particle cannot exist without a Euclidean space, and similarly, it cannot execute motion in a Euclidean plane without energy or a force driving it. Thus, perspective (a) constitutes an element of the construct of rectilinear motion as outlined in Lemma (1). Conversely, when objects are launched from a common point under the rigor of uniform motion and devoid of external forces, they will consistently follow the same path throughout. This idea aligns with the notion established in Lemma (1), indicating that all straight lines constructed through points O and A are parallel and identical geometrically. The proof of Lemma (1) offers comprehensive conditions reflecting situations in the N^{1st} perspective. Perspective (b) becomes clearer when considering a point-particle moving with uniform instantaneous velocities in a thermodynamic system. Here, the geometric consideration is that instantaneous velocities can be defined as geometric magnitudes, equidistant from two distinct basepoints. Furthermore, the scientific and geometric significance, denoting a non-zero driving force ($F \neq 0$) for the point-particle, operating with two distinct instantaneous geometric magnitudes (velocities in this case) is demonstrated by Definition 10.

Example (Application of *Lemma 1*).

Consider a point-particle initially at rest on a frictionless surface. At time $t = 0$, a constant force F is applied to the point-particle in the positive $x - direction$. Using the geometric principles outlined in *Lemma 1*, determine the position of the point-particle at a given time t.

***Solution*. Establishing t as a geometric property.**

In the geometric framework provided by *Lemma 1*, time t can be established as a geometric property through a construction involving straightedge and compass operations. Considering the inherent properties of the geometric construction, we can ensure that t remains invariant throughout the analysis.

Physics interpretation.

Newton's second law states that the force F acting on an object is equal to its mass times its acceleration ($F = ma$). In this scenario, since the force F is constant, the acceleration a will also be constant. Using the kinematic equation $x = x_0 + v_0 t + \frac{1}{2}at^2$, where x_0 is the initial position, v_0 is the initial velocity, and t is the time, we can determine the position of the point-particle at any given time t.

Geometric interpretation.

Lemma 1 establishes the empirical identity property for addition of geometric points. This property ensures that for any point $A, A \oplus O$ is equal to A, where O is the origin. In this scenario, we can consider O as the initial position of the

point-particle, and A as its position after a certain time t. Therefore, the displacement of the point-particle ($A \oplus O$) is equal to its final position (A), which allows us to compute the final position based on the applied force and time elapsed.

Using the kinematic equation $x = x_0 + v_0 t + \frac{1}{2}at^2$, and given that the initial velocity ($v_0 = 0$) (since the point-particle starts from rest), we can compute the final position x of the point-particle at time t as follows.

$$x = x_0 + \frac{1}{2}at^2 \qquad \text{(E1.1)}$$

Since the force F is equal to ma, we have $a = \frac{F}{m}$. Therefore, the equation (E1.1) becomes;

$$x = x_0 + \frac{1}{2}\left(\frac{F}{m}\right)t^2 \qquad \text{(E1.2)}$$

E1.2 gives us the position of the point-particle at time t, based on the applied force F, the mass of the particle m, and the initial position x_0.

This solution provides an approach to solving a physics problem using the principles established in *Lemma 1*, integrating both physics and geometric interpretations to arrive at a solution.

4.4 Geometric scheme for N^{3st}

The N^{3rd} can be conceptualized through directionality notation, and its geometric interpretation aligns with the form defined in Definition 6.

Definition 6.

Given an arbitrary origin point O and two distinct points A and B in a Euclidean plane, we define the geometric operation $A \ominus B$ through; $A \ominus B \equiv A \oplus (-B)$.

Lemma (2) shows that the geometric operation $\ominus$ has the following cancellation property.

***Lemma* 2.**

Given a point A, the geometric operation $A \ominus B \cong O$ constructs the inverse of the point A with respect to the geometric operation $\oplus$.

1. If $A \cong O$, construct the point O. Otherwise, proceed through step (2).
2. Construct line L_1 passing the points O and A.
3. Construct circle C_1 of radius L_1 cantered at the point O.
4. Construct a point A', the intersection of the line L_1 and circle C_1.
5. Construct circle C_2 of radius L_1 cantered at the point A'.
6. Construct points C and D, the intersections of the line L_1 and circle C_2 according to Figure 5.

Proof for Lemma (2).

Utilizing the given construction algorithm, we assert the congruence $\overline{OA} \cong \overline{OA'} \cong \overline{A'D} \cong \overline{A'C} \cong L_1$. Consequently, by definition, the point O is geometrically equivalent to the point, D. Furthermore, circles C_1 and C_2 are congruent, implying that the straight line formed through points C and A' passes evenly through points O, D, and, A. Employing vector notation, the relationship $A = -A'$ holds, a consequence of the cancelation property. This property, interpretable geometrically as the equality in magnitude between OA and OA' (implying the geometric subtraction of the magnitude OA from itself), definitively establishes the cancelation property in an $ETIS$, thereby proving the law.

Remark 7.

In Euclidean geometry, the cancellation property applies exclusively to equal magnitudes of similar kinds.

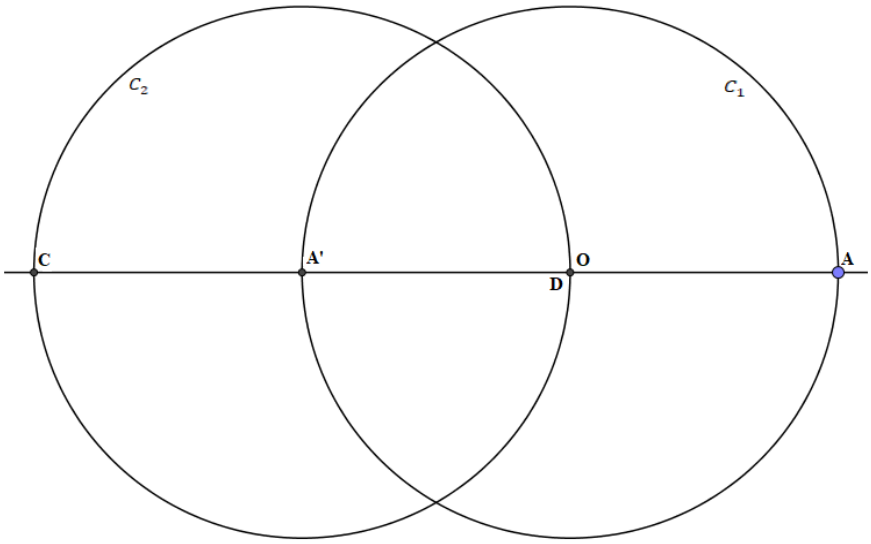

Figure 5. Geometric illustration of a cancelation property in a Euclidean Plane. (The figure illustrates the cancellation property in a Euclidean plane based on Lemma (**2**). Starting with a point ***A***, the construction proceeds through steps (1) to (5) to create points ***C*** and ***D***, highlighting the geometric operation $\ominus$, which constructs the inverse of the point ***A*** with respect to the geometric operation $\oplus$).

4.4.1 *Translation of Lemma (2) to its physics equivalence*

The physics concept of cancellation, rooted in equality between similar physical quantities, is applied in dimensions, dimensional analysis, forces, Newton's third law, and various other contexts. Although Euclidean geometry lacks a precise definition of equality, its contextual use aligns exactly with the concept of equality in physics. In the physical perspective, Newton's third law exhibits a cancellation feature expressed as $q_{1\_2} = -q_{2\_1}$ (Equation (12)). Thus, Lemma (2), besides being deductive, introduces a distinct aspect of cancellation, allowing the modeling of interactions between point-particles.

4.4.2 *Deriving the N^{3rd} from the N^{2nd}*

Consider two point-particles in a $ETIS$ interacting without the influence of external forces. We set the two point-particles q_1 and q_2 interacting in $ETIS$, with enough energy such that q_1 impacts q_2 by a force designated by q_{1_2}, and q_2 has a responsive equivalent force expressed as q_{2_1} that acts on q_1. The rate of change of momentum of $q_1 = \frac{dp_1}{dt}$ and the rate of change of momentum of $q_2 = \frac{dp_2}{dt}$.

Thus, according to N^{2nd},

$$q_{1\_2} = \frac{dp_2}{dt} \text{ and } q_{2\_1} = \frac{dp_1}{dt} \tag{10}$$

Adding the two in Equations (10) we obtain;

$$q_{1\_2} + q_{2\_1} = \left(\frac{dp_2}{dt} + \frac{dp_1}{dt}\right) = \frac{d(p_2+p_1)}{dt} \tag{11}$$

In the absence of external forces, interactions between point-particles with charges q_1 and q_2 result in uniform motion, yielding zero change in momentum.

It turns out from Equation (11) that $\frac{d(p_2+p_1)}{dt} = 0$, implying that $q_{1\_2} + q_{2\_1} = 0$.

Thus,

$$q_{1\_2} = -q_{2\_1} \tag{12}$$

Equation (12) is derived N^{3rd} from N^{2nd}.

Examining the impact of force on a body, Equation (12) takes on geometric significance in connection with point-particles, particularly within a force field or the $ETIS$. When considering the quantities q_{1_2} and q_{2_1} for point-particles in a Euclidean plane, their geometric equivalence points to relations among the points ; O, D, A and A'. This indicates that Equation (12) serves as a physical translation of Lemma (2). Consequently, N^{3rd} emerges as a fundamentally mathematical concept, supported by a robust geometric proof affirming the inherent validity of the law, even in the absence of experiments.

Remark 8.

Mathematical proofs in physics typically rely on assumptions within a physical system. However, the demonstration of the N^{1st} and the N^{3rd} reveals that proofs in physics need not always stem from assumptions within a physical setup. Instead, it has been established that proofs in physics can be inherently natural, where assumptions, whether from within or outside a described physical system, hold true regardless of experimental observations. The Euclidean geometric system provides a broad framework for constructing physics proofs by leveraging factual axioms inherent to the system.

Example (Application of Lemma 2).

Consider two point-particles, q_1 and q_2, with charges of $+2C$ and $-2C$ respectively, interacting in an isolated system. Use *Lemma 2* to determine the magnitude and direction of the force exerted by q_1 on q_2 and vice versa.

Solution.

Lemma 2 demonstrates the cancellation property of the geometric operation $\ominus$, which constructs the inverse of a point with respect to another point. In this scenario, $A \ominus B$ constructs the inverse of point A with respect to the geometric operation $\oplus$.

Given data

- Charge of $q_1 = +2\text{C}$
- Charge of $q_2 = -2\text{C}$

The cancellation property (A geometric scheme).

Lemma 2 establishes that $A \ominus B$ constructs the inverse of point A with respect to the operation $\oplus$. This property applies to the interaction between point-particles in a Euclidean plane.

Contextual proof for Lemma 2.

Utilizing the construction algorithm outlined in *Lemma 2*, we can demonstrate the cancellation property geometrically. By following the steps outlined in the lemma, we can construct points C and D, showcasing the cancellation property of the geometric operation $\ominus$.

Physics equivalence.

In the physics context, the cancellation property of *Lemma 2* applies to the equal and opposite nature of forces between interacting point-particles. The force exerted by q_1 on q_2 ($F_{1\to2}$) is equal in magnitude and opposite in direction to the force exerted by q_2 on q_1 ($F_{2\to1}$).

Magnitude of force.

By applying *Lemma 2*, the force exerted by q_1 on q_2 ($F_{1\to2}$) is equal in magnitude to the force exerted by q_2 on q_1 ($F_{2\to1}$). Thus, the magnitude of ($F_{1\to2}$) is equal to the magnitude of ($F_{2\to1}$).

Direction of force.

Since q_1 has a positive charge and q_2 has a negative charge, the force exerted by q_1 on q_2 is attractive, directed towards q_2. Similarly, the force exerted by q_2 on q_1 is attractive, directed towards q_1.

Using *Lemma 2*, this example has determined that the forces exerted by q_1 and q_2 on each other are equal in magnitude and opposite in direction, consistent with the principles of Newton's third law. Further, the example illustrates how geometric principles can be applied to understand the interactions between point-particles in a physics context.

5 The main result-proving the law of energy conservation

This section provides a methodical proof of the Law of Energy Conservation (LEC) through two approaches; classical version and its geometric equivalent.

5.1 Proof of the Work-Energy theorem (A classical perspective on the LEC)

This section dives into the Work-Energy Theorem, offering a physical perspective on the Law of Energy Conservation (LEC). It acknowledges the complexity of energy, recognizing both directional and chaotic forms [96]. Examples include organized kinetic energies like mechanical motion and electrical current, contrasted with the chaotic thermal energy of atomic and molecular motion [96]. The paper emphasizes that system energy can be defined based on position within various force fields, such as elastic potential energy, gravitational potential energy, or electromagnetic field energy. It highlights the vast spectrum of energy forms, suggesting even more might be discovered. Here, the focus is not on absolute energy levels but rather on energy changes during a process, from an initial state (i) to a final state (f). Therefore, zero-point references for different energy forms are irrelevant and often chosen arbitrarily for convenience. The section then provides basic correlations for energy changes in common forms including: kinetic energy $E_k = KE$ as function of system velocity (v); spring elastic potential energy E_{ps} as function of spring deformation displacement (x); gravitational potential energy $E_{pg} = PE_g$ as function of gravitational elevation (z); and sensible thermal energy $E_u = U$ as function of system temperature (T). According to the LEC, the different forms of energy can be transformed from one form to the other. This energy transformation hypothesis due to the LEC is briefly addressed in a later section of the proof.

5.1.1 Classical formulation of the LEC

Typically, all matter is energy-driven (energy is a characteristic property of matter) [97,98]. Thus going back to the earlier formulation, we adopt the notion of matter for energy by considering an acting system (A) that accelerates a responding system (R) with average force F_A along displacement d_{AR} during mater interaction.

We set,

$W_{F_A} = \int_0^{d_{AR}} F_A ds = \int_0^{d_{AR}} \left(m\frac{dV_R}{dt}\right) ds = \int_0^{d_{AR}} \left\{m\frac{dV_R}{ds}\left(\frac{ds}{dt}\right)\right\} ds = \int_{V_{R_1}}^{V_{R_2}} mV_R dV_R.$ This leads to Equation (13).

$$W_{F_A} = \frac{1}{2}m\{V_{R_2}^2 - V_{R_1}^2\} \quad (13)$$

If we let the quantities $\frac{1}{2}mV_{R_2}^2$ and $\frac{1}{2}mV_{R_1}^2$ be the system kinetic energies expressed as $\frac{1}{2}mV_{R_2}^2 = E_{R_2}$ and $\frac{1}{2}mV_{R_1}^2 = E_{R_1}$ respectively, then Equation (13) is expressible as:

$$W_{F_A} = E_{R_2} - E_{R_1} = \Delta E_R \quad (14)$$

Equation (14) proves the work-energy theorem.

At the same time, the acting system (A) will decelerate under the equilibrium reaction force of

system (R), $F_R = -F_A$, along the same displacement, d_{AR}. Therefore we set;

$W_{F_R} = \int_0^{d_{AR}} F_R ds = \int_0^{d_{AR}} \left(m\frac{dV_A}{dt}\right) ds = \int_0^{d_{AR}} \left\{m\frac{dV_A}{ds}\left(\frac{ds}{dt}\right)\right\} ds = \int_{V_{A_1}}^{V_{A_2}} mV_A dV_A$, leading to Equation (15).

$$W_{F_R} = \frac{1}{2}m\{V_{A_2}^2 - V_{A_1}^2\} \quad (15)$$

If we let the quantities $\frac{1}{2}mV_{A_2}^2$ and $\frac{1}{2}mV_{A_1}^2$ be the system kinetic energies expressed as $\frac{1}{2}mV_{A_2}^2 = E_{A_2}$ and $\frac{1}{2}mV_{A_1}^2 = E_{A_1}$ respectively, then Equation (15) is expressible as:

$$W_{F_R} = E_{A_2} - E_{A_1} = \Delta E_A \quad (16)$$

$$\int_0^{d_{AR}} (F_R) ds = \int_0^{d_{AR}} (-F_A) ds = -\Delta E_R \quad (17)$$

In classical physics, the above correlation is known as the "work-energy principle" [99]. We extend the work-energy principle to include work of gravitational force and gravitational potential energy as well as elastic spring force and potential elastic spring energy.

$W_{F_A} = \int_0^{d_{AR}} (F_A) ds = \int_{s_1}^{s_2} (Ks) ds = (PE_{R2} - PE_{R1}) = (E_{R2} - E_{R1}) = \Delta E_R$, leading to Equation (18).

$$W_{F_A} = \int_0^{d_{AR}} (-F_R) ds = (KE_{A2} - KE_{A1}) = (E_{A2} - E_{A1}) = -\Delta E_A \quad (18)$$

Therefore, during an interaction between two material particles or systems, the acting system energy will be reduced and transferred in the same amount to the resisting system so that the totality of energy of the two interacting systems is unchanged. It then follows that;

$\Delta E_A = -\Delta E_R$, implying Equation (19).

$$E_{A2} - E_{A1} = -(E_{R2} - E_{R1}) \Longrightarrow (E_{A2} + E_{R2}) = (E_{R1} + E_{A1}) = Constant. \quad (19)$$

Relation (19) is expressible in the form of Equation (20) which puts together; potential energy (being converted to kinetic energy of the falling body), and the total mechanical energy (sum of kinetic and potential mechanical energies) in a free fall configuration. Similarly, the mechanical energy is also conserved if a mass freely vibrates on an ideally elastic spring (generally, in simple harmonic trajectories) in the absence of dissipative effects. In general, for work of conservative forces only, the mechanical energy, E_{mech}, for N isolated systems, is conserved since there is no dissipative conversion in thermal energy and thus no heat transfer.

$$E_{mech} = E_K + E_{Pg} + E_{Ps} = \sum_{i=1}^{N} \left(\frac{1}{2}mv^2 + mgz + kx\right)_i = constant. \quad (20)$$

Equation (20) offers a generic algebraic expression for interpreting empirical observations due to the energy conservation principle. In regard to Definition 3 and Definition 5, Equation (20) projects a misconstruction of what an isolated thermodynamics system is. It projects a thermodynamics isolated system as that which corresponds to Definition 1 thus contradicting proposition (1). For consistency throughout the workflow, we restate in the summation operator index (N); $\left(\sum_{i=1}^{N} \left(\frac{1}{2}mv^2 \oplus mgz \oplus kx\right)_i\right)$ such that N corresponds to the number of point-particles considered from a system of interacting point-particles in an TIS, rather than having $TISs$ interacting with each other. This view is based on the consideration that the existence of multiple TIS suggests the existence of distinct multiple universes, contradicting the earlier clarified geometric characteristic $ETIS$ (Definition 3).

5.2 Establishing geometric principles of the LEC

While there's no single, universally accepted genetic proof for the Law of Energy Conservation (LEC), existing mathematical expressions rely on the general theory of motion for various energy forms [1,99,100]. This section offers a different approach; a natural, observation-independent proof based on geometric principles. The proof translates physical relationships derived from the theory of object motion under applied forces into a geometric framework. It leverages established Euclidean geometric proofs and translates them into Cartesian geometric operations that align with our understanding of object geometries in physics. This approach draws upon René Descartes' work (La Géométrie, 1637) [36], which laid the foundation for Cartesian geometry with its practical applications. Descartes' method demonstrates how arithmetic operations can be constructed geometrically using basic tools like a straightedge and compass. Notably, his work not only solves abstract algebraic equations but also geometric problems translated into algebraic form. The geometric-arithmetic operations of G_m and G_d are well founded in the Descartes' scheme. For instance, the G_m of two magnitudes can have two characteristic similar operations; a) taking the two magnitudes as straight-line segments (l_1 and l_2), the operation $l_1 G_m l_2$ corresponds to constructing the l_1 at l_2 times. b) Taking l_1 and l_2 as side lengths of a quantrilateral (say rectangle) then the geometric operation $l_1 G_m l_2$ corresponds to constructing a region bound between the two straight lines. On the other hand, the G_d operation involves practices such as the geometric bisection of a geometric magnitude, or the $n - sectioning$ of a given magnitude (very often G_d operates as the inverse of G_m). The succeeding sections concerns operations based on the G_m of geometric magnitudes, as the G_d is considered a straightforward exercise whenever desired (to the focus of this paper).

5.2.1 Scaling points in the Euclidean plane

We start by defining a way of scaling points in the Euclidean plane with respect to a basepoint, O, by whole number multiples.

Definition 7 (Scaling a point by a whole number multiple with respect to a basepoint).

Given a basepoint O, $n \in \mathbb{N}$, and a point A, we define the n_{th} multiple of A with respect to O, denoted $n \odot A$, inductively by;

i. $n \odot A \equiv O$.
ii. For $n > 0$, $n \odot A \equiv \big((n-1) \odot A\big) \oplus A$.

Within the Euclidean system, the base operation (i) implies that the basepoint O and the point A are exactly the same in a Euclidean plane, and thus, no motion can be experienced. Similarly, the arithmetic operation shows that a sequence of construction cannot be started, as every Euclidean geometric construction stems from two distinct points basepoints. Recursive operation (ii) offers a valid Euclidean geometric statement in that it strictly considers only the positive integers as the rational multiples. Combining these operations conceives a geometric practical extension of the $\odot$ operation to rational numbers. Genetically, the operations provide a piece of significant geometric machinery for interpreting Equation (20).

Definition 8 (Geometric multiplication of a pair of equidistant points A and B relative to a pair of equidistant distinct basepoints O and U).

We define the geometric multiplication of a pair of equidistant points A and B with respect to a pair of equidistant distinct basepoints $\{O, U\}$, denoted as $A \otimes B$ via the following construction beginning from $\{O, U, A, B\}$.

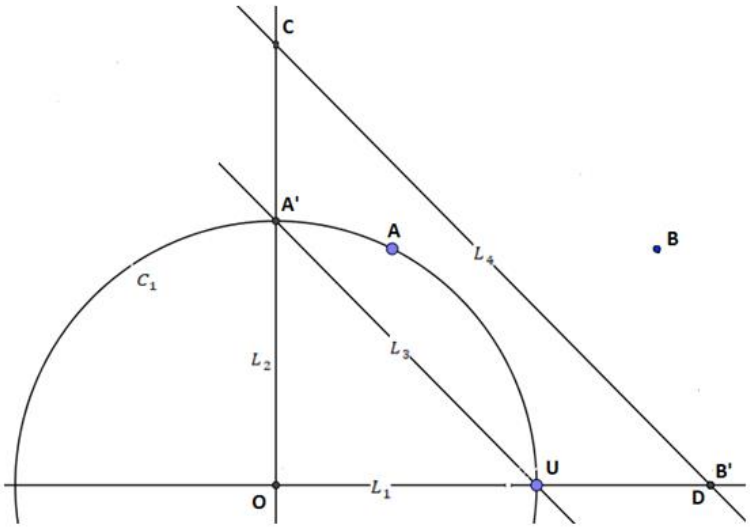

Figure 6. Geometric multiplication of similar points in a Euclidean plane

1. If $U \cong O$, construct the point O. Otherwise, proceed to step (2).
2. Construct line L_1 through the points O and U.
3. Construct line L_2 perpendicular to L_1 through point O.
4. Construct circle C_1 centered at O though point A.
5. Let A' denote the intersection of C_1 and L_2.
6. Construct line L_3 passing through the points A' and U.
7. Construct the point B', a geometric rotation of the point B onto $\overline{OU}$ (see appendix 2).
8. Construct line L_4 parallel to line L_3, through the point B'.
9. Construct the point C, the intersection of L_2 and L_4.
10. Construct the point D, a geometric rotation of the point C onto $\overline{OU}$ (see appendix 2).

Proof.

Definition 8 provides a geometric configuration corresponding to the scheme; $\overline{OA} \cong \overline{UB} \cong \overline{OU} \cong \overline{AB}$, since the point, D is a geometric rotation of the point C (see appendix 2). This is quite a unique feature that can be directly interpreted from algebra as characterizing any quadrilateral. We can deduce from Figure 6 that the point D is the geometric "*product point*" and the magnitude $\overline{OD}$ is the geometric "*product*". To complete the proof, we set through the construction; that the point $A = A'$ implying that $D = U = B'$. Since $U \ncong O$, the focus is to show that $D = U = B'$. By definition, $L_4 \parallel L_3$ and following claim 1 (which proves lemma (1)) it has been shown that for two similar and equal-parallel lines through two distinct points in a Euclidean plane, all their points defining the two parallel lines are geometrically the same.

Translation and the physical interpretation of Definition 8.

Proceeding from Equation (20), this section asserts and shows that Definition 8 has an important physical relation in physics. We consider the i^{th} point-particle given a system of point-particles in the $ETIS$. We let the i^{th} point-particle be energy driven such that it executes motion useful in describing the energy terms of the form projected in Equation (21). Therefore, characteristically, the i^{th} point-particle possess kinetic energy expressible as $\frac{1}{2}mv^2$, gravitational potential energy expressed by mgz, and, in a spring system, the i^{th} point-particle becomes an element of the spring experiencing motion leading to the energy term kx.

$$E_{mech} = \sum_{i=1}^{N} \left(\frac{1}{2}mv^2 + mgz + kx\right)_i = constant \qquad (21)$$

To reduce Equation (21), we make two assumptions; a) in distinct field settings, the mass of the i^{th} point-particle remains constant, and so we set m, g, and k as non-geometric constants (scalars). b) The three constants m, g, and k only correspond to positive real number integers (let these constants be the scaling multiples for the inherent geometric operations). The deduction reduces Equation (21) for the i^{th} point-particle, to its geometric equivalence in Equation (22).

$$E_{mech} = \sum_{i=1}^{N} \left(\frac{1}{2}v^2 \oplus z \oplus x\right)_i = constant \qquad (22)$$

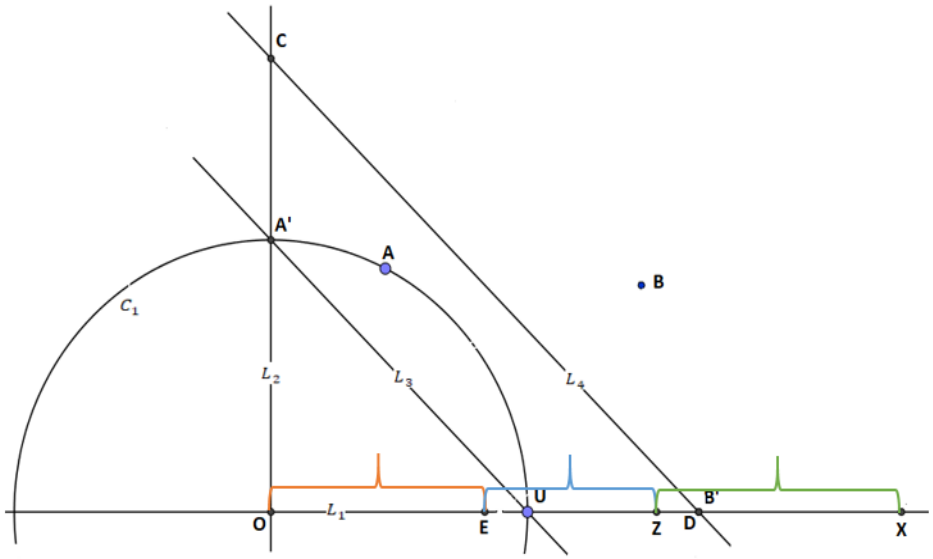

Figure 7. Geometric proof of the ***LEC*** in a ***ETIS*** for the i^{th} point-particle

The quantities v^2, z, and x have a significant geometric essence. Considerably, the quantity v^2 corresponds to a G_m operation on two equal and similar magnitudes expressible as $v \otimes v$. In regard to the aim of this proof, we will consider the quantity v for a straight line segment between two distinct points, in a Euclidean plane. Following this perspective, we apply the G_d operation (corresponding to straightedge and compass sectioning of a straight line) to scale down the geometric operation $(v \otimes v)$ to $\frac{1}{2}(v \otimes v)$. We then consider the quantities z and k as straight line segments geometrically put together with the magnitude $\frac{1}{2}(v \otimes v)$ through the following straightedge and compass algorithm.

1. If $U \cong O$, construct the point O. Otherwise, proceed to step (2).
2. Construct line L_1 through the points O and U.
3. Construct line L_2 perpendicular to L_1 through point O.
4. Construct circle C_1 centered at the point O though point A.
5. Let the point A' denote the intersection of C_1 and L_2.
6. Construct line L_3 passing through the points A' and U.
7. Construct the point B', a geometric rotation of the point B onto $\overline{OU}$ (see appendix 2).
8. Construct line L_4 parallel to line L_3, through the point B'.
9. Construct the point C, the intersection of L_2 and L_4.
10. Construct the point D, a geometric rotation of the point C onto $\overline{OU}$ (see appendix 2).
11. Construct the point E, the bisection pint of $\overline{OD}$.
12. Construct the circle C_2 centered at the point E and radius $\overline{OZ}$, to the side of point E.
13. Let the point Z denote the intersection of C_2 and L_1.
14. Construct the circle C_3 centered at the point Z and radius $\overline{OX}$, to the side of point Z.
15. Let the point X denote the intersection of C_3 and L_1.

The circles C_2 and C_3 can be stifled after obtaining the magnitudes $\overline{EZ}$ and $\overline{ZX}$, according to Figure 7.

Proof. Following Definition 8, $\overline{OD} = (v \otimes v)$ (proven). Therefore by definition, $\overline{OE} = \frac{1}{2}(v \otimes v)$. Further, given a Euclidean plane, a straight line segment can always be extended using straightedge-compass constructions [43]. Thus, it is geometrically possible to put together the three magnitudes $\overline{OE}$, $\overline{EZ}$ and $\overline{ZX}$ such that;

$(\overline{OE} \oplus \overline{EZ} \oplus \overline{ZX}) \cong \overline{OX}$. Therefore, the LEC (Equations (20, 21, and 22)) is proven. (23)

Equation (23) is inherently geometric, and its evaluation reflects the fundamental principles of Euclidean constructions. Throughout the paper, we have assumed that every Euclidean operation requires two distinct points. If points coincide, the operation becomes undefined. This concept translates directly to the energy equation's segments, which represent geometric magnitudes. The magnitude $\overline{OE}$ is the kinetic energy term which implies that the i^{th} point-particle must execute motion between two distinct points in

a Euclidean space. Otherwise, the kinetic energy term does not exist. The magnitude $\overline{EZ}$ defines the gravitational potential energy due to the motion of the i^{th} point-particle from some height above the Euclidean plane (virtually in reference to the earth's surface). So similarly, the magnitude $\overline{EZ}$ is only constructible between two distinct points. Lastly, the magnitude $\overline{ZX}$ corresponds to the energy possessed by an element of a spring (the i^{th} point-particle) in motion due to a spring extended between two distinct points. Practically (this is not part of the proof but an illustration), taking $U \cong O$ results to $\overline{OE} \cong O$, hence validating the assumption that for a valid geometric construction corresponding to a physical relationship in a Euclidean space, $U \ncong O$. This proof demonstrates that the LEC can be derived logically from self-evident geometric principles within the Euclidean system, independent of experimental observations. The paper argues that considering the LEC "*unprovable*" is an oversight. Rather, it reflects a lack of exploration at the intersection of physics and geometry, where both inductive and deductive reasoning can be applied.

5.3 Exploring the possibility of breaking the law of energy conservation

This section introduces an unconventional perspective on the potential violation of the Law of Energy Conservation (LEC), focusing on phenomena within classical systems rather than the conventional development of a Perpetual Motion Machine (PMM). The approach theorizes a specific, practical model of an electrical short circuit as an example of an anomalous event capable of challenging traditional interpretations of energy conservation. Unlike models grounded in abstract notions or "nothingness", the proposed framework relies on physical quantities conceptualized as point particles. The primary objective is to illustrate how a transient event, such as a short circuit, can evolve into a steady-state system while maintaining coherence with geometric principles. The analysis redefines the perception of short circuits, which are traditionally considered transient phenomena characterized by significant energy dissipation as heat and governed by internal resistances and potential differences. Instead, this framework establishes a steady-state model for short circuits, using unconventional circuit representations. These models highlight the possibility of higher current magnitudes arising in steady-state conditions without adhering strictly to anomaly-free interpretations. The aim is to shift the discussion toward a structured and investigable domain where short circuits serve as critical cases for re-evaluating the scope of the LEC. Experimental validation of such steady-state behaviors is acknowledged as a significant challenge, requiring tools and methodologies that extend beyond the current scope of physics. While this paper limits itself to theoretical proofs and geometric modeling, ongoing research aims to develop experimental setups capable of measuring, analyzing, and applying electrical quantities such as current, voltage, and resistance during short circuit events. These efforts will be presented in separate publications to complement the theoretical framework outlined here. Section 2 identified the limitations of modern physics in addressing chaotic systems like short circuits, particularly in defining energy conservation under such conditions. The inability to provide absolute clarity on the LEC in these scenarios raises questions about whether the principle is universally applicable. This section explores those questions by examining the theoretical feasibility and underlying motivations for potential violations of the LEC. The discussion also aims to clarify misconceptions about the principle, often fueled by growing energy demands and a limited understanding of its boundaries. The notion of introducing a new element termed the "*Chaotic Magnitude*" into the governing equations of energy conservation (Equations 21 and 22) is proposed as a way to address these challenges. While not formally proven, this element is supported by physical principles and geometric axioms, offering a conceptual extension of the LEC. Figure 8 demonstrates the application of this concept in an electrical short circuit, emphasizing its potential to refine our understanding of energy conservation.

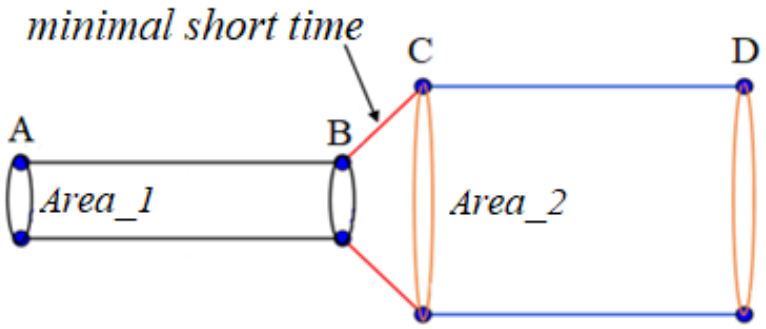

Figure 8. Geometric Interpretation of Electrical Short Circuit in Ordered and Chaotic States. (This figure illustrates the electric current flow within a conductor $\overline{\boldsymbol{AD}}$ in two distinct states: ordered and chaotic. The ordered flow is represented in section $\overline{\boldsymbol{AB}}$, while the chaotic short circuit is depicted in section $\overline{\boldsymbol{CD}}$. The region $\overline{\boldsymbol{BC}}$ marks the critical transition from ordered to chaotic current flow, identified as the "*minimal short time*", an interval during which the system undergoes a shift. The figure encapsulates the steady-state mode of the short circuit, challenging conventional models that assume zero resistance or voltage during such events. The diagram serves as a basis for understanding the short circuit as a dynamic phenomenon that can be explored for its potential in energy generation).

Figure 8 presents a detailed model of the electric current flow in two distinct scenarios within a conductor labeled $\overline{AD}$. The section $\overline{AB}$ of the conductor represents an ordered, regular flow of current, while the section $\overline{CD}$ corresponds to the chaotic state induced by the occurrence of a short circuit. The region $\overline{BC}$, positioned between $\overline{AD}$ and $\overline{CD}$, represents the transition from the ordered state to the chaotic flow. This region marks a critical point in the evolution of the short circuit and is referred to as the "*minimal short time*", an interval during which the system undergoes a shift from ordered to chaotic current flow. The conductor's stability is assumed to support both energy flows and a constant energy source, ensuring that no additional external power input interferences disrupt the constant chaotic flow through $\overline{CD}$. Short circuits, whether intentional or unintentional, are integral to various applications, including power protection system design and the determination of protective device capacities [101-104]. Unintentional short circuits frequently arise in power circuits, highlighting the practical relevance of understanding their dynamics. The transition from ordered to chaotic current flow, represented by $\overline{BC}$, is thus defined by the elemental magnitude of the "*minimal short time*", a key parameter for studying the phenomenon. Traditional models assume that the "*minimal short time*" is associated with negligible conductor resistance, often treated as zero in theoretical models. However, this assumption is rigorously challenged in this paper. Contrary to the assumption of zero resistance, the argument here is that electrical resistance cannot be zero during a short circuit. This insight is expanded upon in separate work that addresses experimental models for the "*minimal short time*" and explores the behavior of quantities such as current, voltage, and resistance during electrical short circuits. To derive a basic formulation for an electrical short circuit, the current expression from Ohm's Law is employed. Previous sections established that motion-energy processes occur strictly between distinct spatial points, prompting an inquiry into the practical and theoretical validity of applying Ohm's law in this context. Specifically, this exploration critically examines the claim that electrical resistance, denoted as R, can be zero for a given conductor. Through this investigation, the paper aims to demonstrate the potential benefits of utilizing electrical short circuits not merely as hazardous occurrences, but as mechanisms for energy generation, offering new insights into their practical applications. The electrical current formulation derived from Ohm's law is presented in Equation (24), providing the foundation for the subsequent analysis.

$$I = \frac{V}{R} \tag{24}$$

In the ideal form, Equation (24) implies that;

$$I = \frac{V}{0} = \infty \tag{25}$$

Equation (25) suggests the possibility of obtaining an infinite quantity from a finite physical relation(s). The subsequent discussion concerns objecting to this view. It also establishes an intelligible objection to the possibility of the mathematical relation for electrical resistance in a conductor as, $R = 0$.

The genetic definition of electrical resistance is presented in Equation (26):

$$R = \rho \frac{L}{A} \tag{26}$$

where ρ denotes the material resistivity, L represents the conductor length, and A is the cross-sectional area.

To critically examine the notion $R = 0$, two hypothetical experiential instances are proposed for analysis.

Premise 1 (When $\mathbf{L = 0 \Rightarrow A = 0}$).

We start by opening up the expression for A; $A = \pi r^2$. A has a geometrical property of the conductor and so we can relate L to r such that; when $L = 0$, $r = 0$ implying the existence of electrical conductors without cross-sectional areas in their geometries. This results to a typical mathematical string that gives the quite strange observation projected in Equation (27).

$$R = \rho \frac{0}{0} = \infty \tag{27}$$

Equation (27) illustrates that if the relations $L = r = 0$ possibly existed, then the conductor's electrical resistance would be infinitely ever large, and not zero. This is obscure enough since we cannot have infinitely large electrical resistance without the electrical conductor. However, the equation could have a simplified reinterpretation as; in the case of an open circuit, resistance tends to ∞ as it is assumed in the studies on electrical voltage and current using Norton-Thevenin relations [105,106]. Note that genetically, Equation (27) rightfully implies that the geometries of the conductor influence its electrical resistance, and this paper completely subscribes to this view.

Premise 2 (When either $\boldsymbol{\rho = 0}$).

Setting $\rho = 0$ in Equation (26) we end up with $R = 0$. This seems scientifically sensible. However, this paper asserts that the expression $R = 0$ offers quite an ambiguous physical relation and a highly refutable observation since ρ is a genetic property of the electrical conductor. Therefore, the $\rho = 0$ denotes an electrical conductor free of resistivity property or the material, and it is known that such a material cannot practically exist. Ensuing these deductions, it is judicious to opine conclusively that material resistance equals zero only when there is no conducting material or in the absence of voltage and current source (reasonably, because any power source will have some resistance as studied in the Norton-Thevenin concepts [106]).

Premises (1 and 2) categorically reject the possibility of the relation $R = 0$, both theoretically and practically. Therefore, asserting $R = 0$ reflects a fundamental misunderstanding of the nature of an electrical short circuit. Equations (24-27) demonstrate that Ohm's law imparts understandable geometrical properties to electrical

conductors, precluding the possibility of $R = 0$. In the following section, we will explore a condition of very low electrical resistance in a conductor, using this concept to illustrate the perpetual breach of the LEC in both physical and theoretical contexts.

5.4 A geometric projection to breaking the LEC

This section aims to establish a geometric perspective defining theoretical and physical models targeting the violation of the LEC. Within a population of point-particles, denoted as i^{th}, exemplified by the transition of electric charges from an ordered to chaotic state through a conductor, we designate two instantaneous velocities: v_o for ordered current flow and v_c for chaotic current flow. Throughout, we assume that during ordered current flow, point-particles move uniformly at an instantaneous velocity magnitude, v_o. Conversely, in the case of a short circuit (maintaining constant conductor geometries), we assume an increase in electric field strength between interacting point-particles, intensifying force interactions due to uniformly charged particles, resulting in stronger repulsive forces. We assume that an increase in repulsive force strengths corresponds to an increase in the strengths of electric fields, leading to an enhanced flow of the respective electric fields through the conductor. The velocity, v_c, of interacting point-particles increases with higher speeds of the interacting fields. The geometric projection of this phenomenon necessitates the use of instantaneous velocity magnitudes between the ordered and chaotic sections of the current flow process. We proceed by considering the velocity magnitudes for both v_o and v_c for the i^{th} point-particle through the ordered and chaotic sections of the flow, denoting them as geometric relations $\overline{OA}_o \cong v_o$ for the ordered velocity magnitude and $\overline{OB}_c \cong v_c$ for the chaotic velocity magnitude, both taken from a fixed point O. Once explicitly defined, the sub-scripts o and c on the magnitudes $\overline{OA}_o$ and $\overline{OB}_c$ will be omitted throughout the workflow. The geometric solutions will involve two schemes concerning the basepoints O and U in a Euclidean plane, as per Definition 10.

Definition 9 (Chaotic Magnitude).

Here, a Chaotic Magnitude is defined as a physical quantity that cannot be discerned using standard scales of physics. These magnitudes arise in anomalous processes and may encompass velocities, forces, or energies experienced by charged particles, such as those in an electrical short circuit.

Remark 9.

The defined chaotic velocity v_c serves as a illustrative instance of the mentioned chaotic magnitude.

Chaotic kinetic energy.

Definition 8 demonstrates the geometric squaring of ordered instantaneous velocities, denoted as v_o. In this section, the aim is to expand Equations (21) and (22) by introducing a corresponding instantaneous velocity, v_c, for chaotic flow. The quantities v_o and v_c will then be combined geometrically, employing operations bridging classical physics and relativity. Despite limited knowledge of chaos in classical physics, studies indicate its prevalence [96,107,108]. To establish chaotic kinetic energy on a Newtonian scale, this section initiates by illustrating that chaotic flows can occur within the framework of classical physics, dependent on the velocities of the moving bodies. Although the velocities driving chaotic bodies are not fully understood, we assume that the considered point-particles in chaotic flows move at speeds less than the speed of light.

Remark 10.

Significantly, for a body moving at a fraction of the speed of light, employing relativistic mechanics is sensible for calculating its kinetic energy. This enhanced kinetic energy, termed chaotic kinetic energy in this paper, results from such speeds. In the context of special relativity theory, modifications to the expression for linear momentum are introduced, with m representing the object's rest mass, v denoting its velocity, and c indicating the speed of light in a vacuum.

We then apply the expression for linear momentum;

$$p = m\gamma v \tag{28}$$

where the quantity $\gamma = \frac{1}{\sqrt{1-\frac{v^2}{c^2}}}$.

Applying the integration by parts we obtain;

$$E_k = \int v.dp = \int v.d(m\gamma v) = m\gamma v.v - \int m\gamma v.dv = m\gamma v^2 - \frac{m}{2}\int \gamma d(v^2) \tag{29}$$

Having previously defined the quantity $\gamma = \frac{1}{\sqrt{1-\frac{v^2}{c^2}}}$,

$$E_k = m\gamma v^2 - \frac{-mc^2}{2}\int \gamma d\left(1-\frac{v^2}{c^2}\right)$$

$$E_k = m\gamma v^2 + mc^2\left(1-\frac{v^2}{c^2}\right)^{1/2} - E_0 \tag{30}$$

And E_0 is a constant of integration for the indefinite integral.

Simplifying the expression Equation (30) reduces to;

$$E_k = m\gamma\left(v^2 + c^2\left(1-\frac{v^2}{c^2}\right)\right) - E_0$$

$$E_k = m\gamma(v^2 + c^2 - v^2) - E_0$$

$$E_k = m\gamma c^2 - E_0 \tag{31}$$

Where E_0 is found to obey $v = 0$, $\gamma = 1$, $E_k = 0$, resulting to;

$$E_0 = mc^2 \tag{32}$$

Proceeding from Equation (32), following this relation we have;

$$E_k = m\gamma c^2 - mc^2 = \frac{mc^2}{\sqrt{1-\frac{v^2}{c^2}}} - mc^2 = (\gamma - 1)mc^2 \quad (33)$$

Equation (33) illustrates that as speed approaches the speed of light, the work needed to accelerate an object from rest approaches infinity. The implication, discussed in detail in a separate article, leads us to assume that no object can exceed the speed of light limits. This computation results in the mass-energy equivalence formula, asserting that a body at rest must possess energy content.

$$E_{rest} = E_0 = mc^2 \quad (34)$$

From a Newtonian perspective, the classical kinetic energy actually approximates the relativistic kinetic energy at low speeds ($v \ll c$). Therefore, we assume that this condition is observed in this intuitionistic-contextual deduction. We then employ use of the Taylor expansion on the first two terms or a binomial approximation to get the reciprocal square root, as follows;

$$E_k \approx mc^2\left(1 - \frac{1}{2}\frac{v^2}{c^2}\right)^{\frac{1}{2}} - mc^2 = \frac{1}{2}mv^2 \quad (35)$$

Equation (35) shows that the total energy E_k can be partitioned into the rest mass energy plus the Newtonian kinetic energy at low speeds. The energy expression $\frac{1}{2}mv^2$ resulting from the computation will be considered the chaotic kinetic energy expressed as $\frac{1}{2}mv_c^2$ through the proof.

Relationship between ordered and chaotic kinetic energies.

Here, we establish an abstract relationship between the stated chaotic velocity and the ordered velocity based on simple kinetic energy formulation. Kinetic energy is the energy of motion of a mass (so it is not always that a motion starts from a rest state). From physics understanding, velocity is the displacement covered by the body in motion, scaled by the time required to cover the displacement. Denoting the change in displacement as Δd and a change in time through the displacement as Δt, we can define average velocity according to Equation (36).

$$v_{av} = \frac{\Delta d}{\Delta t} \quad (36)$$

From Equation (36) we can then define average acceleration as follows;

$$a_{av} = \frac{\Delta v}{\Delta t} \quad (37)$$

We redefine Equation (8) to average force using Equation (37).

$$F_{av} = ma_{av} = m\left(\frac{\Delta v}{\Delta t}\right) \quad (38)$$

Thus in the time Δt the object is displaced some magnitude Δd. We recall the assumption that the motions throughout the paper are free of external forces, and consider the sort of motion in which the mass m moves in the direction of the force.

We then compute the work done in this situation as follows;

$$W = F_{av}\Delta d = m\left(\frac{\Delta v}{\Delta t}\right)\Delta d \quad (39)$$

We consider a motion situation that starts with some velocity v_b and ends with velocity v_a.

It then follows from Equation (39) that;

$$W = F_{av}\Delta d = m\left(\frac{v_a - v_b}{\Delta t}\right)\Delta d \quad (40)$$

By definition,

$$\Delta d = (v_{av} \times \Delta t) \Longrightarrow \Delta d = \frac{1}{2}(v_a + v_b)\Delta t \quad (41)$$

Using Equation (41) in Equation (40) we obtain;

$$W = F_{av}\Delta d = m\left(\frac{v_a - v_b}{\Delta t}\right)\left(\frac{1}{2}(v_a + v_b)\Delta t\right) \Longrightarrow W = \frac{1}{2}m(v_a - v_b)(v_a + v_b) \quad (42)$$

$$W = \frac{1}{2}m({v_a}^2 - {v_b}^2) \quad (43)$$

Equation (43) is a consequence of motion due to a body with sort of mass m that is moving at two distinct velocities.

Ordinarily, the quantity v_b is assumed to be zero ($v_b = 0$) and thus Equation (43) is reducible to the kinetic energy Equation in (44).

$$K_E = W = \frac{1}{2}m{v_a}^2 \Longrightarrow K_E = \frac{1}{2}m{v_a}^2 \quad (44)$$

However, following Figure 8, Equation (43) holds as ($v_b \neq 0$). So reasonably, Equation (43) can be related to the chaotic kinetic energy and rewritten to Equation (45).

$$E_k = \frac{1}{2}m({v_c}^2 - {v_0}^2) \quad (45)$$

Equation (45) puts together both the ordered and the chaotic velocities and the corresponding kinetic energies. The equation is geometrically established following proposition 2.

Proposition 2.

In a classical system involving both ordered and chaotic kinetic energy flows, the Law of Energy Conservation is violated when the chaotic kinetic energy exceeds the ordered kinetic energy according to the geometric formulation of chaotic and ordered velocities and their corresponding

kinetic energies. Specifically, when the geometric difference between the squares of chaotic and ordered velocity magnitudes is non-zero, energy is not conserved.

Proposition (2) will be proven following Definition 10.

Definition 10 (Geometric difference between the squares of chaotic and ordered magnitudes with respect to distinct basepoints O and U).

Consider the geometric product of a pair of distinct equidistant points A and B with respect to a pair of distinct basepoints $\{O, U\}$, and, a geometric product of a pair of distinct points E and F equidistant from and with respect the pair of distinct basepoints $\{O, U\}$, defined via the following construction algorithm beginning from $\{O, U, A, B\} \subseteq \{O, U, E, F\}$.

1. If $U \cong O$, construct the point O. Otherwise, proceed to step (2).
2. Construct line L_1 through the points O and U.
3. Construct line L_2 perpendicular to L_1 through the point O.
4. Construct circle C_1 centered at the point O though point A.
5. Let the point A' denote the intersection of C_1 and L_2.
6. Let the point N denote the intersection of C_1 and L_1.
7. Construct line L_3 passing through the points A' and U.
8. Construct the point B', a geometric rotation of the point B onto $\overline{OU}$ (see appendix 2).
9. Construct line L_4 parallel to line L_3, through point B'.
10. Construct the point C, at the intersection of L_2 and L_4.
11. Construct the point D, a geometric rotation of the point C onto $\overline{OU}$ (following appendix 2, let C_2 denote the rotation configuration).
12. Construct circle C_3 centered at the point U of radius $\overline{ND}$.
13. Let the point N' denote the intersection of C_3 and L_4, from the point C.
14. Construct circle C_4 centered at the point O though point E.
15. Construct the point E', the intersection of C_4 and L_2.
16. Construct line L_5 passing through the points E' and U.
17. Construct the point F', a geometric rotation of the point F onto $\overline{OU}$ on the side of point U (see appendix 2).
18. Construct line L_6 parallel to line L_5, through the point F'.
19. Construct the point G, the intersection of L_2 and L_6.
20. Construct the point H, a geometric rotation of the point G onto $\overline{OU}$ on the side of point U (following appendix 2, let the circle circumference C_5 denote the rotation configuration).
21. Construct circle C_6 centered at the point U of radius $\overline{E'G}$.
22. Let the point P' denote the intersection of C_6 and L_6, from the point G.

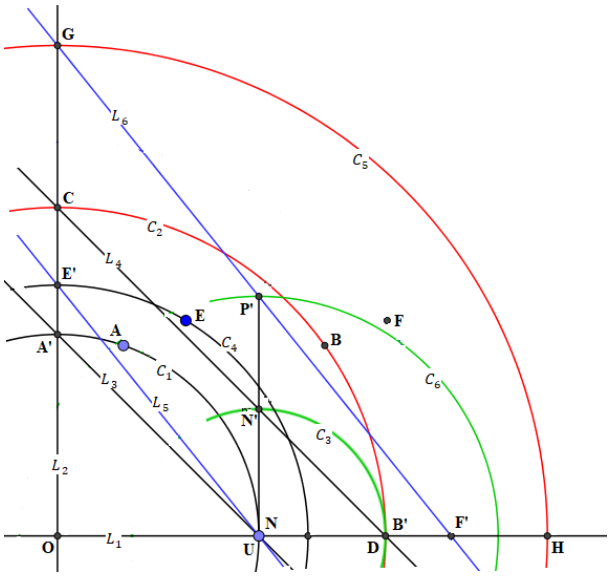

Figure 9. The Energy Conservation Revision Scheme

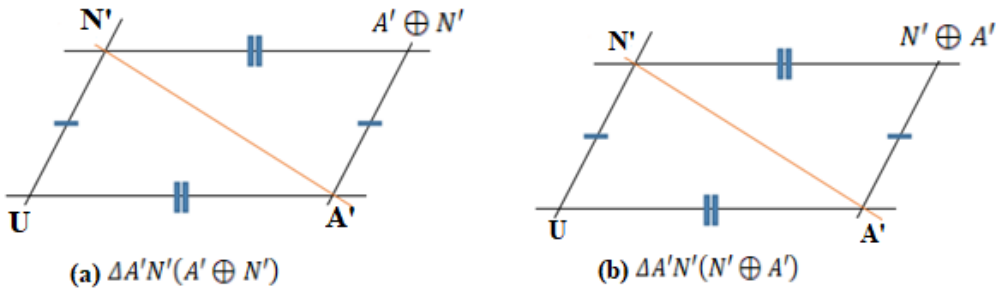

Figure 10. Geometric proof for Claim 2

Claim 2.

The circle C_3 intersects L_4 through point N', implying that the lines $\overline{UN'} \cong \overline{A'C}$ and, $\overline{UA'} \cong \overline{N'C}$.

Proof.

Considering the quadrilateral $UN'CA'U$ in Figure 9 we can extract Figure 10 according following deductions.

We set the point C corresponding to the point $N' \oplus A'$ in the diagram (a), Figure 10 and in a distinct view, we let the point C correspond to $A' \oplus N'$ according to diagram (b), Figure 10.

Starting with Figure 9, since $\overline{ND} \cong \overline{A'C}$ (corresponding to $\overline{UN'} \cong \overline{A'(A' \oplus N')}$ in the diagram (a) and $\overline{UN'} \cong \overline{A'(N' \oplus A')}$ in the diagram (b) of Figure 10), we deduce from Figure 10 that $\overline{UN'} \parallel \overline{A'(A' \oplus N')}$, $\overline{UA'} \parallel \overline{N'(A' \oplus N')}$ for diagram (a). Similarly, $\overline{UN'} \parallel \overline{A'(N' \oplus A')}$, $\overline{UA'} \parallel \overline{N'(N' \oplus A')}$ for diagram (b). The geometric consequence of these deductions is congruence expressed as $\Delta A'N'(A' \oplus N') \cong \Delta A'N'(N' \oplus A')$. The two congruent triangles $\Delta A'N'(A' \oplus N')$ and $\Delta A'N'(N' \oplus A')$ share two points (A' and N') such that the third points lie on the side of $\overline{A'N'}$. It can be shown through the following deductions that the thirds points are equidistance from $\overline{A'N'}$.

Starting with $\Delta A'UN'$, we set the angles;

$$\angle UA'N' = \alpha \text{ and } \angle UN'A' = \theta \tag{46}$$

It then follows that

$$\angle A'UN' = \pi - (\alpha + \theta)$$
(Angles sum in a triangle) (47)

We now focus on $\Delta A'N'(A' \oplus N')$, in the diagram (a) of Figure 10.

The $\angle N'A'(A' \oplus N') = \theta$, and the $\angle A'N'(A' \oplus N') = \alpha$
(alternate angles to $\angle UN'A'$ and $\angle UA'N'$ respectively). (48)

Therefore,
$$\angle A'(A' \oplus N')N' = \pi - (\alpha + \theta),$$
(Angles sum in a triangle) (49)

Next, we consider $\Delta A'N'(N' \oplus A')$ in diagram (b) of Figure 10.

$\angle N'A'(N' \oplus A') = \theta$ and the $\angle A'N'(N' \oplus A') = \alpha$
(alternate angles to $\angle OBA$ and $\angle OAB$ respectively). (50)

Therefore,
$$\angle A'(N' \oplus A')N' = \pi - (\alpha + \theta),$$
(Angles sum in a triangle) (51)

Since,
$\angle A'(A' \oplus N')N' = \angle A'(N' \oplus A')N'$, $\overline{UN'} \parallel \overline{A'(A' \oplus N')}$ and $\overline{UN'} \parallel \overline{A'(N' \oplus A')}$, implying that;

$$\overline{UN'} = \overline{A'(A' \oplus N')}. \tag{52}$$

A very significant consequence of statement (52) is that; in allusion to Figure 9, the equation leads to a rigorous Euclidean geometric fact based on the theory of similar triangles. Comparing $\Delta COB'$ and $\Delta N'UB'$, it is geometrically reasonable to assert that $\frac{OC}{UN'} \cong \frac{OB'}{UB'}$, implying that $\Delta COB' \cong \Delta N'UB'$ (due to a similarity property on SAS). Similarly, by the provided construction, the proof for claim 2 is inductively equally deducible for the quadrilateral $GE'UP'G$. Hence Definition 10 is proven. The analytical benefits of Definition 10 are elaborated in the following section.

6 Discussion

The proof for Definition 10 concludes the intended perspective on the LEC within the paper's scope. However, the bisection of product lines $\overline{OD}$ and $\overline{OH}$ is not explicitly addressed in the proof. The primary objective was to demonstrate the derivation of the difference between the squares of the magnitudes v_c and v_o. It is asserted inductively that bisecting the product lines $\overline{OD}$ and $\overline{OH}$ yields bisection points that exhibit behavior analogous to points D and H in the experimental framework for both v_c and v_o, given that $\overline{OD} \subseteq \overline{OH}$. There is no inconsistency in performing these bisection operations to establish a relationship akin to the projection in Equation (23). Consequently, Equation (23) can be reformulated as follows: Let E denote the bisection point of the product $\overline{OD}$, and let J represent the bisection point of the product $\overline{OH}$. This allows rewriting Equation (23),

$(\overline{OE} \oplus \overline{EZ} \oplus \overline{ZX}) \cong \overline{OX})$ as; $([\overline{OJ} - \overline{OE}] \oplus \overline{EZ} \oplus \overline{ZX}) \cong \overline{OX})$. In the context of the electrical short circuit example applied to electrical energy models, the difference $([\overline{OJ} - \overline{OE}])$ is anticipated to consistently result in a positive magnitude. The methodology for measuring electrical short circuit current based on a given circuit power input is addressed in a separate article that focuses on experimental investigations. Definition 10 provides both natural and experimental geometric interpretations of the relationship between the magnitudes $({v_c}^2 - {v_0}^2)$ in Equation (45), as outlined in Claim 2. This section focuses on expanding the established proofs for the Law of Energy Conservation (LEC) from two perspectives: the validity and limitations of the LEC statement and the potential for its practical violation. The geometric proof associated with Equation (45) suggests that energy-driven systems do not always initiate motion from rest or zero-velocity conditions. Equation (45) finds practical application in scenarios such as electrical short circuits, as illustrated in Figure 8, where the point particles under consideration exhibit distinct instantaneous velocities. The first phase of the proof for Definition 10 concerns the geometric multiplication of two distinct points (A and B), equidistant from given two distinct basepoints (O and U), to $\overline{OU}$. These operations can be translated to the geometric multiplication of two equal magnitudes so that we have the relations $\overline{OA} \cong v_o$ and $\overline{OB} \cong v_o$ geometrically put together such that $(\overline{OA} \otimes \overline{OB}) \cong {v_0}^2$ when the point-particle is executing discernible kind of motion (we name this kind of discernible motion the ordered motion and the associated quantities, ordered quantities (magnitudes) as mentioned earlier, for v_o). In this configuration, $\overline{OA} \cong \overline{AB} \cong \overline{BU} \cong \overline{OU}$. The second segment in the proof for Definition 10 involves the geometric multiplication of two distinct points (E and F) taken equidistant from the two distinct basepoints (O and U) such that $\overline{OH} \cong \overline{UF} \ncong \overline{OU}$, with no restrictions to the basepoints condition, provided $(\overline{OA} \cong \overline{AB} \cong \overline{BU} \cong \overline{OU}) \ncong (\overline{OH} \cong \overline{UF})$. Likewise, we translate the geometric relations $\overline{OH} \cong v_c$ and $\overline{OF} \cong v_c$ geometrically put together such that $(\overline{OH} \otimes \overline{UF}) \cong {v_c}^2$ when the point-particle is executing chaotic kind of motion (we name this kind of undiscernible motion the chaotic motion and the associated quantities, chaotic quantities as established, for v_c).

6.1 Geometric modification of Equation 21

Equation (21) necessitates the incorporation of a geometrically squared magnitude to account for the chaotic velocity of an electric charge. To explore how energy can be generated, a shift in the physical perspective of Equation (21) is required. Following the assumptions underlying Equation (22), the equation can be reduced to its geometric counterpart. Given the previously established geometric definitive condition, where $(\overline{OA} \cong \overline{AB} \cong \overline{BU} \cong \overline{OU}) \ncong (\overline{OH} \cong \overline{UF})$, the mechanical energy expression becomes:

$$E_{mech} = \sum_{i=1}^{N} \left(\left[\frac{1}{2} m {v_c}^2 - \frac{1}{2} m {v_o}^2 \right] + mgz + kx \right)_i \neq constant \quad (53)$$

Further refinements lead to the following geometric formulation:

$$E_{mech} = \sum_{i=1}^{N} \left(\left[\frac{1}{2} {v_c}^2 \ominus \frac{1}{2} {v_o}^2 \right] \oplus z \oplus x \right)_i \neq constant \quad (54)$$

Equations (53) and (54) indicate that under classical limits, the Law of Energy Conservation (LEC) has consistently been violated. Under the specified set construction condition $(\overline{OA} \cong \overline{AB} \cong \overline{BU} \cong \overline{OU}) \ncong (\overline{OH} \cong \overline{UF})$, it becomes evident that ${v_c}^2 > {v_o}^2$. This inequality suggests that a geometric subtraction in Equations (54) demonstrates that a system comprising both chaotic and ordered motions inherently results in an excess of a measurable quantity. To address this paradox, attention is directed to adjusting the position of point U in Figure 10 towards point O. Observations reveal that as point U approaches point O, the magnitude $({v_o}^2)$ diminishes while $({v_c}^2)$ increases significantly. Through Definitions (8) and (10), the geometric multiplication of distinct points, given two distinct base points on a plane, translates into the geometric multiplication of distinct magnitudes relative to a specific base point. Consequently, the geometric difference between the terms in the square brackets in Equations (53) and (54) corresponds to the geometric difference between two distinct product magnitudes, obtained as the geometric squares of two unique straight-line segments. Each magnitude's geometric square is definable as: $OA \otimes OB : OU \cong \left({}^{OA}/_{OU}\right) \otimes \left({}^{OB}/_{OU}\right)$. This result adheres to the principles of René Descartes' operation, as illustrated in Appendix 1. Throughout the paper, significant advancements have been achieved. The complete establishment of the LEC for a thermodynamics isolated system configuration in physics prompted an investigation into the meaning of a thermodynamics isolated system. The deductions revealed that the current understanding of a thermodynamics isolated system is scientifically flawed and vague. The notion of multiple isolated systems in the entire universe was identified as a serious scientific and mathematical misinterpretation. The paper proposed an alternative and definitive perspective on the thermodynamics isolated system, referred to as TIS (Definition 5), within a Euclidean plane. Geometrically, the established workflow operates within an interface named $ETIS$. Building on the TIS definition, the review refutes the false hypothesized multiverse concepts [109], particularly when considering the universe as a practical example of a TIS. It has been established that the Law of Energy Conservation (LEC) operates within defined classical bounds and has been consistently challenged in classical systems. The electrical short circuit, serving as an exemplary model transitioning from ordered to chaotic modes, provided a foundation for completing this proof. This was achieved through the introduction of chaotic magnitudes within the proposed steady-state mode in a classical system. However, it is important to emphasize that the short circuit concept was employed illustratively, as depicted in Figure 8. The exploration of short circuits as a potential means of energy generation remains a topic for a separate study. Equation

(54) fundamentally reinterprets Equation (22), indicating that the difference between the terms within the square brackets will always exceed the initial state of the system. Geometrically, when the construction is completed as mentioned previously, Equation (54) corresponds to the operation $([\overline{OJ} - \overline{OE}] \oplus \overline{EZ} \oplus \overline{ZX}) \cong \overline{OX}$), where the magnitude $\overline{OX}$ is large enough, in proportions to the difference due to the terms in the square braces. Thus, as it was desired, it is proven that the LEC can be broken in the ordinary physical settings. Considerably, processes go through in a particular direction and not the opposite. In the exposed workflow, directionality was observed following the rigor of Euclidean geometric constructions. This was in caution though, as direction is not constrained by the LEC. In thermodynamics, adherence to the first law (LEC) and second law is crucial for a process to occur [86,110]. Notably, this principle remains consistent across the established proofs. The presented proof for the Law of Energy Conservation (LEC) proposes a novel approach, challenging the traditional reliance on the impossibility of perpetual motion. Instead, it asserts that the LEC can be derived from the fundamental principle that 'something cannot originate from nothing', particularly when the two entities are inherently similar. This paper paves the way for a more philosophical exploration of the LEC, moving beyond purely physical considerations.

Remark 11 (energy generation perspective).

In the context of this paper, we consider "*creating energy*" as establishing a scheme that defines a higher energy output given some energy input to a system, without external interferences to the specific processes. Consider Theorem 2.

Theorem 2 (Violation of the law of energy conservation in chaotic-ordered systems).

Let v_o represent the ordered velocity magnitude and v_c represent the chaotic velocity magnitude of point-particles in a classical system. If the chaotic velocity exceeds the ordered velocity, i.e., $v_c > v_o$, then the system breaks the Law of Energy Conservation according to Equation (45).

Geometric setup (Elaborated proof).

Consider the instantaneous velocity magnitudes v_o for ordered flow and v_c for chaotic flow in a classical system. Let O and U be distinct basepoints from which we measure these velocities geometrically.

- Let the ordered velocity be represented geometrically by the line segment OA_o.
- Let the chaotic velocity be represented geometrically by the line segment OB_c.

Energy Relationship.

The kinetic energy corresponding to each flow state (ordered and chaotic) is given in Equation (45) can be broken as follows:

Ordered kinetic energy. $KE_E^{(o)} = \frac{1}{2}m{v_o}^2$

Chaotic kinetic energy. $KE_E^{(c)} = \frac{1}{2}m{v_c}^2$

Conditions for energy violation.

The Law of Energy Conservation is broken under the following conditions.

- In a conserved energy system, the kinetic energy cannot simultaneously exist in both chaotic and ordered states.
- Velocity Condition. Violation of the Law of Energy Conservation occurs if $v_c \neq v_o$. Implying that the geometric difference between the squared chaotic and ordered velocities must be positive.
- Geometric Difference and Kinetic Energy Imbalance. In particular, if $v_c > v_o$, the chaotic kinetic energy $KE_E^{(c)}$ exceeds the ordered kinetic energy $KE_E^{(o)}$ implying that $E_k = \frac{1}{2}m({v_c}^2 - {v_0}^2) > 0$.
- Absence of External Input. No external energy is introduced to account for the increase in chaotic kinetic energy.

Geometric justification.

According to Definition 10, the geometric difference between chaotic and ordered magnitudes with respect to basepoints O and U is non-zero when $v_c \neq v_o$. This geometric non-equivalence directly translates to an energetic non-equivalence.

Implication for energy conservation.

If $v_c > v_o$, the difference ${v_c}^2 - {v_0}^2$ is positive, and thus the chaotic kinetic energy exceeds the ordered kinetic energy. In classical physics, this extra kinetic energy does not originate from any discernible source, thus implying a violation of the Law of Energy Conservation. The system has more energy in the chaotic state than it had in the ordered state, with no external input.

Therefore, under the assumption that $v_c > v_o$, the system violates the Law of Energy Conservation, according to Definition 10. The difference in kinetic energies breaks the standard conservation rule, thus establishing the theorem.

6.2 A significance of the provable review

This paper fundamentally redefines the geometric framework underpinning the Law of Energy Conservation (LEC) by introducing and rigorously establishing chaotic magnitudes within a Euclidean plane. Central to this exploration is the geometric proof tied to Equation (45), which conclusively demonstrates that energy systems can deviate from traditional assumptions of initiation from rest or zero velocity. This insight highlights the innovative realization that classical physical settings can indeed exhibit violations of the LEC under specific configurations. The geometric proofs presented herein emphasize the critical relationship between chaotic and ordered motions, offering a novel lens for understanding energy interactions in both theoretical and practical domains. The established chaotic magnitude plays a pivotal role in extending the expressibility of the LEC. Firstly, it provides a robust framework for addressing discrepancies between traditional and modern interpretations of mechanical energy. Secondly, it

establishes a geometric foundation for analyzing transitions between ordered and chaotic systems, particularly in scenarios like electrical short circuits. Finally, it enables the formulation of new mathematical constructs to describe energy interactions beyond classical constraints, offering insights into phenomena that were previously deemed impossible within the established confines of energy conservation.

6.3 Implications of the study

This paper introduces a paradigm shift in understanding the LEC by exploring its aspects under chaotic and complex phenomena, specifically within steady-state modes of electrical short circuits. This approach challenges the conventional transient-focused perspective, offering a deeper understanding of energy systems when transitioning between ordered and chaotic modes. Such insights provide corrections to long-standing misconceptions regarding the universality of the LEC, presenting opportunities for novel interpretations and applications. The implications of this paper extend to practical domains, including the global energy crisis. By proposing a framework where energy generation aligns with the explored steady-state models, the study highlights potential pathways to reduce dependence on finite energy resources. This aligns with the pursuit of green and clean energy systems, where the proposed constructs could minimize noise and air pollution, paving the way for sustainable innovations. Moreover, this paper fosters advancements in understanding energy conservation under extreme conditions, suggesting broader applications in high-efficiency technologies. These include minimizing energy losses in power transmission and enabling breakthroughs in energy storage systems. Finally, the presented proofs contribute to the broader scientific discourse, providing a solid mathematical foundation for future explorations of energy phenomena in complex physical systems.

7 Conclusion

The paper has provided a detailed exploration of the Law of Energy Conservation (LEC) from both scientific and mathematical perspectives. A two-pronged approach was utilized to assess the validity of the LEC. A novel geometric proof, independent of experimental validation, was developed, revealing a remarkable implication: the LEC might be systematically violated in certain classical systems. Such a violation could arise from the non-universality of energy creation or destruction or by challenging the conventional understanding of energy transformation in specific contexts. The electrical short circuit model, characterized by excessive flow or accumulation of electric charges at a specific point within a conductor—viewed as point particles in a chaotic system—illustrated a plausible scenario for such a violation in classical frameworks. This study underscores the potential limitations of scientific understanding when it relies exclusively on inductive, observation-based methodologies. The necessity of rigorous, deductive proofs, developed independently of experimental constraints, is emphasized as critical for constructing a more robust and comprehensive scientific framework. The analysis suggests that technological advancements can facilitate the establishment of demonstrable proofs for fundamental natural phenomena, even in scenarios where traditional experimental validation is impractical. The presented findings reveal potential gaps in the current understanding of physics, which may arise from inadequacies in the philosophical and mathematical frameworks employed to study natural systems. The investigation further proposes that violations of the Law of Energy Conservation (LEC) could occur in classical systems, such as electrical short circuits (when considered as an example model of a chaotic system), particularly when analyzed within a steady-state framework. However, validating or invalidating this requires a new approach. Developing a comprehensive scheme applicable across dimensions, ensuring consistency beyond mathematical formalization, is essential. This would enable the design of experiments or proofs that definitively demonstrate LEC violation. Furthermore, improved formulations for calculating short-circuit currents, incorporating the concepts introduced in this paper, are necessary for a more complete understanding of this phenomenon. Further validation of the geometric proof and the concept of "*Chaotic Magnitude*" is crucial. This validation could involve applying these ideas to other physical systems and comparing the results with established physical laws. Additionally, exploring the philosophical and mathematical implications of the proposed framework for studying the LEC could lead to significant advancements in our understanding of energy and its behavior. The paper argues that perpetual motion machines are not a valid method for proving the LEC. The reasons for this include potential violations occurring within the system itself, masked by our current understanding. Hence, this paper presented a novel approach to the LEC, employing geometric proofs and highlighting the limitations of purely experimental methods. The potential violation of the LEC in classical systems, particularly during electrical short circuits (as the examples assert the generation of higher electrical current than the systems input current), highlights the need for a more comprehensive scientific framework. Future research should focus on developing a cross-dimensional validation scheme, improving short-circuit current calculations, and further validating the geometric proof and the concept of "*Chaotic Magnitude*". These advancements can lead to a deeper understanding of the LEC and its role in the physical world.

Conflict of interest

The author declares that there is no conflict of interest.

Similarity rate (Drillbit): 6%

References

[1] H. Goldstein, C. P. Poole, and J. L. Safko, *Classical mechanics*, 3. ed., [Nachdr.]. San Francisco Munich: Addison Wesley, 2008.

[2] G. Kalies and D. D. Do, "Momentum work and the energetic foundations of physics. I. Newton's laws of motion tailored to processes," *AIP Adv.*, vol. 13, no. 6, p. 065121, Jun. 2023, https://doi.org/10.1063/5.0147910.

[3] F. Verhulst, “Henri Poincaré (1854–1912) Engineer, Mathematician, Physicist and Philosopher,” in IUTAM Symposium on Exploiting Nonlinear Dynamics for Engineering Systems, vol. 37, I. Kovacic and S. Lenci, Eds., in IUTAM Bookseries, vol. 37. , Cham: Springer International Publishing, 2020, pp. 15–26. https://doi.org/10.1007/978-3-030-23692-2_2.

[4] “Poincaré, Jules Henri | Internet Encyclopedia of Philosophy.” Accessed: Jan. 10, 2025. [Online]. Available: https://iep.utm.edu/poincare/.

[5] M. Silberstein, W. M. Stuckey, and T. McDevitt, “Beyond Causal Explanation: Einstein’s Principle Not Reichenbach’s,” Entropy, vol. 23, no. 1, p. 114, Jan. 2021, https://doi.org/10.3390/e23010114.

[6] L. Guzzardi, “Energy, Metaphysics, and Space: Ernst Mach’s Interpretation of Energy Conservation as the Principle of Causality,” Sci. Educ., vol. 23, no. 6, pp. 1269–1291, Jun. 2014, https://doi.org/10.1007/s11191-012-9542-9.

[7] J. B. Pitts, “Conservation of Energy: Missing Features in Its Nature and Justification and Why They Matter,” Found. Sci., vol. 26, no. 3, pp. 559–584, Sep. 2021, https://doi.org/10.1007/s10699-020-09657-1.

[8] N. Banerjee and S. Sen, “Einstein pseudotensor and total energy of the universe,” Pramana, vol. 49, no. 6, pp. 609–615, Dec. 1997, https://doi.org/10.1007/BF02848334.

[9] L. Patton, “Experiment and theory building,” Synthese, vol. 184, no. 3, pp. 235–246, Feb. 2012, https://doi.org/10.1007/s11229-010-9772-9.

[10] “Chapter 1: The Nature of Science.” Accessed: Jan. 10, 2025. [Online]. Available: https://www.project2061.org/publications/sfaa/online/chap1.htm?

[11] P. Fara, “What Is Science? AHistorian’s Perplexities,” Mètode Rev. Difus. Investig., vol. 0, no. 5, Apr. 2015, https://doi.org/10.7203/metode.84.3915.

[12] R. V. Blystone and K. Blodgett, “WWW: The Scientific Method,” CBE—Life Sci. Educ., vol. 5, no. 1, pp. 7–11, Mar. 2006, https://doi.org/10.1187/cbe.05-12-0134.

[13] K. Morsanyi, T. McCormack, and E. O’Mahony, “The link between deductive reasoning and mathematics,” Think. Reason., vol. 24, no. 2, pp. 234–257, Apr. 2018, https://doi.org/10.1080/13546783.2017.1384760.

[14] Liaqat Khan, “What is Mathematics - an Overview,” 2015, Unpublished. https://doi.org/10.13140/RG.2.1.3626.8967.

[15] Jaydip Datta, “MATHEMATICS: An Inductive & Deductive Review,” 2022, https://doi.org/10.13140/RG.2.2.25473.99683/9.

[16] B. Shea, “Karl Popper: Philosophy of Science,” 2016.

[17] S. El-Badawy, “The Importance of Inductive Reasoning in Science: A Critical Analysis,” 2022, https://doi.org/10.13140/RG.2.2.18728.14087.

[18] B. Hepburn and H. Andersen, “Scientific Method,” in The Stanford Encyclopedia of Philosophy, Summer 2021., E. N. Zalta, Ed., Metaphysics Research Lab, Stanford University, 2021. Accessed: Jan. 10, 2025. [Online]. Available: https://plato.stanford.edu/archives/sum2021/entries/scientific-method/.

[19] R. Meer, “Immanuel Kant’s Theory of Objects and Its Inherent Link to Natural Science,” Open Philos., vol. 1, no. 1, pp. 342–359, Nov. 2018, https://doi.org/10.1515/opphil-2018-0025.

[20] A. Botica, “Intended’ and ‘Experienced’ Meaning: Reevaluating the Reader-Response Theory,” J. Educ. Soc. Res., Oct. 2013, https://doi.org/10.5901/jesr.2013.v3n7p519.

[21] H. Meyer-Ortmanns and T. Reisz, Principles of Phase Structures in Particle Physics, vol. 77. in World Scientific Lecture Notes in Physics, vol. 77. WORLD SCIENTIFIC, 2006. https://doi.org/10.1142/3763.

[22] A. Szegleti and F. Márkus, “Dissipation in Lagrangian Formalism,” Entropy, vol. 22, no. 9, p. 930, Aug. 2020, https://doi.org/10.3390/e22090930.

[23] D. Mušicki, “Extended Lagrangian formalism and the corresponding energy relations,” Eur. J. Mech. - ASolids, vol. 23, no. 6, pp. 975–991, Nov. 2004, https://doi.org/10.1016/j.euromechsol.2004.01.010.

[24] R. M. Marinho, “Noether’s theorem in classical mechanics revisited,” Eur. J. Phys., vol. 28, no. 1, pp. 37–43, Jan. 2007, https://doi.org/10.1088/0143-0807/28/1/004.

[25] K. Brading and E. Castellani, “SYMMETRIES AND INVARIANCES IN CLASSICAL PHYSICS,” in Philosophy of Physics, Elsevier, 2007, pp. 1331–1367. https://doi.org/10.1016/B978-044451560-5/50016-6.

[26] S. Bilbao, M. Ducceschi, and F. Zama, “Explicit exactly energy-conserving methods for Hamiltonian systems,” J. Comput. Phys., vol. 472, p. 111697, Jan. 2023, https://doi.org/10.1016/j.jcp.2022.111697.

[27] G. Kalies and D. D. Do, “Momentum work and the energetic foundations of physics. III. The unification of mechanics and electrodynamics,” AIP Adv., vol. 13, no. 9, p. 095322, Sep. 2023, https://doi.org/10.1063/5.0166847.

[28] H. Liu, X. Cai, Y. Cao, and G. Lapenta, “An efficient energy conserving semi-Lagrangian kinetic scheme for the Vlasov-Ampère system,” J. Comput. Phys., vol. 492, p. 112412, Nov. 2023, https://doi.org/10.1016/j.jcp.2023.112412.

[29] D. E. Chang, A. M. Bloch, N. E. Leonard, J. E. Marsden, and C. A. Woolsey, “The Equivalence of Controlled Lagrangian and Controlled Hamiltonian Systems,” ESAIM Control Optim. Calc. Var., vol. 8, pp. 393–422, 2002, https://doi.org/10.1051/cocv:2002045.

[30] C. Woolsey, C. K. Reddy, A. M. Bloch, D. E. Chang, N. E. Leonard, and J. E. Marsden, “Controlled Lagrangian Systems with Gyroscopic Forcing and Dissipation,” Eur. J. Control, vol. 10, no. 5, pp. 478–

496, Jan. 2004, https://doi.org/10.3166/ejc.10.478-496.
[31] P. Holland, "Hamiltonian theory of wave and particle in quantum mechanics I. Liouville's theorem and the interpretation of the de Broglie-Bohm theory," Il Nuovo Cimento B, vol. 116, Sep. 2001.
[32] V. Rastogi, A. Mukherjee, and A. Dasgupta, "A review on extension of Lagrangian-Hamiltonian mechanics," J. Braz. Soc. Mech. Sci. Eng., vol. 33, no. 1, pp. 22–33, Mar. 2011, https://doi.org/10.1590/S1678-58782011000100004.
[33] C. R. Galley, "Classical Mechanics of Nonconservative Systems," Phys. Rev. Lett., vol. 110, no. 17, p. 174301, Apr. 2013, https://doi.org/10.1103/PhysRevLett.110.174301.
[34] J.-T. Xing, "Generalised energy conservation law for chaotic phenomena," Acta Mech. Sin., vol. 35, no. 6, pp. 1257–1268, Dec. 2019, https://doi.org/10.1007/s10409-019-00886-7.
[35] R. Trudeau, "Euclidean Geometry," 2001, pp. 22–105. https://doi.org/10.1007/978-1-4612-2102-9_2.
[36] C. Sasaki, "The Géométrie of 1637," in Descartes's Mathematical Thought, vol. 237, in Boston Studies in the Philosophy of Science, vol. 237. , Dordrecht: Springer Netherlands, 2003, pp. 205–280. https://doi.org/10.1007/978-94-017-1225-5_6.
[37] M. Panza, "Rethinking geometrical exactness," Hist. Math., vol. 38, no. 1, pp. 42–95, Feb. 2011, https://doi.org/10.1016/j.hm.2010.09.001.
[38] A. Ostermann and G. Wanner, "The Elements of Euclid," in Geometry by Its History, in Undergraduate Texts in Mathematics. , Berlin, Heidelberg: Springer Berlin Heidelberg, 2012, pp. 27–59. https://doi.org/10.1007/978-3-642-29163-0_2.
[39] R. Hartshorne, "Teaching Geometry According to Euclid," Not. Am. Math. Soc., vol. 47, Jan. 2000.
[40] A. M. Kimuya, "Constructability and Rigor of Angles Multiples of 3 in Euclidean Geometry," Trends J. Sci. Res., vol. 2, no. 1, pp. 1–27, Jan. 2024, https://doi.org/10.31586/jml.2024.841.
[41] N. F. Shul'ga, V. V. Syshchenko, A. I. Tarnovsky, V. I. Dronik, and A. Yu. Isupov, "Regular and chaotic motion domains in the channeling electron's phase space and mean level density for its transverse motion energy," J. Instrum., vol. 14, no. 12, pp. C12022–C12022, Dec. 2019, https://doi.org/10.1088/1748-0221/14/12/C12022.
[42] F. Borceux, "Euclid's Elements," in An Axiomatic Approach to Geometry, Cham: Springer International Publishing, 2014, pp. 43–110. https://doi.org/10.1007/978-3-319-01730-3_3.
[43] R. J. Trudeau, "Euclidean Geometry," in The Non-Euclidean Revolution, Boston, MA: Birkhäuser Boston, 2001, pp. 22–105. https://doi.org/10.1007/978-1-4612-2102-9_2.
[44] P. Mancosu, "Descartes and Mathematics," in A Companion to Descartes, John Wiley & Sons, Ltd, 2007, pp. 103–123. https://doi.org/10.1002/9780470696439.ch7.
[45] G. Kalies, "Fundamental laws of nature confirmed by free fall," Jun. 18, 2021. https://doi.org/10.21203/rs.3.rs-624477/v1.
[46] L. Guzzardi, "Energy, Metaphysics, and Space: Ernst Mach's Interpretation of Energy Conservation as the Principle of Causality," Sci. Educ., vol. 23, no. 6, pp. 1269–1291, Jun. 2014, https://doi.org/10.1007/s11191-012-9542-9.
[47] C. R. Palmerino, "Law of Free Fall in Renaissance Science," in Encyclopedia of Renaissance Philosophy, M. Sgarbi, Ed., Cham: Springer International Publishing, 2019, pp. 1–7. https://doi.org/10.1007/978-3-319-02848-4_939-1.
[48] E. Goren and I. Galili, "Newton's Law - A Theory of motion or force?," J. Phys. Conf. Ser., vol. 1287, no. 1, p. 012061, Aug. 2019, https://doi.org/10.1088/1742-6596/1287/1/012061.
[49] J. Avigad, E. DEAN, and J. Mumma, "A Formal System for Euclid'S Elements," Rev. Symb. Log., vol. 2, pp. 700–768, Dec. 2009, https://doi.org/10.1017/S1755020309990098.
[50] M. Bunge, "Energy: Between Physics and Metaphysics," Sci. Educ., vol. 9, no. 5, pp. 459–463, Sep. 2000, https://doi.org/10.1023/A:1008784424048.
[51] P. Davies and N. H. Gregersen, Eds., Information and the Nature of Reality: From Physics to Metaphysics, 1st ed. Cambridge University Press, 2014. https://doi.org/10.1017/CBO9781107589056.
[52] C. Annamalai and A. M. D. O. Siqueira, "Mass-Energy Equivalence derived from Newtonian mechanics," J. Eng. Exact Sci., vol. 9, no. 8, pp. 15963–01e, Jun. 2023, https://doi.org/10.18540/jcecvl9iss8pp15963-01e.
[53] G. D'Abramo, "Mass–energy connection without special relativity," Eur. J. Phys., vol. 42, no. 1, p. 015606, Jan. 2020, https://doi.org/10.1088/1361-6404/abbca2.
[54] B. Muhyedeen, "New Concept of Mass-Energy Equivalence," Eur. J. Sci. Res., vol. ISSN 1450-216X Vol.26 No.2 (2009), pp.161–175, Feb. 2009.
[55] R. Gobato, A. Gobato, and D. F. G. Fedrigo, "Energy and matter," Sep. 02, 2015, arXiv: arXiv:1509.02892. https://doi.org/10.48550/arXiv.1509.02892.
[56] C. Barreiro, J. M. Barreiro, J. A. Lara, D. Lizcano, M. A. Martínez, and J. Pazos, "The Third Construct of the Universe: Information," Found. Sci., vol. 25, no. 2, pp. 425–440, Jun. 2020, https://doi.org/10.1007/s10699-019-09630-7.
[57] T. R. Mongan, "Origin of the Universe, Dark Energy, and Dark Matter," J. Mod. Phys., vol. 09, no. 05, pp. 832–850, 2018, https://doi.org/10.4236/jmp.2018.95054.
[58] N. Raos, "Atomism in greek philosophy," Kem. U Ind. Chem. Chem. Eng., vol. 51, pp. 385–392, Jan. 2002.

[59] C. Masolo and L. Vieu, "Atomicity vs. Infinite Divisibility of Space," in Spatial Information Theory. Cognitive and Computational Foundations of Geographic Information Science, vol. 1661, C. Freksa and D. M. Mark, Eds., in Lecture Notes in Computer Science, vol. 1661. , Berlin, Heidelberg: Springer Berlin Heidelberg, 1999, pp. 235–250. https://doi.org/10.1007/3-540-48384-5_16.

[60] V. Villani, "The Way Ahead," in Perspectives on the Teaching of Geometry for the 21st Century, vol. 5, C. Mammana and V. Villani, Eds., in New ICMI Study Series, vol. 5. , Dordrecht: Springer Netherlands, 1998, pp. 319–327. https://doi.org/10.1007/978-94-011-5226-6_11.

[61] A. Oliveira, "Coriolis' Theory of Machines and Mechanisms," Jan. 1980.

[62] "Descartes, Rene | Internet Encyclopedia of Philosophy." Accessed: Jan. 10, 2025. [Online]. Available: https://iep.utm.edu/rene-descartes/.

[63] R. Descartes, The geometry of René Descartes. New York, NY: Dover Publications, 1996.

[64] R. Hershkowitz et al., "Reasoning in Geometry," in Perspectives on the Teaching of Geometry for the 21st Century, vol. 5, C. Mammana and V. Villani, Eds., in New ICMI Study Series, vol. 5. , Dordrecht: Springer Netherlands, 1998, pp. 29–83. https://doi.org/10.1007/978-94-011-5226-6_3.

[65] D. Lomas, "Geometry starting with Euclid," Can. J. Sci. Math. Technol. Educ., vol. 5, no. 2, pp. 271–276, Apr. 2005, https://doi.org/10.1080/14926150509556659.

[66] W. Halbfaß, "Descartes, René: Principia philosophiae," in Kindlers Literatur Lexikon (KLL), H. L. Arnold, Ed., Stuttgart: J.B. Metzler, 2020, pp. 1–3. https://doi.org/10.1007/978-3-476-05728-0_9540-1.

[67] E. Mach, "ON THE PRINCIPLE OF THE CONSERVATION OF ENERGY," The Monist, vol. 5, no. 1, pp. 22–54, 1894.

[68] J.-P. Anfray, "Leibniz and Descartes," in The Oxford Handbook of Descartes and Cartesianism, S. Nadler, T. M. Schmaltz, and D. Antoine-Mahut, Eds., Oxford University Press, 2019, pp. 720–737. https://doi.org/10.1093/oxfordhb/9780198796909.013.45.

[69] Y. Kato and K. Sakamoto, "Between Cartesianism and orthodoxy: God and the problem of indifference in Christoph Wittich's Anti-Spinoza," Intellect. Hist. Rev., pp. 1–19, Dec. 2020, https://doi.org/10.1080/17496977.2020.1852373.

[70] G. E. Smith, "The vis viva dispute: A controversy at the dawn of dynamics," Phys. Today, vol. 59, no. 10, pp. 31–36, Oct. 2006, https://doi.org/10.1063/1.2387086.

[71] M. N. Hidayat, S. P. Chairandy, and F. Ronilaya, "Design and Analysis of A Perpetual Motion Machine Using Neodymium Magnets as A Prime Mover," J. Southwest Jiaotong Univ., vol. 56, no. 2, pp. 211–219, Apr. 2021, https://doi.org/10.35741/issn.0258-2724.56.2.17.

[72] S. V. Kukhlevsky, "Breaking of Energy Conservation Law: Creating and Destroying of Energy by Subwavelength Nanosystems," 2006, arXiv. https://doi.org/10.48550/ARXIV.PHYSICS/061000.

[73] J. F. Rodríguez-León, I. Cervantes, E. Castillo-Castañeda, G. Carbone, and D. Cafolla, "Design and Preliminary Testing of a Magnetic Spring as an Energy-Storing System for Reduced Power Consumption of a Humanoid Arm," Actuators, vol. 10, no. 6, p. 136, Jun. 2021, https://doi.org/10.3390/act10060136.

[74] A. P. David, "Electro-Magnetic Induction: Free Electricity Generator," May 18, 2017, Social Science Research Network, Rochester, NY: 3486740. https://doi.org/10.2139/ssrn.3486740.

[75] N. Coppedge, "TOP PERPETUAL MOTION MACHINES," May 2022.

[76] M. S. Berman, "On the Zero-Energy Universe," Int. J. Theor. Phys., vol. 48, no. 11, pp. 3278–3286, Nov. 2009, https://doi.org/10.1007/s10773-009-0125-8.

[77] M. Berman, "On the Zero-Energy Universe," Int. J. Theor. Phys., vol. 48, May 2006, https://doi.org/10.1007/s10773-009-0125-8.

[78] "Descartes, Rene: Scientific Method | Internet Encyclopedia of Philosophy." Accessed: Jul. 16, 2022. [Online]. Available: https://iep.utm.edu/rene-descartes-scientific-method/.

[79] J. F. Scott, The scientific work of René Descartes (1596-1650). in Routledge library editions: René Descartes, no. volume 3. London: Routledge, 2017.

[80] A. Micheli and P. Iturralde, "[On the evolution of scientific thought]," Arch. Cardiol. Mex., vol. 85, Aug. 2015, https://doi.org/10.1016/j.acmx.2015.06.003.

[81] Y. Guan et al., "Burden of the global energy price crisis on households," Nat. Energy, vol. 8, no. 3, Art. no. 3, Mar. 2023, https://doi.org/10.1038/s41560-023-01209-8.

[82] M. Farghali et al., "Strategies to save energy in the context of the energy crisis: a review," Environ. Chem. Lett., vol. 21, no. 4, pp. 2003–2039, Aug. 2023, https://doi.org/10.1007/s10311-023-01591-5.

[83] J. Mitali, S. Dhinakaran, and A. A. Mohamad, "Energy storage systems: a review," Energy Storage Sav., vol. 1, no. 3, pp. 166–216, Sep. 2022, https://doi.org/10.1016/j.enss.2022.07.002.

[84] R. Machotka, "Euclidean Model of Space and Time," J. Mod. Phys., vol. 09, pp. 1215–1249, Jan. 2018, https://doi.org/10.4236/jmp.2018.96073.

[85] O. Ericok and J. Mason, Foundations of a Finite Non-Equilibrium Statistical Thermodynamics: Extrinsic Quantities. 2022.

[86] U. Seifert, "First and Second Law of Thermodynamics at Strong Coupling," Phys. Rev. Lett., vol. 116, no. 2, p. 020601, Jan. 2016, https://doi.org/10.1103/PhysRevLett.116.020601.

[87] Y.-F. Chang, "Entropy Decrease in Isolated Systems: Theory, Fact and Tests: Physics," Int. J. Fundam. Phys. Sci., vol. 10, no. 2, Art. no. 2, Jun. 2020, https://doi.org/10.14331/ijfps.2020.330137.

[88] H. Choi, "Size and Expansion of the Universe in Zero Energy Universe (Logical defenses for the Model 'We are living in a black hole')," Nov. 2016.

[89] P. Halpern and N. Tomasello, "Size of the Observable Universe," Adv. Astrophys., vol. 1, Nov. 2016, https://doi.org/10.22606/adap.2016.13001.

[90] R. Hershkowitz et al., "Reasoning in Geometry," in Perspectives on the Teaching of Geometry for the 21st Century: An ICMI Study, C. Mammana and V. Villani, Eds., in New ICMI Study Series. , Dordrecht: Springer Netherlands, 1998, pp. 29–83. https://doi.org/10.1007/978-94-011-5226-6_3.

[91] "Euclid's Elements, Book II, Proposition 10." Accessed: Jun. 29, 2023. [Online]. Available: http://aleph0.clarku.edu/~djoyce/elements/bookII/propII10.html.

[92] C. Masolo and L. Vieu, "Atomicity vs. Infinite Divisibility of Space," in COSIT, 1999. https://doi.org/10.1007/3-540-48384-5_16.

[93] N. Raos, "Atomism in greek philosophy," Kem. U Ind. Chem. Chem. Eng., vol. 51, pp. 385–392, Jan. 2002.

[94] S. W. Gaukroger, "Descartes' Conception of Inference," in Metaphysics and Philosophy of Science in the Seventeenth and Eighteenth Centuries: Essays in honour of Gerd Buchdahl, R. S. Woolhouse, Ed., in The University of Western Ontario Series in Philosophy of Science. , Dordrecht: Springer Netherlands, 1988, pp. 101–132. https://doi.org/10.1007/978-94-009-2997-5_6.

[95] Heath, Thomas L, The Thirteen Books of Euclid's Elements, translated from the text of Heiberg, with introduction and commentary, 2nd ed., vol. 3 vols. Cambridge (available in Dover reprint): University Press, 1926.

[96] N. F. Shul'ga, V. V. Syshchenko, A. I. Tarnovsky, V. I. Dronik, and A. Y. Isupov, "Regular and chaotic motion domains in the channeling electron's phase space and mean level density for its transverse motion energy," J. Instrum., vol. 14, no. 12, pp. C12022–C12022, Dec. 2019, https://doi.org/10.1088/1748-0221/14/12/C12022.

[97] B. T. Utelbayev, E. Suleimenov, and U. A.B., "Elementary Particles and Properties of Material Objects Review Article," Dec. 2018.

[98] S. Reucroft and E. Williams, "The Structure and Properties of Elementary Particles," Oct. 2019.

[99] R. Abreu and V. Guerra, "The concepts of work and heat and the first and second laws of thermodynamics," Mar. 2012.

[100] S. Shahsavari and P. Torkaman, "Energy Conservation Principle from the Perspective of the Energy Structure Theory," Asian J. Appl. Sci., vol. 10, no. 5, Nov. 2022, https://doi.org/10.24203/ajas.v10i5.6950.

[101] B. Xia, Z. Chen, C. Mi, and B. Robert, "External short circuit fault diagnosis for lithium-ion batteries," in 2014 IEEE Transportation Electrification Conference and Expo (ITEC), Dearborn, MI: IEEE, Jun. 2014, pp. 1–7. https://doi.org/10.1109/ITEC.2014.6861806.

[102] Z. Chen, R. Xiong, J. Tian, X. Shang, and J. Lu, "Model-based fault diagnosis approach on external short circuit of lithium-ion battery used in electric vehicles," Appl. Energy, vol. 184, pp. 365–374, Dec. 2016, https://doi.org/10.1016/j.apenergy.2016.10.026.

[103] A. Berizzi, A. Silvestri, D. Zaninelli, and S. Massucco, "Short-circuit current calculation: A comparison between methods of IEC and ANSI standards using dynamic simulation as reference," IEEE Trans. Ind. Appl. Inst. Electr. Electron. Eng. U. S., vol. 30:4, https://doi.org/10.1109/IAS.1993.299168.

[104] F. V. Conte, P. Gollob, and H. Lacher, "Safety in the battery design: The short circuit," World Electr. Veh. J., vol. 3, Dec. 2009, https://doi.org/10.3390/wevj3040719.

[105] M. F. Moad, "On Thevenin's and Norton's Equivalent Circuits," IEEE Trans. Educ., vol. 25, no. 3, pp. 99–102, Aug. 1982, https://doi.org/10.1109/TE.1982.4321556.

[106] J. D. Enderle, "Thévenin's and Norton's Theorems," in Bioinstrumentation, in Synthesis Lectures on Biomedical Engineering. , Cham: Springer International Publishing, 2006, pp. 53–61. https://doi.org/10.1007/978-3-031-01616-5_6.

[107] R. V. Jensen, "Classical Chaos," Am. Sci., vol. 75, no. 2, pp. 168–181, 1987.

[108] M. C. Gutzwiller, "Soft Chaos and the KAM Theorem," in Chaos in Classical and Quantum Mechanics, M. C. Gutzwiller, Ed., in Interdisciplinary Applied Mathematics. , New York, NY: Springer, 1990, pp. 116–141. https://doi.org/10.1007/978-1-4612-0983-6_10.

[109] G. F. R. Ellis, U. Kirchner, and W. R. Stoeger, "Multiverses and physical cosmology," Mon. Not. R. Astron. Soc., vol. 347, no. 3, pp. 921–936, Jan. 2004, https://doi.org/10.1111/j.1365-2966.2004.07261.x.

[110] J. Wisniak, "Conservation of Energy: Readings on the Origins of the First Law of Thermodynamics. Part I," Educ. Quím., vol. 19, pp. 159–171, Jan. 2008, https://doi.org/10.22201/fq.18708404e.2008.2.25806

Appendix I. (Rene' Descartes' multiplication with geometric construction method)

Descartes [36] presents a mechanical method for multiplying straight-line segments through geometric constructions. To simplify, we deviate slightly from Euclid's strict construction by introducing measurements and assuming a unity measure throughout. This scientific technique contrasts with and serves as a source of inspiration for the earlier developed straightedge and compass geometric operations.

Definition 11 (Geometric multiplication of a straight line segment r_2 and a given baseline r_1). Given a baseline r_1 between two distinct basepoints points B and D and an arbitrary line segment r_2 contained between two distinct points B and C , the geometric multiplication of r_1 and r_2 is obtained through the following construction starting from $\{r_1, r_2\}$.

1. Construct the point A, a unit between point B and point D on the side of the point D.
2. Construct line L_1 through the points A and C.
3. Construct line L_2 that is parallel to L_1 through the point D.
4. Construct an extension of BC to intersect L_2 at a point, E.

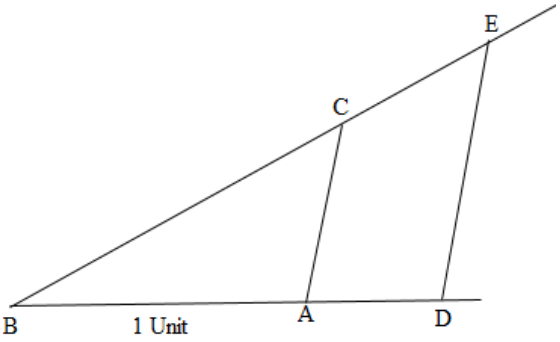

Figure 11. An Illustration of Descartes' Geometric Multiplication of Points in a Euclidean Plane. (This figure illustrates Descartes' geometric multiplication of points in a Euclidean Plane. The construction involves a baseline r_1 between basepoints B and D and a line segment r_2 between points B and C. Points A, C, D, and E are constructed accordingly, demonstrating the steps for geometric multiplication as per Definition 11).

Claim 3. $\overline{BD} \otimes \overline{BC} = \overline{BE}$

Proof. L_2 is parallel to L_1, implying ΔABC is similar to ΔDBE. We set, as 1 is to L_1 as $r_1 = 1 + AD$ is to L_2.

If $L_1 = (1 + AD) : L_2$, then $L_2 = (1 + AD) \times L_1$.

Also, let $BE = r_p$ so that $r_p : L_2 = r_2 : L_1$.

In this case;

$$r_p = \frac{r_2 \times L_2}{L_1} = \frac{r_2 \times (1+AD) \times L_1}{L_1} = r_2 \times (1 + AD) = r_2 \times r_1$$

Thus, $r_p = r_2 \times r_1$, hence claim 3} is proven.

Appendix 2. Point Rotation by Straightedge-Compass Construction

Definition 12 (Rotation of a point to a baseline through O and P): Given two distinct basepoints points O and P and an arbitrary point Q, the rotation of Q to the bassline through point O and point P can be defined by a construction starting from $\{O, P, Q\}$ as follows.

1. Construct the baseline l through the points O and P.
2. Construct a circle c centered at the point P through point Q.
3. Label Q' the intersection point between c and l.

The point Q' is a geometric rotation of the point Q to the baseline. By Definition, the magnitude $\overline{OQ} \cong \overline{OQ'}$.

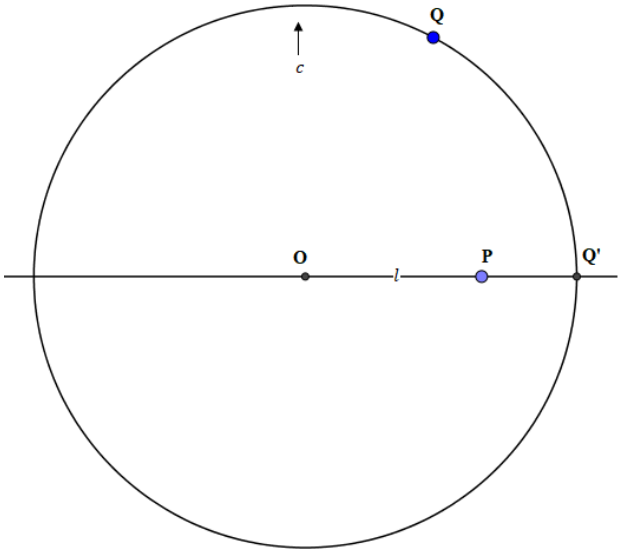

Figure 12. Geometric Rotation of a point in a Euclidean Plane.

Appendix 3 Important Notations. The following shorthand convention is employed throughout the paper workflow.

PMM	$: Perpetual\ Motion\ Machines$
LEC	$: Law\ of\ Energy\ conservation$
$ETIS$	$: Euclidean - Thermodynamic\ Isolated\ System$
TIS	$: Thermodynamics\ Isolated\ System$
$\mathrm{N}^{\mathrm{nth}}$	$: A\ Newton's\ Law\ and\ n = 1,2,\ and\ 3$
ΔABC	$: Triangle\ ABC$
$\overline{L_1} \parallel \overline{L_2}$	$: Two\ parallel\ lines\ L_1\ and\ L_2$
$\overline{OA}$	$: Straight - line\ through\ points\ O\ and\ A$
$A > B$	$: Magnitude\ A\ is\ greater\ than\ magnitude\ B$

Eurasian J. Sci. Eng. Tech., 2025; 6(1): 036-040

Eurasian Journal of Science Engineering and Technology

Research article

www.dergipark.org.tr/tr/pub/ejset / www.dergipark.org.tr/en/pub/ejset

Enhancing optoelectronic performance: Structural and optical properties of MZO thin films

Ali Altuntepe [1,*], Serkan Erkan [2]

[1] *Sivas of Science and Technology University Optical Excellence Application and Research Center, 58000, Sivas, Türkiye*
[2] *Nigde Omer Halisdemir University, Nanotechnology Research and Application Center, 51240, Niğde, Türkiye*

Abstract

This work reports on the feasibility of using molybdenum-doped zinc oxide (MZO) thin films as transparent conductive electrode (TCE) material in optoelectronic applications, especially in solar cells. MZO films were deposited by RF magnetron sputtering in the thickness range of 100-500 nm and their electrical, optical, and structural properties were systematically studied. The results indicated that the electrical conductivity increased with the increase in film thickness, while the sheet resistance decreased; the 500 nm MZO film had the least resistance, which was about 362.4 Ω/sq. The optical measurements presented an average transmittance of about 77–84% in the visible range, with minor variations attributed to graphene integration in hybrid MZO+Graphene structures. The bandgap energy of MZO films decreased from 3.29 eV to 3.21 eV with increasing thickness, indicating the transition from quantum confinement toward bulk-like properties. SEM and EDXS analyses confirmed successful doping with molybdenum and gave insight into the surface morphology and chemical composition of the films. While MZO films with improved electrical and optical performances were reported when compared to undoped zinc oxide (ZnO), the hybrid structures showed a high sheet resistance due to inherent characteristics of graphene. The presented work demonstrates the MZO films as potential alternatives for more conventional TCE materials like indium tin oxide (ITO), considering their cost and availability issues, as well as their structure-related shortcomings.

Keywords: MZO, Magnetron sputtering, Pressure, Graphene

1 Introduction

In silicon-based solar cells, one of the primary cost-increasing factors is the amount of material used (~180 µm). The main reason thin-film technology is widely studied is the significantly reduced material usage (2–10 µm) compared to Si-based solar cells. Another major cost factor in Si-based solar cells is the transparent conductive electrode (TCE) material, indium tin oxide (ITO) [1]. ITO thin films exhibit low thickness and sheet resistance while maintaining high optical transparency in the visible region. Despite its advantages, ITO has some inherent issues. The main drawbacks include the lack of a uniform crystalline structure and a high density of structural defects. In its amorphous form, substitutional reactions between +3 valence indium and +4 valence tin do not occur, and the film structure contains high levels of impurities. Consequently, the carrier density and mobility remain quite low, which significantly limits cell efficiency (Mazur vd., 2010). In addition to ITO, zinc oxide-based TCEs are used to a limited extent. Structural defects and high sheet resistance in zinc oxide (ZnO) require various structural enhancement methods for solar cell applications. Chemical doping has facilitated the use of ZnO-based TCEs in such applications. Aluminum-doped zinc oxide (AZO), molybdenum-doped zinc oxide (MZO), and gallium-doped zinc oxide (GZO) are particularly employed in optoelectronic applications such as sensors, transistors, and thin-film solar cells [2-5].

Molybdenum (Mo)-doped ZnO (MZO) films have recently emerged as popular TCE materials. Like gallium, molybdenum enables stable doping due to its ionic radius (0.062 nm), which is close to that of Zn. Molybdenum, in its 4+ or 6+ oxidation states, integrates into the Zn structure and contributes two or four electrons to ZnO's conduction band, thereby enhancing electrical conductivity. Studies on MZO films report resistivity values in the range of approximately 10−3-10−4 ohm-cm [6]. Despite these promising features, MZO films also present challenges, primarily low oxidation resistance [7]. Moreover, the electrical properties of MZO films can vary depending on the production method. Research continues on parameters such as doping ratios, temperature effects, and film thickness in MZO structures [8, 9]. In general, the disadvantages of TCEs include structural defects and the limited carrier density at similar levels. To address these issues, graphene—a carbon-based material often referred to as a "miracle material"—stands out as one of the best candidates. Graphene, defined as the first two-dimensional material synthesized with a hexagonal honeycomb lattice, was isolated in 2004 by Novoselov and colleagues using mechanical exfoliation. It quickly became a focus of interest due to its exceptional properties, including high strength (1 TPa Young's modulus), excellent electrical conductivity, and high optical transparency (97%). These combined properties make graphene applicable in a wide range of fields [10]. Graphene is utilized in solar cells, fuel cells, sensors, transistors, and many other electronic and

* Corresponding author, e-mail: altuntepeali@gmail.com (A. Altuntepe)
Recieved: 20.12.2024 Accepted: 09.01.2025 Published: 30.01.2025
doi: 10.55696/ejset.1604813

optoelectronic applications. Notably, it offers a strong alternative to ITO, which is commonly used as a transparent conductive electrode in solar cells [11]. The brittle nature of ITO, its limited natural reserves, and its significantly lower carrier density compared to graphene highlight the importance of integrating graphene as a TCE. In summary, while the growth parameters for MZO have been optimized, this study presents research on hybrid TCEs combining graphene.

2 Material and method

All films were deposited using an RF power source and a single target. Before initiating the deposition process, the sputtering system was evacuated to a pressure below $1.6x10^{-6}$ Torr after placing the substrates. High-purity argon (Ar, 99.999%) gas was then introduced into the system to generate the plasma required for sputtering, preparing the system for the deposition process. Each TCE film was deposited by applying 50 W of power. MZO films with thicknesses of 100, 200, 300, 400, and 500 nm were deposited on glass substrates. This approach allowed the investigation of the effect of film thickness on the electrical and optical properties of the TCE layer. The CVD system used for graphene synthesis comprises three zones and six gas flow control units. Polycrystalline copper substrates with a thickness of 25 µm were utilized, sourced from Alfa Easer. Methane (CH_4, 99.9995% purity) served as the carbon source, while hydrogen (H_2, 99.9999% purity) acted as the decomposition agent. The gas flow parameters for single-layer graphene synthesis were previously optimized in our studies [12]. To transfer graphene from the metal substrate to a desired surface, the "wet transfer" method, which employs a polymer support, was used. Initially, the graphene on the copper substrate was coated with poly(methyl methacrylate) (PMMA) using a spin-coating device to protect its surface. The copper substrate was then dissolved in an ammonium persulfate ($(NH_4)_2S_2O_8$) solution, releasing the graphene+polymer structure from the metal surface. This structure was rinsed multiple times in deionized water baths to remove residual impurities. The graphene was subsequently transferred onto a chosen substrate. After the transfer, the substrate was heated on a hot plate at approximately 50-60°C for 3 minutes to remove excess water from the structure, followed by heating at 80°C for 5 minutes. Finally, the polymer layer used during the transfer process was removed from the graphene surface using acetone.

Table 1. Growth process of MZO

Growth Process	
Base Pressure	$1.6x10^{-6}$ Torr
Growth Pressure	$3x10^{-3}$ Torr
RF Power	50 Watt
Deposition Rate	0.2 Å/s
Temperature	RT

3 Results and discussion

MZO films were growth at varying thicknesses (100–500 nm). A significant factor in the improved electrical properties of MZO films compared to ZnO is the four-valence difference between Mo^{6+} and Zn^{2+}. The presence of Mo as a dopant contributes additional electrons to electrical conductivity, enhancing the electrical properties of ZnO-based MZO films and making them suitable for TCE applications. Sheet resistance measurements of MZO+Graphene films showed an increase in resistance compared to MZO films alone (Table 2). Similar to AZO films, the sheet resistance of MZO films being higher or comparable to that of graphene leads to an increase in the overall sheet resistance of the MZO+Graphene structure. Despite this, the decrease in sheet resistance with increasing MZO film thickness was also observed in MZO+Graphene films. The measurements revealed that MZO films have lower sheet resistance compared to AZO films. This indicates that different dopants significantly influence the electrical properties of ZnO-based films. As the film thickness increases, the sheet resistance of MZO films decreases, which is accompanied by an improvement in crystal quality. This contributes to an increase in carrier concentration, thereby enhancing the electrical properties [13]. For example, a 100 nm MZO film exhibits a sheet resistance of 819 ohm/sq, while a 500 nm MZO film has a resistance of 362 ohm/sq. The sheet resistance continued to decrease for films of all thicknesses up to 500 nm.

Table 2. The sheet resistance, optical transmission, and bandgap values of MZO films.

			MZO		
	MZO	**MZO+Graphene**	**MZO**	**MZO+Graphene**	**MZO**
Thickness (nm)	**Sheet Resistance (ohm/sq)**	**Sheet Resistance (ohm/sq)**	**Transmission (%)**	**Transmission (%)**	**E_g (eV)**
100	751.98	1051	81	83	3.29
200	643.26	843.6	79	81	3.28
300	588.9	730	78	78	3.27
400	498.3	589.8	80	76	3.24
500	362.4	434.2	80	80	3.21

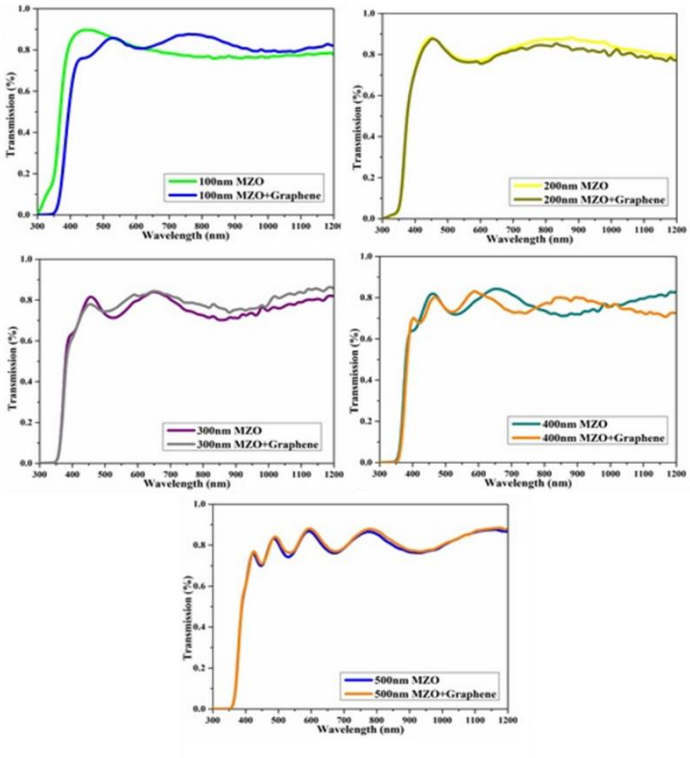

Figure 1. The optical transmission values of MZO and MZO+Graphene films.

MZO films exhibit average optical transmittance values ranging between 77% and 84% in the visible region. It is observed that graphene coating causes partial increases and decreases in transmittance values; however, these variations are considered within the margin of error. Nevertheless, in MZO+Graphene films, an improvement in optical transmittance values was generally noted beyond a wavelength of 700 nm. This can be attributed to the material used in the hybrid TCE structure being graphene. Graphene's low absorption values beyond 700 nm contribute positively to the optical transmittance values in the hybrid structures. The band gap is an important characteristic of semiconductors, and it determines their electrical and optical properties. The optical properties of the MZO films growth on glass substrate were determined by using the bandgap values calculated from the absorption coefficient obtained by the transmittance spectra of the samples. The bandgap energy values of the samples were calculated by measuring the transmittance spectra with an ellipsometer (J.A. Woollam-VASE) system in our research center. The absorption coefficients of the samples were calculated using the Lambert-Beer law [14] with the measured transmittance values at room temperature in the range of 200-1200 nm and the thicknesses of the MZO films.

$$\alpha = \frac{1}{d}\ln\frac{1}{T} \quad (1)$$

The absorption coefficient (α) in Equation (1) represents the absorption coefficient, d represents the thickness of the sample, and T represents the optical transmittance. Using the calculated absorption coefficients with Equation (1), the bandgap energy values of the MZO films were calculated using Equation (2), where E_g is the bandgap energy, A is the constant, $h\nu$ is the photon energy, and n is the nature of the transition, which takes the value of 1/2 for direct bandgap semiconductors [15].

$$(\alpha h\nu)^2 = A(h\nu - E_g)^n \quad (2)$$

The optical band gap MZO films shows a slight decreasing trend as the film thickness increases. At 100 nm, the band gap is 3.29 eV, and as the thickness increases, it gradually decreases, reaching 3.21 eV at 500 nm. This reduction in band gap can be attributed to several factors. First, in very thin films, quantum confinement effects are more pronounced, which leads to a wider band gap. As the film thickness increases, these quantum effects diminish, allowing the material to approach bulk-like properties where the band gap is generally smaller. Additionally, thicker films tend to have fewer strain effects, as they may relax more compared to thinner films, which can contribute to a slight narrowing of the band gap. The defect density, often higher in thinner films, can also lead to localized states within the band gap, which reduces as the film thickens, resulting in a more stable electronic structure and a smaller band gap. This behavior reflects the transition from quantum confinement to bulk-like properties, which is typical for semiconductor thin films. As shown in the Figure 2, graphene coating does not appear to have an impact on the bandgap energy. An observed decrease in bandgap energy occurs with increasing

film thickness (Table 1). Similarly, studies in the literature have also demonstrated the effect of film thickness on bandgap energy [16-17]. Fundamentally, with increasing film thickness, grain boundaries expand, and the crystal structure improves accordingly. This can be correlated with the changes observed in the bandgap energy.

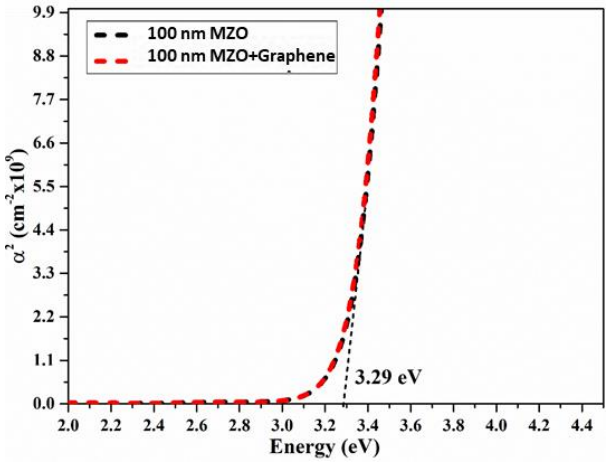

Figure 2. Band gap for the 100 nm MZO film.

The SEM and EDXS measurements of the optimized thickness MZO films have been performed (Table 2). Based on the obtained SEM-EDXS results, information regarding the surface microstructures and chemical compositions of the films has been gathered. These techniques provide valuable insights into the morphology, grain size, surface uniformity, and the distribution of elements within the films. SEM imaging helps to visualize the surface structure, while EDXS analysis allows for the precise determination of the elemental composition, confirming the successful doping of molybdenum and the overall material consistency. This analysis is crucial for understanding the relationship between the film's structural characteristics and its electrical and optical properties. It has been observed that the presence of Mo atoms within the structure of MZO films is at a very low level. This can be explained by either the inability of Mo atoms to incorporate into the structure during sputtering or the lack of sufficient sensitivity in the EDXS measurements.

Table 3. Chemical compositions of MZO film.

TCE	Atomic Ratio (%)		
	O	Zn	Mo
100nm MZO	62.55	37.37	0.08

The SEM surface images of the 100 nm MZO film are shown in Figure 3, providing insights into the morphological characteristics of the film. As observed, the surface exhibits a uniform and dense structure, indicating good coverage and homogeneity. This suggests that the deposition process resulted in a consistent film formation without significant defects or irregularities.

However, the grain boundaries in the SEM images appear less defined, and the individual grains are not prominently visible. This can be attributed to two primary factors. First, the relatively low thickness of the film (100 nm) limits the growth of larger grains, as thinner films typically have smaller grain sizes due to the limited material available for crystallization. Second, the absence of thermal treatment, such as annealing, prevents further recrystallization and grain growth. Thermal processes are known to enhance grain boundary mobility, allowing grains to coalesce and grow, leading to a more distinct grain structure.

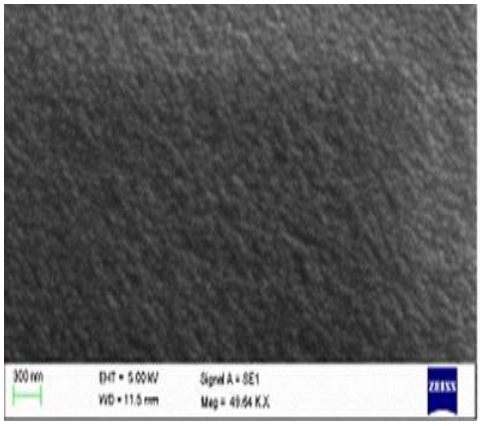

Figure 3. SEM surface images of MZO thin film

When the electrical and optical properties of MZO films were examined, it was determined that 050 nm MZO film exhibited better properties compared to other films. In this sense, it was determined that the most suitable film thickness for MZO films to be used as TCE in solar cell applications was 100 nm.

4 Conclusion

MZO films showed enhanced electrical and optical properties with increasing film thickness, such as lower sheet resistance, higher carrier concentration, and better crystal quality. The reduction in bandgap energy with increasing film thickness was explained by quantum confinement effects and structural improvements. The incorporation of graphene into MZO structures led to significant changes in optical transmittance, especially in the near-infrared region. Although the addition of graphene slightly increased sheet resistance compared to pure MZO films, its low absorption characteristics enhanced optical transmittance beyond 700 nm. This suggests the synergistic possibility of hybrid TCE structures in applications that demand both high transparency and electrical conductivity.

The study also underlines the importance of optimizing parameters related to film thickness, doping levels, and deposition methods for achieving maximum performance. Notwithstanding the challenges in achieving uniform Mo doping, besides variability in electrical properties arising out of production methods, MZO+Graphene structures present an encouraging alternative to traditional TCEs like ITO. More research is required for addressing the challenges, refining the fabrication techniques, and exploring scalability for industrial applications. This will help develop further understanding of hybrid TCEs and create pathways for their incorporation into next-generation optoelectronic devices,

such as solar cells, for which issues of cost, efficiency, and material sustainability will remain pressing.

Conflict of interest

The authors declare that there is no conflict of interest.

Similarity rate (iThenticate): .15 %

References

[1] A. M. Bagher, M. M. A. Vahid, and M. J. Mohsen, "Types of solar cells and application," *Photonics*, vol. 3, no. 2, pp. 94–113, 2015, doi: 10.1515/pn-2015-0005.

[2] S.-W. Ko, J.-G. Jung, K.-S. Park, and S.-M. Lim, "Adhesion change of AZO/PET film by ZrCu insertion layer," *J. Korean Phys. Soc.*, vol. 49, no. 2, pp. 252–259, 2016, doi: 10.1007/s00339-015-9459-4.

[3] G. Gonçalves, E. Elangovan, P. Barquinha, L. Pereira, R. Martins, and E. Fortunato, "Influence of post-annealing temperature on the properties exhibited by ITO, IZO and GZO thin films," *Thin Solid Films*, vol. 515, no. 22, pp. 8562–8566, Sep. 2007, doi: 10.1016/j.tsf.2007.03.034.

[4] F. Bittau et al., "Analysis and optimisation of the glass/TCO/MZO stack for thin film CdTe solar cells," *Sol. Energy Mater. Sol. Cells*, vol. 187, pp. 15–22, Sep. 2018, doi: 10.1016/j.solmat.2018.07.001.

[5] K. Girija et al., "Enhanced H_2S sensing properties of gallium doped ZnO nanocrystalline films as investigated by DC conductivity and impedance spectroscopy," *Mater. Chem. Phys.*, vol. 214, pp. 297–305, Jul. 2018, doi: 10.1016/j.matchemphys.2018.04.063.

[6] S. Zhang, S.-H. Wei, and A. Zunger, "Intrinsic n-type versus p-type doping asymmetry and the defect physics of ZnO," *Phys. Rev. B*, vol. 63, no. 7, p. 075205, Feb. 2001, doi: 10.1103/PhysRevB.63.075205.

[7] C. Wu et al., "Electrical and optical properties of molybdenum-doped ZnO transparent conductive thin films prepared by dc reactive magnetron sputtering," *Semicond. Sci. Technol.*, vol. 24, no. 12, p. 125012, Dec. 2009, doi: 10.1088/0268-1242/24/12/125012.

[8] A. Ali et al., "Mo-doped ZnO nanoflakes on Ni-foam for asymmetric supercapacitor applications," *RSC Adv.*, vol. 9, pp. 27432–27438, 2019, doi: 10.1039/C9RA05046A.

[9] J.-Y. Chun, J.-W. Han, and D.-S. Seo, "Molybdenum-doped zinc oxide electrodes for organic light-emitting devices," *Electron. Lett.*, vol. 45, no. 12, pp. 604–606, 2009, doi: 10.1049/el.2009.0200.

[10] A. K. Geim and K. S. Novoselov, "The rise of graphene," *Nanoscience and Technology: A Collection of Reviews from Nature Journals*, pp. 11–19, 2010, doi: 10.1142/9789814287005_0002.

[11] P. Avouris and F. Xia, "Graphene applications in electronics and photonics," *Mater. Today*, vol. 15, no. 3, pp. 122–130, Mar. 2012, doi: 10.1016/S1369-7021(12)70058-3.

[12] R. Zan et al., "Integration of graphene with GZO as TCO layer and its impact on solar cell performance," *Renew. Energy*, vol. 173, pp. 45–52, 2021, doi: 10.1016/j.renene.2021.03.001.

[13] R. Swapna et al., "Microstructural, electrical and optical properties of ZnO: Mo thin films with various thickness by spray pyrolysis," *J. Alloys Compd.*, vol. 553, pp. 68–75, Jun. 2013, doi: 10.1016/j.jallcom.2012.03.100.

[14] J. I. Pankove, *Optical Processes in Semiconductors*. New York, NY, USA: Dover, 1971.

[15] J. Tauc, "Optical properties and electronic structure of amorphous Ge and Si," *Mater. Res. Bull.*, vol. 3, no. 1, pp. 37–46, 1968, doi: 10.1016/0025-5408(68)90023-8.

[16] X. Xiu et al., "Transparent conducting molybdenum-doped zinc oxide films deposited by RF magnetron sputtering," *Appl. Surf. Sci.*, vol. 253, no. 8, pp. 3345–3348, Feb. 2007, doi: 10.1016/j.apsusc.2006.07.106.

[17] R. Zan, A. Altuntepe, and S. Erkan, "Substitutional boron doping of graphene using diborane in CVD," *Phys. E*, vol. 128, p. 114629, Mar. 2021, doi: 10.1016/j.physe.2021.114629.

Eurasian J. Sci. Eng. Tech., 2025; 6(1): 041-046

Eurasian Journal of Science Engineering and Technology

Research article

www.dergipark.org.tr/tr/pub/ejset / www.dergipark.org.tr/en/pub/ejset

Effect of microwave roasting and different solvents on the extraction of bioactive compounds from date seed

Gözde Doğanay [1,*], Hande Baltacıoğlu [2]

[1,2]*Niğde Ömer Halisdemir University, Food Engineering Department, 51240, Niğde, Türkiye*

Abstract

In this study, phenolic compounds were extracted from date seeds treated with different roasting methods (microwave (MW) and traditional) with three different solvents (water, acidic water, and alcohol), and their changes were investigated. The best results for total phenolic content (TPC) and antioxidant activity were given by 80% methanol (%1 HCI) solvent. The highest amount of TPC was determined in MW roasting at 300 W (7601.71 ± 155.759 mg GAE/100 g dry weight), followed by unroasted (7333.64± 3.12 mg GAE/ 100g dry weight) samples. On the other hand, traditional roasting was less effective than MW roasting at 300 W in terms of TPC, it had the highest antioxidant activity in all samples. HPLC results showed that date seeds contained individual phenolics like caffeic acid, p-cumaric acid, gallic acid, 3,4-dihydroxybenzoic acid, and rutin, and their amounts were affected by different roasting methods. As a multivariate analysis, PCA was a successful method for the classification of roasting treatments based on the bioactive compounds and antioxidant activity. According to these results, roasting had a significant effect on the extraction of phenolic compounds from date seed.

Keywords: Antioxidant activity, Date seed, Extraction, Microwave roasting, TPC

1 Introduction

The date palm (*Phoenix dactylifera* L.) is one of the oldest plants, cultivated and known to mankind, and has more than 2000 varieties. It has been grown in a wide geography including the Middle East and North Africa. Dates have been consumed as food for about 6000 years, and have different flavors, colors, and appearances [1]. Dates are mainly consumed as dried. Dates are a good source of dietary fiber, minerals (potassium, calcium, magnesium), and B and C vitamins with low fat and protein but high phenolic content [2], [3]. There are many phytochemical compounds in date seeds as well as dates. In contrast to the fruit, date seeds have a high phenolic, protein, and fat content [4]. The seed constitutes almost 13-15% of the fruit. Date seeds are mainly used as a supplement to animal feed. However, later studies have shown that date seeds have medicinal value due to their beneficial bioactive compounds [5]. There are several animal studies reporting biological effects of date seed such as lowering blood sugar as an anti-diabetic effect [6], improving Alzheimer's, memory and learning disorders [7], reducing oxidative damage [8]. Phytochemicals, found in date seeds include flavonoids, sterols, phenolic acids, and tocopherols. Phenolic compounds predominantly found in dates are ferulic acid, proanthocyanidins, p-coumaric acid, gallic acid, quercetin, and rutin [9]. In a study, it was determined that the total phenolic content in different date seeds ranged between 3102-4430 mg GAE/100 g fresh weight, and the antioxidant content ranged between 58,000-92900 µmol Trolox equivalents/100 mg fresh weight [10]. Bouhlali et al. [11] found that date seeds contain high levels (1224-1844 mg rutin equivalents/100g dry weight (DW)) of flavonoids and determined antioxidant activity of seeds, ranging from 10 to 23 mmol trolox equivalents/100 g DW for FRAP, 4-8 mmol trolox equivalents/100 g DW for ABTS, and 0.11-0.16 g/L for IC50 of DPPH.

Roasting is heating the seeds between 170-240 ºC for a certain time. With this process, changes in the color and structure of the seeds are observed and its unique aroma is formed due to various reactions [12]. In the literature, studies examine the effect of different roasting processes on the quality characteristics and bioactive components of coffee obtained from date seed [13], [14], [15]. In a study, palm seeds were roasted at 180, 200, and 220 °C for 20 minutes and it was observed that the highest antioxidant activity was determined in the sample roasted at 220 °C for 20 minutes [16]. In a study investigating the effect of roasting conditions on the physicochemical, chemical, and sensory properties of coffee obtained from date seeds, it was reported that roasting temperature and time were highly effective on quality and the optimum roasting temperature was 199.9 °C and the optimum roasting time was 21.5 minutes [12].

In recent years, microwave roasting has been applied as an alternative to traditional roasting due to the negative effects of high roasting temperatures and long processing times on quality [17]. In studies investigating the effect of microwave roasting on the physicochemical properties and bioactive properties of peanut and sesame seeds, it was determined that microwave roasting increased the antioxidant activity and total phenolic content compared to controls [17], [18]. Phenolic compounds are naturally present in the structure of fruits and vegetables as bioactive compounds and these compounds can be obtained by extraction with different solvents[19].

* Corresponding author, e-mail: gdoganay33@gmail.com (G. Doğanay)
Recieved: 17.01.2025 Accepted: 27.01.2025 Published: 30.01.2025
doi: 10.55696/ejset.1622241

In this study, date seeds were subjected to roasting at different power by microwave. Phenolic compounds in unroasted (control) and roasted (microwave and hot air oven) date seeds were extracted by classical solvent extraction method with water, acidic water (containing 1% HCl), alcohol (80% methanol containing 1% HCl). The effect of roasting processes on bioactive compounds was compared by determining total phenolic content and antioxidant activity (DPPH). Phenolic compounds were determined by HPLC and those change with the roasting process was examined. As a multivariate analysis, PCA was used for the classification of roasting treatments based on the bioactive compounds and antioxidant activity.

2 Material and methods

2.1 Material

Date seeds used in this study were obtained from local markets. All date seeds were stored at +4 °C until the production process.

2.2 Methods

2.2.1 Roasting

100 g of date seeds were weighed for each roasting process. The date seeds were heated in an oven at 180 ℃ for 20 minutes in the traditional roasting method. The microwave roasting process was carried out in a household microwave oven (Samsung MS23K3515AW) at different power and times. Roasting times were determined according to the degree of roasting and applied at 300 W for 12 minutes, 450 W for 6 minutes, 600 W for 5 minutes, and 800 W for 4 minutes. Unroasted seeds were used as control. Date seeds were ground with a grinder (HC100, Lavion, Türkiye) and passed from a 250 µm sieve.

2.2.2 Extraction of bioactive compounds

All samples were extracted with water, acidic water (containing 1% HCl), and alcohol (80% methanol containing 1% HCl) by classical solvent extraction at 30 °C for 6 hours. The centrifugation was done to the extracted samples at 5000 rpm for 20 minutes and filtered.

2.2.3 Total phenolic content (TPC)

Folin- Ciocaltaeu method was applied to the samples for determining TPC. The results were represented as gallic acid equivalent (mg GAE / 100 g dry weight) [19]. Extract (0.1 ml) was added on 0.75 ml of Folin- Ciocaltaeu (%10), and after waiting for 5 minutes, 0.75 ml of Na_2CO_3 (75 g/L) was added. After vortexing, the solution was kept in the dark under room conditions for 60 minutes and absorbance was read at 725 nm.

2.2.4 Antioxidant activity

Antioxidant activity was carried out using DPPH (1,1-diphenyl-2-picrylhydrazyl) radical. The extract (0.1 ml) and 3.9 ml of 0.1 mM DPPH solution (in 80% methanol) was mixed. After vortexing, the mixing solution was kept in the dark under room conditions for 30 minutes and the absorbance was recorded at 517 nm. 0.1 ml of methanol (80%) was used instead of the sample as a control under the same conditions. Antioxidant activity was calculated by Equation (1) as inhibition (%) [19].

$$\%\ Inhibition = \left[\frac{A_c - A_s}{A_c}\right] \text{x}100 \qquad (1)$$

Ac: Absorbance of control
As: Absorbance of sample

2.2.5 Determination of phenolic compounds by HPLC

HPLC was used to determine the phenolic compounds of the samples unroasted and roasted with traditional and microwave described by Okur et al. [20] with slight modifications. Before injection, the extracts were filtered through a 0.45 µm teflon membrane filter. Then, 20 µl of the filtered extracts were injected into the HPLC (Shimadzu Corporation, Kyoto Japan) with the SIL 10AD vp automatic sampling system. The HPLC system had a pump (LC-10ADvp), degasser (DGU-14A), control oven (CTO-10Avp), and a UV-VIS detector. Polyphenols were separated using a C18 column (GL Sciences, 250x4.60 mm, 5 microns, Japan). The column temperature was 30 °C. The separation was done by applying a gradient program with a binary solvent system. The mobile phases were 5% formic acid (A) and 20% A + 80% ACN (B). The flow rate was 1.0 ml/min. Phenolic compounds were carried out at 320 nm. The gradient program for phenolic compounds was applied as follows: 0–0.01 min: A 100%; 15 min: 90% A + 10% B; 90.00 min: 60% A + 40% B; 93.00 min: 100% B; 98 min: 100% A.

2.2.6 Multivariate analysis

Principal component analysis (PCA) was used to differentiate unroasted and roasted samples, and the results were presented as a score plot. PCA analysis was performed with the Minitab 17 (State College, PA, USA) program. The TPC and antioxidant activity of the samples were chosen as variables [19].

2.2.7 Statistical analysis

The Minitab (17.1.0.0, State College, PA, USA) was applied for the statistical analysis of the results. One-way ANOVA (analysis of variance) and Tukey's multiple range test were employed to determine the statistical differences.

3 Results and discussions

Roasted and unroasted samples were subjected to classical solvent extraction with different solvents. The TPC and antioxidant activity were determined in the extracted samples. The total phenolic content of unroasted and roasted samples extracted with different solvents was shown in Table 1.

According to Table 1, the highest TPC was determined in the sample subjected to microwave roasting at 300 W for 12 minutes ($p < 0.05$). The amount of TPC determined in the sample subjected to traditional roasting was lower than in the unroasted sample ($p < 0.05$).

Table 1. The TPC of unroasted and roasted samples extracted with different solvents

Treatment	TPC (mg GAE/100 g dry weight)		
	80% methanol (1% HCI)	Acidic water (1% HCI)	Water
Unroasted	7333.64± 3.12^{Aab}	542.10 ± 34.99^{Ca}	1331.32 ± 23.91^{Bb}
Traditional roasting	7139.43 ± 24.45^{Abc}	448.13 ± 12.85^{Ca}	1749.88 ± 21.85^{Ba}
MW roasting-300 W	7601.71 ± 155.75^{Aa}	231.98 ± 59.24^{Cb}	984.09 ± 85.73^{Cc}
MW roasting-450 W	6757.23 ± 153.99^{Ad}	484.77 ± 84.09^{Ca}	886.37 ± 51.49^{Cc}
MW roasting-600 W	6865.31 ± 223.55^{Acd}	428.36 ± 9.42^{Ca}	1335.71 ± 3.07^{Cb}
MW roasting-800 W	6789.30 ± 32.03^{Acd}	202.86 ± 48.76^{Cb}	1374.50 ± 105.87^{Cb}

Different uppercase letters (A, B, C) in the same line indicated a significant difference between the extraction solvents; Different lowercase letters (a, b, c) in the same column indicated a significant difference between the treatments

Table 2. The antioxidant activity of unroasted and roasted samples extracted with different solvents

Treatment	% inhibition		
	80% methanol (1% HCI)	Acidic water (1% HCI)	Water
Unroasted	49.18 ± 0.72^{Abc}	14.71 ± 1.75^{Ca}	18.93 ± 1.95^{Ba}
Traditional roasting	54.79 ± 0.15^{Aa}	14.25 ± 0.87^{Ba}	10.66 ± 0.93^{Cc}
MW roasting-300 W	46.81 ± 0.51^{Ac}	8.53 ± 0.61^{Bb}	9.88 ± 1.02^{Bc}
MW roasting-450 W	51.29 ± 1.18^{Aab}	7.45± 0.46^{Cb}	14.09 ± 0.30^{Bb}
MW roasting-600 W	48.92 ± 1.29^{Abc}	9.93 ± 0.26^{Bab}	10.25 ± 0.46^{Bc}
MW roasting-800 W	50.87 ± 2.11^{Aabc}	8.39± 1.08^{Cb}	18.82 ± 2.37^{Ba}

Different uppercase letters (A, B, C) in the same line indicated a significant difference between the extraction solvents; Different lowercase letters (a, b, c) in the same column indicated a significant difference between the treatments

The highest TPC in classical solvent extraction was determined with methanol in terms of solvents used. Similarly, methanol was found to be more effective than water for the extraction of phenolic compounds from date because the extraction of phenolic contents has been influenced by the polarity of extracting solvents [21] The antioxidant activity of unroasted and roasted samples extracted with different solvents was shown in Table 2.

Contrary to the TPC of the samples, the highest antioxidant activity was determined in the sample subjected to traditional roasting ($p < 0.05$). The antioxidant activity of the samples, treated with traditional roasting, was statistically higher than that of the samples, treated with microwave roasting. In the literature similar results reported that date seeds roasted with MW had higher antioxidant activity than those roasted with hot air [22] Similarly, it was determined that extraction with 50% methanol showed the highest total antioxidant activity compared to all other solvents [21]. Jdaini et al. (2023) [23]determined that binary extracts water-acetone and water-methanol revealed the highest antioxidant activity in date fruit. The sample, treated with MW roasting at 300 W showed the lowest antioxidant activity and this was significantly different from the results of the samples roasted with MW. The samples treated at 450 W, 600 W, and 800 W have antioxidant activity that are statistically similar to each other, but still different from the samples of unroasted and traditional roasting.

Phenolic compounds and their amounts determined by HPLC in roasted and unroasted samples were shown in Table 3. HPLC chromatogram of roasted and unroasted samples of date seed was shown in Figure 1.

Table 3. Phenolic compounds and their amounts in roasted and unroasted samples

	Gallic acid (mg/kg)	3,4-Dihydroxybenzoic acid (mg/kg)	Caffeic acid (mg/kg)	*p*-coumaric acid (mg/kg)	Rutin (mg/kg)
Unroasted	ND	ND	73.61 ± 1.04	18.14 ± 0.56^{a}	790.48±36.92^{a}
MW roasting-300 W	2936.91±136.31^{b}	690.42 ± 30.03^{b}	ND	15.57± 0.35^{b}	229.85 ±8.44^{b}
Traditional roasting	4907.45±108.34^{a}	1477.83 ± 63.60^{a}	ND	14.97± 1.04^{b}	97.34±1.50^{c}

ND: Not detected
Different letters (a, b, c) in the same column indicated a significant difference between the treatments

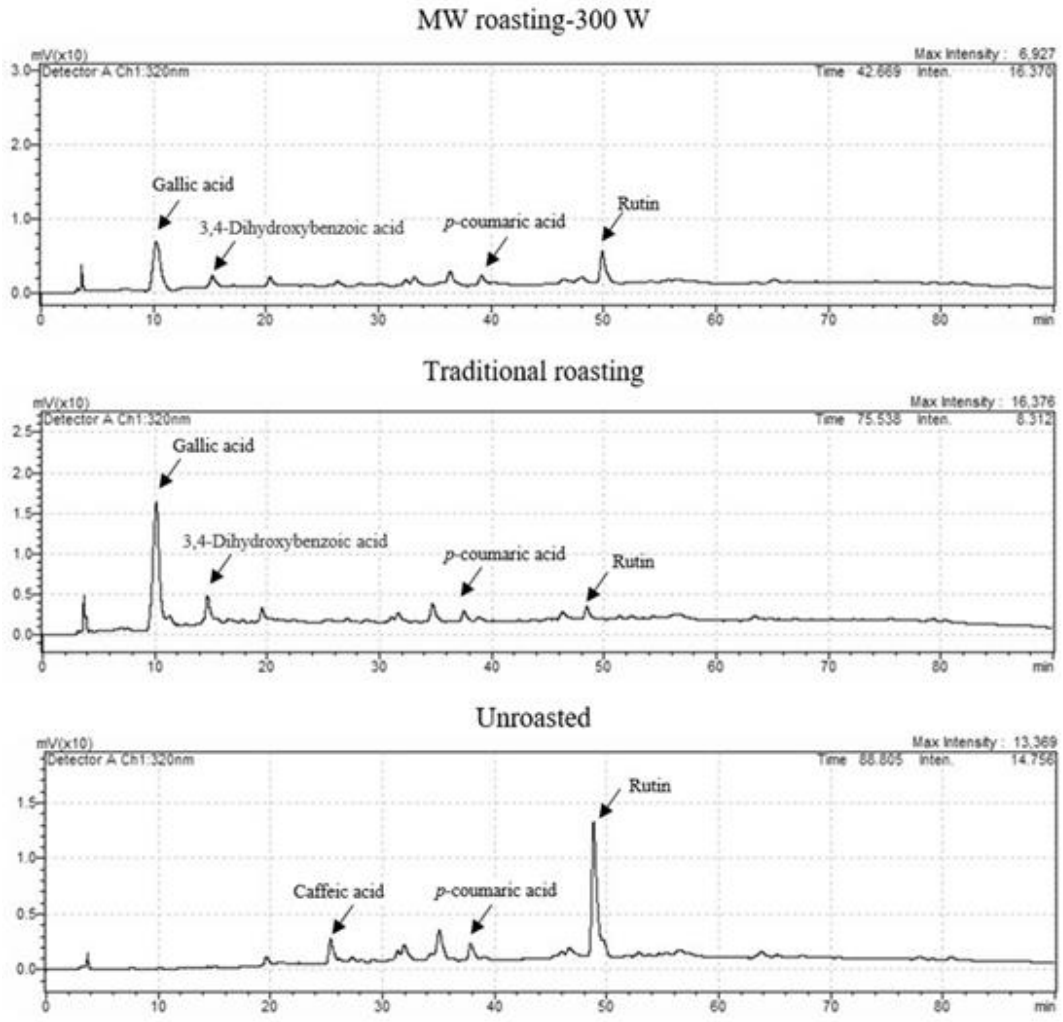

Figure 1. HPLC chromatogram of roasted and unroasted samples of date seed at 320 nm.

According to Table 3, the phenolic compounds detected in unroasted date seeds were caffeic acid, p-coumaric acid, and rutin, while gallic acid and 3,4-dihydroxybenzoic acid were found differently in roasted date seeds. Similarly determined that the dominant phenolic components of the roasting and unroasting date seed were (+)-catechin, 1,2-dihydroxybenzene, 3,4- dihydroxybenzoic acid, quercetin, syringic acid, and gallic acid [24] The effect of roasting on phenolic components in date seed showed significant changes ($p < 0.05$). The roasting process enables the release of phenolic compounds in the structure. Another research also reported roasting enables the release of polyphenols incorporated with various cellular components [22]. On the other hand, roasting caused a decrease in the amount of p-cumaric acid and rutin compounds. The phenolic compound determined in the highest amount in roasted samples was gallic acid. MW roasting was less effective than traditional roasting in terms of the release of bound phenolic compounds in the structure.

Principal component analysis (PCA) was used as a multivariate analysis and categorized the samples that were unroasted and roasted according to different methods based on the bioactive compounds (Figure 2).

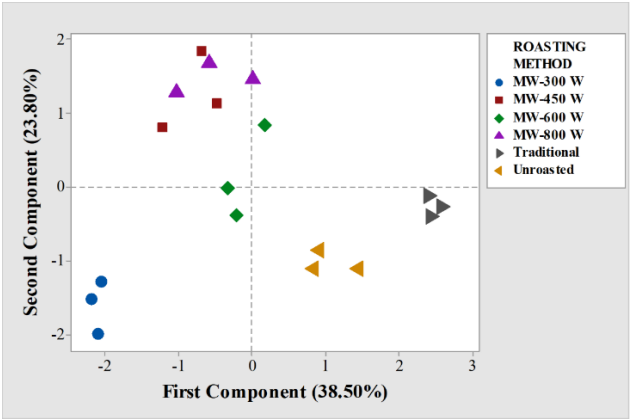

Figure 2. Score plot of two components for the effect of different roasting methods on the extraction of date seeds.

As shown in the PCA score plot, two principal components explained 62.20% of the total variance whereas the total variance was 38.50 % for PC1 and 23.80 % for PC2. The samples roasted by MW were mostly differentiated from the samples that were unroasted and roasted with the traditional method according to PC1. However, the samples

unroasted, roasted with MW at 300W, and traditional roasting were differentiated from those roasted with MW at 450, 600, and 800 W according to PC2. Similarly, PCA results revealed a positive relationship between antioxidant activity and phenolic compounds of date seed extracts roasted at 160 and 180 °C for 45 minutes [25].

4 Conclusions

According to our research, date seeds had high phenolic compounds and antioxidant activity. Among the solvents, 80% methanol (1% HCl) was selected as the best extraction solvent. Moreover, roasting had a significant effect on the extraction of phenolic compounds, the best results were obtained for TPC with MW roasting at 300 W and for antioxidant activity with traditional roasting. These results were in accordance with the PCA results. HPLC results showed that the roasting process caused the release of bound phenolic compounds in the structure like gallic acid and 3,4-dihydroxybenzoic acid. In further studies, the effects of new extraction techniques such as microwave and ultrasound on the extraction of phenolic compounds from roasted and unroasted date seeds can be investigated.

Acknowledgement

This research has been supported by the Scientific Research Projects Coordination Unit of Niğde Ömer Halisdemir University. Project Number: TGT 2023/14-LÜTEP.

Conflict of interest

The authors declare that there is no conflict of interest.

Similarity rate (iThenticate): 19%

References

[1] S. Ghnimi, S. Umer, A. Karim, and A. Kamal-Eldin, “Date fruit (Phoenix dactylifera L.): An underutilized food seeking industrial valorization,” *NFS Journal*, vol. 6, pp. 1–10, 2017. https://doi.org/10.1016/j.nfs.2016.12.001

[2] H. Taleb, S. E. Maddocks, R. K. Morris, and R. K. , K. A. D. Morris, “Chemical characterisation and the anti-inflammatory, anti-angiogenic and antibacterial properties of date fruit (Phoenix dactylifera L.),” *J Ethnopharmacol*, vol. 194, pp. 457–468, 2016. https://doi.org/10.1016/j.jep.2016.10.032

[3] A. H. El-Far *et al.*, “Date palm (Phoenix dactylifera): Novel Findings and future directions for food and drug discovery,” *Curr Drug Discov Technol*, vol. 16, no. 1, p. 2, 2019. https://doi.org/10.2174/1570163815666180320111937

[4] A. Golshan Tafti, N. Solaimani Dahdivan, and S. A. Yasini Ardakani, “Physicochemical properties and applications of date seed and its oil,” *Int Food Res J*, vol. 24, no. 4, pp. 1399–1406, 2017.

[5] S. S. Al Harthi, A. Mavazhe, H. Al Mahroqi, and S. A. Khan, “Quantification of phenolic compounds, evaluation of physicochemical properties and antioxidant activity of four date (Phoenix dactylifera L.) varieties of Oman,” *J Taibah Univ Med Sci*, vol. 10, no. 3, pp. 346–352, 2015. https://doi.org/10.1016/j.jtumed.2014.12.006

[6] Hasan M and Mohieldein A, “In vivo evaluation of anti diabetic, hypolipidemic, antioxidative activities of saudi date seed extract on streptozotocin ınduced diabetic rats,” *J Clin Diagn Res*, vol. 10, no. 3, 2016. doi: 10.7860/JCDR/2016/16879.7419

[7] F. Dehghanian *et al.*, “Date seed extract ameliorates β-amyloid-induced impairments in hippocampus of male rats,” *Biomedicine & Pharmacotherapy*, vol. 89, pp. 221–226, 2017. https://doi.org/10.1016/j.biopha.2017.02.037

[8] H. M. Habib, E. M. El-Fakharany, U. D. Souka, F. M. Elsebaee, M. G. El-Ziney, and W. H. Ibrahim, “Polyphenol-rich date palm fruit seed (Phoenix dactylifera L.) extract inhibits labile iron, enzyme, and cancer cell activities, and DNA and protein damage,” *Nutrients*, vol. 14, p. 3536, 2022. https://doi.org/10.3390/nu14173536

[9] S. Maqsood, O. Adiamo, M. Ahmad, and P. Mudgil, “Bioactive compounds from date fruit and seed as potential nutraceutical and functional food ingredients,” *Food Chem*, vol. 308, 2020. https://doi.org/10.1016/j.foodchem.2019.125522

[10] M. Al-Farsi, C. Alasalvar, M. Al-Abid, K. Al-Shoaily, M. Al-Amry, and F. Al-Rawahy, “Compositional andfunctional characteristics of dates, syrups, and their by-products,” *Food Chem*, vol. 104, pp. 943–947, 2007. https://doi.org/10.1016/j.foodchem.2006.12.051

[11] E. D. T. Bouhlali, C. Alem, J. Ennassir, M. Benlyas, A. N. Mbark, and Y. F. Zegzouti, “Phytochemical compositions and antioxidant capacity of three date (Phoenix dactylifera L.) seeds varieties grown in the Southeast Morocco,” *Journal of the Saudi Society of Agricultural Sciences*, vol. 16, pp. 350–357, 2017. https://doi.org/10.1016/j.jssas.2015.11.002

[12] M. Fikry *et al.*, “Effect of the roasting conditions on the physicochemical, quality and sensory attributes of coffee-like powder and brew from defatted palm date seeds,” *Foods*, vol. 8, no. 2, 2019. https://doi.org/10.3390/foods8020061

[13] S. Niazi *et al.*, “An overview: date palm seed coffee, a functional beverage,” *International Journal of Public Health and Health Systems*, vol. 2, no. 2, pp. 18–25, 2017.

[14] S. Warnasih, A. H. Mulyati, D. Widiastuti, Z. Subastian, L. Ambarsari, and P. Sugita, “Chemical characteristics, antioxidant activity, total phenol, and caffeine contents in coffee of date seeds (Phoenix dactylifera L.) of red sayer variety,” *The Journal of Pure and Applied Chemistry Research*, vol. 8, no. 2, pp. 179–184, 2019. DOI: 10.21776/ub.jpacr.2019.008.02.475

[15] B. Souda, R. Rami, B. Jalloul, and D. Mohamed, “Roasted date palm seeds (Phoenix dactylifera) as an alternative coffee: chemical composition and bioactive properties,” *Biomass Convers Biorefin*, 2020. DOI:10.1007/s13399-020-00896-7

[16] G. Atasoy, "Determination of the effect of different heat treatments on bioactive properties and the the production of date seed coffee," M. S. thesis, The Graduate School of Naturel and Applied Sciences of Selcuk University, Konya, 2019.

[17] R. K. Raigar, R. Upadhyay, and H. N. Mishra, "Optimization of microwave roasting of peanuts and evaluation of ıts physicochemical and sensory attributes," *J Food Sci Technol*, vol. 54, no. 7, pp. 2145–2155, 2017. https://doi.org/10.1007/s13197-017-2654-0

[18] I. A. Mohamed Ahmed *et al.*, "Effect of microwave roasting on color, total phenol, antioxidant activity, fatty acid composition, tocopherol, and chemical composition of sesame seed and oils obtained from different countries," *J Food Process Preserv*, vol. 44, 2020. https://doi.org/10.1111/jfpp.14807

[19] C. Baltacıoğlu, H. Baltacıoğlu, İ. Okur, M. Yetişen, and H. Alpas, "Recovery of phenolic compounds from peach pomace using conventional solvent extraction and different emerging techniques," *J Food Sci*, vol. 89, no. 3, pp. 1672–1683, 2024. https://doi.org/10.1111/1750-3841.16972

[20] I. Okur, C. Baltacıoğlu, E. Ağçam, H. Baltacıoğlu, and H. Alpas, "Evaluation of the effect of different extraction techniques on sour cherry pomace phenolic content and antioxidant activity and determination of phenolic compounds by FTIR and HPLC," *Waste Biomass Valorization* , vol. 10, p. 3545, 2019. https://doi.org/10.1007/s12649-019-00771-1

[21] W. Kchaoua, Abbès F, Blecker C, H. Attiaa, and Besbes S, "Effects of extraction solvents on phenolic contents and antioxidant activities of Tunisian date varieties (Phoenix dactylifera L.)," *Ind Crops Prod*, vol. 45, pp. 262–269, 2013. https://doi.org/10.1016/j.indcrop.2012.12.028

[22] Abdel-Karim N.A.A, E. A. A. Abdrabou, and Osman A.A.A, "Influence of roasting and microwave heating on nutritional value and bioactive compounds of siwi date seed," *J Food Sci*, vol. 52, no. 1, pp. 123–137, 2024. DOI: 10.21608/ejfs.2024.223982.1190

[23] K. Jdaini, Alla F, Mansouri F, Parmar A, and M. A. Elhoumaizi, "Optimizing the extraction of phenolic antioxidants from date palm fruit by simplex-centroid solvent mixture design," *Heliyon*, vol. 9, no. 1, p. e12738, 2023. https://doi.org/10.1016/j.heliyon.2022.e12738

[24] E. E. Babiker *et al.*, "Bioactive compounds, minerals, fatty acids, color, and sensory profile of roasted date (Phoenix dactylifera L.) seed," *J Food Process Preserv*, vol. 44, no. 7, Jul. 2020, doi: 10.1111/jfpp.14495. https://doi.org/10.1111/jfpp.14495

[25] Y. Halabi *et al.*, "Optimized roasting parameters of full-fat date palm seed (Phoenix dactylifera L.) using a central composite design and chemometric approach to prepare antioxidant-rich beverage," *Letters in Applied NanoBioScience*, vol. 13, no. 3, pp. 1–19, 2024. https://doi.org/10.33263/LIANBS133.113

Eurasian J. Sci. Eng. Tech., 2025; 6(1): 047-052

Eurasian Journal of Science Engineering and Technology

Research article

www.dergipark.org.tr/tr/pub/ejset / www.dergipark.org.tr/en/pub/ejset

Characterization of physiochemical properties of Cactus Cladodes (*Opuntia ficus indica*) grown in Antalya

Şehriban Gül Bağırsakcı[1], Salih Karasu[2], Erkan Karacabey[3,*]

[1,2,3] *Suleyman Demirel University, Food Engineering Department, Engineering and Natural Sciences Faculty, 32200, Isparta, Türkiye*
[2] *Yıldız Technical University, Chemical and Metallurgical Faculty, Food Engineering Department, 34210, İstanbul, Türkiye*

Abstract

In the current study, the main purpose is to determine the chemical and physical properties of cactus cladode grown in the rural region of Antalya, the Mediterranean region of Türkiye, since it reveals high-yield leaves for potential consumption. Physical and chemical properties were examined. The moisture content and dry matter did not show extra ordinary results, but its ash content emphasized it as a good source of minerals. Total sugar content (TSC) percent was higher than 5%. The functional bioactive components were determined as 8.85 mg/g dry matter, 1.97 mg/g dry matter, 2.43 mg/g dry matter, and 0.468 mg/g dry matter for the total phenolic content (TPC), the total flavonoid content (TFC), the total flavanol content as well as the ascorbic acid content (AAC), respectively. The results indicated that some of the features were superior compared to literature reports, but some were not. In any case, cactus cladodes from the Antalya region of Türkiye reveal high potential as an alternative source of food for human diet. Its carbohydrate content serves as an energy supply, whereas promising bioactive contents including TPC, TFC, total flavanol content and AAC present high potential as a functional nutrient for human consumption. High antioxidant capacity values also support those findings.

Keywords: Antioxidant capacity, Ascorbic acid, Flavonoid content, Phenolic content, Regional effect

1 Introduction

Starvation is the main problem which the humanity has to confront and needs to find solutions. One of the ways is to look for alternative nutritional sources. Towards this purpose, different types of sources have been released from animal and plant worlds. Those findings are promising sources, but increasing population of humanity leads to continue looking for more sources. Thus, more efforts in this way are still well-come.

Opuntia widely grows plant throughout the world, especially on north hemisphere, although it is an endemic plant type of the American continent [1]. It has started spreading from the American continent to the rest of the world, after Christophe Colomb discovered that continent and now it is possible to see the different species of *Opuntia* everywhere. The spreading of this plant in this wide regional areas all over the world is related to its adaptation ability to extremely ranged climatic and/or soil conditions. Thus, this makes it available for human diet and it goes back to ancient times. For example, before the discovery of the American continent by European explorers, continent's hosts had been harvesting *Opuntia* species more than 9000 years [2]. In other words, *Opuntia* species are important nutritional source of human diet in different forms. However, at this point, it is worth to emphasize that it is not common as a diet for most of the cultures except for the American continent, although it is easy to find and harvest. But this does not mean that it is never consumed out of the American lands. This is not to be avoidable for humanity for a long time, only means to need an extra time to re-discover it for human diet.

As mentioned above, beside of the American continent, it grows in the wide land of world from Mediterranean to Middle & South Africa, and Middle East countries, even in India as well as in Australia [3]. Additionally, *Opuntia* species are cultivated in those regions, especially on the American lands. The total area where *Opuntia* species grow wildly or are cultivated is more than three million hectares [4].

One of the most harvested and consumed species is *Opuntia ficus indica*. It is cultivated in 26 countries [4], since it is the most common species of *Opuntia* which is traded in the world [2]. Additionally, *Opuntia ficus indica* is the well-known species and the products originating from *O. ficus indica* are spread all over the world [3]. Although different parts of this plant species are consumed, the most common part for consumption is its leaves known as Cactus Cladode. Cladode yield from *Opuntia ficus indica* has been reported to vary in the range of 30 – 80 tones/hectare depending on the climatic and soil conditions and region and species [5]. However, new taste and/or source always creates a doubt for consumers before consuming new food for the first time, since it may cause serious problems especially due to directly taken into the human body from the intestinal system. Thus, researchers need to investigate any source for human consumption from all aspects. In this context, nutritional and functional potential as well as physical properties are examined and the findings are shared from different channels

* Corresponding author, e-mail: erkankaracabey@sdu.edu.tr (E. Karacabey)
Recieved: 20.01.2025 Accepted: 23.01.2025 Published: 30.01.2025
doi: 10.55696/ejset.1623788

to inform consumers and to make them feel comfortable towards consumption.

In the current study, the main purpose is to discover the chemical and physical properties of Cactus cladode grown in the rural region of Antalya, Mediterranean region of Türkiye, since it reveals high-yield leaves for potential consumption. According to our best knowledge, there are scare number of studies about Cactus cladode grown around Antalya city [6-8] and this study serves to fill that gap in the literature.

2 Material and methods

2.1 Material

Cactus cladodes *Opuntia ficus indica* were harvested in the region be rural area of Yeşilkaraman Village, Aksu, Antalya, Mediterranean Region, Turkiye. Cladode selection were performed according to maturity and shape levels and they were considered to have uniform in those criteria. Until analysis, cladodes were stored at -18°C.

2.2 Analysis

2.2.1 Physical analyses

2.2.1.1 Moisture content

Cactus cladode was subjected to measurement of moisture content. Sample moisture content was measured gravimetrically by using moisture determination equipment (Kern 085, DBS 60-3, Germany) [9].

2.2.1.2 Color measurement

The surface color of the cladode sample was measured using a colorimeter (High-Quality Colorimeter, 3nh, China) and color parameters of CIE were given as L*, a*, and b* [10]. Chroma (C*) and hue values were calculated from the measured color parameters according to the below equations (Equation (1) and (2)).

$$C^*=(a^{*2}+b^{*2})^{1/2} \quad (1)$$

$$Hue°=\tan^{-1}(b^*a^*) \quad (2)$$

2.2.1.3 Texture analysis

Cactus cladode was sliced, before textural analysis. Slice thickness was 5 mm. As textural properties, skin strength and elasticity values of cactus cladode were measured using a texture equipment (Stable Micro Systems, England). Puncture test was performed and the text parameters were adjusted as 1 mm/sec of speed using a 2 mm P/2 prob.

2.2.1.4 Ash content

Ash content of cladode sample was determined by the method by Williams [11]. Amount of the sample was weighted into a dried/pre-weighed porcelain crucible. Burning of sample was carried in an ash furnace at 550±50°C for 6-7 hours until all organic materials was burned off. Ash content was expressed as a percentage of difference in weight before and after analysis.

2.2.2 Chemical analyses

2.2.2.1 Extraction of bioactives

Extraction procedure reported by Ammar et al. [12] was carried to extract bioactive constituents from cactus cladode. Before extraction, sample was sliced and 2 g of sample was transferred into a glass jar and 20 mL of methanol was added as an extraction solution. The mixture was homogenized for 1 min and transferred into an extraction cell. Extra 10 mL of methanol was used to wash out the remaining particles from the glass jar to the extraction cell. Extraction was carried out on a magnetic stirrer for 2 hours. Liquid phase was separated by filtering the extraction medium through filter paper and filtrate was also centrifuged at 4000 rpm for 10 min at 4°C.

2.2.2.2 Determination of total phenolic content

Total phenolic content (TPC) of cladode sample was determined by Folin–Ciocalteu method [13]. In order to determine TPC, the extract obtained in the previous extraction step was used and the absorbance measurement was performed at 765 nm using a spectrophotometer (T70+UV/VIS spectrophotometer, PC Ins., England). Standard curve was prepared using gallic acid standard and the result was given as mg GAE/ 100g dry matter.

2.2.2.3 Determination of flavonoid content

Methanolic extract was evaporated and dissolved by ethanol before flavonoid analysis. Total flavonoid content (TFC) was determined according to the method by Zaporozhets et al. [11]. Rutin was used as a standard material. TFC of the sample was spectrophotometrically measured at 510 nm and given as mg RE/g dry matter [14].

2.2.2.4 Determination of flavanol content

Similar to TFC, ethanolic extract was used to determine total flavanol content of the cladode sample by reading absorbance at 440 nm (T70+UV/VIS spectrophotometer, PC Ins., England) [15]. The standard curve was prepared using rutin as a standard material and the result was given as mg RE/ g dry matter.

2.2.2.5 Phenolic profile analysis

The phenolic profile of the cladode sample was determined chromatographically using HPLC (LC-20AD pump, SPDM20A DAD detector, SIL-20A HT autosampler, CTO-10ASVP column oven, DGU-20A5R degasser, and CMB-20A communication module), (HPLC-DAD, Shimadzu Corp., Kyoto, Japan). The procedure followed was reported by Karadag et al. [16]. A gram of sliced cladode sample was extracted in a 16 mL of methanol for 2 hours and the extract was filtered through a syringe filter (0.45µm) into an amber vial. Each phenolic was given as mg/g dry matter. The mobile phase was 0.1% of Acetic acid (v/v), 0.1% Acetonitrile (v/v) and gradient flow program was applied (Table 1). Inertrsil® ODS C-18 (250×4.6 mm, ID: 5 µm) was used and the column oven temperature was 40°C. The flow rate was 1 mL/min, duration was 63 min, and injection volume was 1 mL. The detection of phenolics was monitored at 278, 320, and 360 nm.

Table 1. Gradient program of phenolic profile analysis

Time (min)	Mobil Phase A-Acetonitrile (%)
0	10%
2	10%
27	30%
50	90%
60	100%
63	10%

2.2.2.6 Ascorbic acid analysis

The ascorbic acid content (AAC) of cladode sample was determined by HPLC [17]. Three gram of sample was mixed with metaphosphoric acid (4.5%) at volume ratio of 1:12.5, and mixture was homogenized. The extraction medium was centrifuged at 4000 rpm at 4°C for 20 min. The supernatant was filtered through a syringe filter of 0.45µm and 20µL of filtrate was injected to HPLC (Agilent 1260 Infinity, Agilent, USA). Agilent XBD C18 (250*4.6 mm, ID: 5 µm) was used as a column and detection was done at 254 nm at column oven temperature of 30°C. Flow rate was 0.8 mL/min. The total flow duration was 35 min. The flow program was isocratic. L-ascorbic acid was used as a standard. The ascorbic acid content of the sample was given as mg/kg dry matter.

2.2.2.7 Antioxidant content

Two antioxidant activity measurement methods were carried out to determine the antioxidant potential of cladode sample.

α, α-diphenyl-β-picrylhydrazyl (DPPH•) Assay:

Free radical scavenging activity (DPPH) of the cladode sample was determined according to the method by Dorman et al. [18]. A 50 µL of methanolic extract was mixed with 450 µL of reactant (Tris-HCl, 50mM, pH 7.4). One mL of 0.10 mM DPPH• (α, α-diphenyl-β-picrylhydrazyl) was added to the solution and the mixture was incubated at room temperature under dark. Absorbance of sample was read at 515 nm using a spectrophotometer (T70 + UV / VIS spectrophotometer, PG Instruments, England). % inhibition of sample was determined using Trolox standard curve and the result was given as µmol TEAC/g dry matter.

2,2'-azinobis (3-ethylbenzothiazoline-6-sulphonic acid (ABTS•+) Assay:

Antioxidant potential of cladode by ABTS assay was determined following the method by Re et al. [19]. In the analysis 7 mM ABTS•+ solution including 2.45 mM potassium persulphate was prepared and the solution was kept for 12-16 hours to form ABTS•+ radicals. Reading was performed at 734 nm using a spectrophotometer (T70 + UV / VIS spectrophotometer, PG Instruments, England). Initial and 6 min later absorbance values of sample was read and the percent reduction was calculated. The result was given as µmol TEAC (Trolox® equivalent antioxidant capacity)/ g dry matter.

2.2.2.8 Determination of total sugar content

Total sugar content (TSC) of cladode was determined by Lane-Eynon method [20]. The result was given as g/100g dry matter.

3 Results and discussions

Current study investigated cactus cladode (*Opuntia ficus indica*) as a potential nutritional source for human diet. For this purpose, first of all physical and chemical properties of cladode sample is required to be defined. Thus, those relevant parameters were analyzed and the cladode sample results were measured. Analyzed properties were mainly classified into two groups. Table 2 summarized the group one being the representation of physical properties.

Table 2. Physical properties of Cactus cladode (*Opuntia ficus indica*)

Physical Properties	Measured Value
Moisture content,%	92.25 ± 0.01
Dry matter, %	7.75 ± 0.01
Ash content, mg/g dry matter	213.23±2.50
Ash percent, %	21.91±0.12
L*	42.42±10.16
a*	-2.04±3.61
b*	23.44±4.66
C*	28.17±4.90
Hue	94.59±9.39
Skin strength, g.force	187.17±0.07
Elasticity, mm	2.61±0.01

All the results were the mean of three replicates with standard deviation.

The moisture content of the cladode sample was higher than 90%. In literature cladode moisture content of *Opuntia ficus indica* was reported as being around 90% [21-22]. Our finding was coincidence with those results. As well known that, water is the most significant molecule of biological materials, since it is required to manage biochemical reactions and microbiological activities. Thus, having information about moisture content makes it be evaluated for any purpose like processing, cooking, and/or consumption. Dry matter content of cladode sample was also determined based on moisture content. Thus, it can be evaluated this product as a low dry matter plant material. This was considered as a significant property, since that low level requires specific process conditions (for example: high temperature level, long process time for drying). The results of mineral content of cladode and its percent level (>20%) indicated that this plant material is a good source of minerals, but the current results do not reveal details like which minerals were rich in the sample. Thus, further study in this context is required. Percent ash value have been studied and reported results were in the range of 20-25% [21, 23]. The ash percent of cactus cladode in the current study was also in that range. Another important parameter is the cladode surface color. Color parameters were seen to be suitable for a green leaf plant material. Cladodes have a moderate lightness. However, higher lightness value (>65) was reported [24]. Difference from literature one may be attributed to climatic conditions, soil, and regional differences. Due to its surface observed color, a value is too low, whereas b value is high. Ayadi et al. [24] reported a* and b* values as −8.17±0.74 and 25.15 ± 0.61. These results of color parameters were very close to the results of the current study. Additionally, these color parameters are

coincidence with green leaf vegetables in general manner. As being another important color parameter, it is well-known that the hue value is the better representation of the color parameter being close to real observation. In the current study, hue value was calculated as more than 90. In other words, it was very close to the green representation level of hue value (120). Textural properties are important in terms of processing and consumption. Skin strength and elasticity values were seen to be around 187 g. force and 2.61 mm, respectively. If the skin strength was too high, it would be hard to process, consume etc. Similarly, elasticity was also important, since it is a response of the sample against to outer forces.

Another group of properties is chemical ones which are important to evaluate any diet source from nutritional and functional aspects. Thus, the chemical analysis was carried and the amount of some important constituents were measured. The calculated results were given in Table 3.

Table 3. Chemical properties of Cactus cladode (*Opuntia ficus indica*)

Chemical Properties	Measured Value
TSC, g/100 g dry matter	5.63±0.19
TPC, mg GAE/g dry matter	8.85±1.12
TFC, mg RE/g dry matter	1.97±0.01
Total flavanol content, mg RE/g dry matter	2.43±0.82
AAC, mg/g dry matter	0.468±0.006
DPPH, µmol TEAC/g dry matter	17.42±1.42
ABTA, µmol TEAC/g dry matter	54.26±2.00

TSC: Total sugar content; TPC: Total phenolic content; TFC: Total flavonoid content; AAC: Ascorbic acid content. All the results were the mean of three replicates with standard deviation.

As can be seen from Table 3, TSC of the cactus cladode sample was the first parameter and it was more than 5% of solid matrix. This value was corresponding to the soluble sugar % and it was found to be coincidence with the literature value published by Ayadi et al. [24]. In that study, total soluble sugar percent was given in the range of 2-6%, which changed depending on species.

The functional potential of any nutrient is another topic on which researchers should focus on and perform on a detailed investigation. Because besides of nutritional contribution to the human diet, food sources should provide functionality managed by its constituents. Phenolics is coming first in this extent, especially for plant-based food sources. Therefore, TPC, TFC, total flavanol content, and AAC were examined and the measured results were given in Table 3. Ayadi et al. [24] also analyzed the total phenolic content of cladodes for two different species. One of them was *Opuntia ficus indica*. The TPC was reported to vary in the range of 825.81 - 975.82 mg /100 g dry matter and this result was compatible with our finding which was equivalent to 885 mg/100 g dry matter. However, cladode belonging to *Opuntia ficus indica* was reported to have lower TPC (varied from 168.6 to 185.8 mg/100g dry matter) compared to the current result. The difference may be attributed to the regional difference, since the variety used in the study was grown in Korea [23]. TFC was also under investigation and the calculated result was found to be higher than the published one (0.81-1.29 mg/g dry matter) by Lee at al. [23]. Similar to TPC values, it was found that cactus cladode grown in Antalya region was a flavonoid-rich source compared to that grown in Korea. Although it is not common in the literature, total flavanol content was also determined in the current study and the result indicated that this group is 23% higher than flavonoids (Table 3). Finally, ascorbic acid was considered in this study and AAC of the cladode sample was determined. Ascorbic acid is a significant vitamin and being in the human diet makes people healthier, since it contributed to the body's self-defense system. Generally, it is sensitive to environmental conditions like temperature, oxidation etc. Thus, its good source has been taken consumer and researcher interests. In our study, this vitamin was detected at the level of 0.468 mg/g dry matter. The AAC of cladode has been extensively in the literature, as well. Chiteva and Wairagu [25] have declared the AAC of *Opuntia ficus indica* cladode sample as 5.17 ± 0.06 mg /100 g dry matter. This AAC value was lower than that found in the current study. In another study, literature survey was performed and the published review gave information about AAC of cladode, as well [26]. In that review, the range was declared as 7-22 mg/100g dry matter. Our finding was also higher than that published range. On the other hand, Lee et al. [20] have reported a compatible AAC result (71.2 mg/100 g dry matter) for cactus cladode compared to that value in the current study. Aragona et al. [27] have revealed the AAC of cactus cladode as 29 mg/100 g. This amount of AA was lower than the achieved result in the current study.

The antioxidant activity potential of cactus cladode was evaluated by two assays; DPPH and ABTS+ methods. The results of DPPH and ABTS+ were found to be as 17.42±1.42 µmol TEAC/g dry matter and 54.26±2.00 µmol TEAC/g dry matter, respectively. Bioactive compounds of *Opuntia ficus indica* plant parts including cladode may act as electron donors to convert free radicals to more stable products, and this has shown that the scavenging effect increases with the concentration of polyphenols [28]. Opuntia plant part also includes flavanol glycosides and it has been proven that those bioactives reveal a potential as an additive in food and cosmetic, as well as pharmaceutical industries due to their antioxidant power [29].

Besides of bioactive content of cladode sample, its phenolic profile has been also examined and resulted phenols were summarized in Table 4.

As in the literature some of the phenolics (ferulic and qumaric acid) are common with the current study that revealed phenolics, but some reported ones in this study have not been seen in literature [26]. It is well-known that phenolics are secondary metabolites of plants against attacks coming from outside to protect its self. Thus, the phenolic profile is totally dependent on the environmental conditions, whether the plant material has been under microbial attack or not, etc. Thus, an identical profile definition is not possible for phenolic profile of the plant materials.

Table 4. Dominant phenolic compounds detected in the cactus cladode of *Opuntia ficus indica*

Ellagic acid	Caffeic acid	p-Qumaric acid	Ferulic acid
3.988±0.0034	2.196±0.006	0.265±0.008	1.050±0.070

All the results were the mean of two replicates with standard deviation.

4 Conclusions

The results of the current study help to characterize the physiochemical properties of cactus cladode grown in Antalya, Mediterranean Region of Türkiye. One of the biggest problems that the world faces is the starvation and increasing population of humanity, and limited sources of food have pushed researchers to look for alternatives. The raw material of the current study has been evaluated in this extent, and the results were found to be promising towards this purpose. However, this study is only accepted as a first step since only the characterization of the physiochemical properties of cladodes was considered in it. However, to accept it as an alternative, it should be investigated from all aspects, like processing, storage, transport, and its availability for the human intestine system. Thus, the current study was classified former step of this area and more efforts should be required in near future to make picture more clear for humanity.

Conflict of interest

The authors declare that there is no conflict of interest.

Similarity rate (iThenticate): 20%

Acknowledgement

This research was financially supported by "Süleyman Demirel University Scientific Research Projects Office," in Türkiye (Project number: FDK-2019-7364).

References

[1] López, R., De Ita, A., Vaca, M., "Drying of Prickly Pear Cactus Cladodes (Opuntia Ficus Indica)," Forced Convection Tunnel. Energy Conversion and Management, vol. 50, no. 9, pp. 2119-2126, 2009. https://doi.org/10.1016/j.enconman.2009.04.014.

[2] Griffith, M.P., "The Origins of an Important Cactus Crop, Opuntia Ficus-Indica (Cactaceae): New Molecular Evidence", American Journal of Botany, vol. 91, no. 11, pp. 1915-1921, 2004. https://doi.org/10.3732/ajb.91.11.1915.

[3] Stintzing, F.C., Carle, R., "Cactus Stems (Opuntia Spp.): A Review on Their Chemistry, Technology, and Uses", Molecular Nutrition Food Research, vol. 49, no. 2, pp. 175-194, 2005. https://doi.org/10.1002/mnfr.200400071.

[4] Msaddak, L., Abdelhedi, O., Kridene, A., Rateb, M., Belbahri, L., Ammar, E., Nasri, M. Zouari, N., "Opuntia Ficus-Indica Cladodes as a Functional Ingredient: Bioactive Compounds Profile and Their Effect on Antioxidant Quality of Bread," Lipids in health disease, vol. 16, no. 1, pp. 1-8, 2017. https://doi.org/10.1186/s12944-016-0397-y.

[5] López-Cervantes, J., Sánchez-Machado, D.I., Campas-Baypoli, O.N., Bueno-Solano, C., "Functional Properties and Proximate Composition of Cactus Pear Cladodes Flours," Food Science Technology, vol. 31, no. 3, pp. 654-659, 2011. https://doi.org/10.1590/S0101-20612011000300016.

[6] Kendir, G., & Köroğlu, A., "Cladode and fruit anatomy of Opuntia ficus-indica (L.) Miller in Türkiye", ACTA Pharmaceutica Sciencia, vol. 62, no. 1, 2024. https://doi.org/10.23893/1307-2080.APS6204.

[7] Yılmaz, C., Türkay, C., Toplu, C., Seday, Ü., Zurnacı, M. "Doğu Akdeniz Bölgesinde Dikenli İncir(Opuntia ficus- indica L.) Genetik kaynaklarının Toplanması, Muhafazası, Değerlendirilmesi ve çeşit olabilecek Tiplerinin Belirlenmesi", Program Kodu: 1001. TÜBİTAK TOVAG Proje 1110135, 2014: pp. 1-99, 2014.

[8] Yılmaz, C., "Dikenli İncir (Opuntia ficus-indica L.) Yetiştiriciliği".Tarım Türk Dergisi, vol. 24, pp. 14-16, 2010.

[9] Lee, M., Chemists, A.o.O.A., "Official Methods of Analysis of AOAC International (16th Edn): Edited by Patricia A. Association of Official Analytical Chemists, Washington, 1995.

[10] Kulcu, R., "Determination of the Effects of Different Packaging Methods and Materials on Storage Time of Dried Apple", International Journal of Science Technology, vol. 4, no. 2, pp. 238-255, 2018. https://doi.org/10.20319/mijst.2018.42.238255.

[11] Williams, S., "AOAC Official Methods of Analysis, Arlington", VA, 1984.

[12] Ammar, I., Ennouri, M., Attia, H., "Phenolic Content and Antioxidant Activity of Cactus (Opuntia Ficus-Indica L.) Flowers Are Modified According to the Extraction Method", Industrial Crops and Products, vol. 64, pp. 97-104, 2015. https://doi.org/10.1016/j.indcrop.2014.11.030.

[13] Matthäus, B., "Antioxidant Activity of Extracts Obtained from Residues of Different Oilseeds", Journal of Agricultural and Food Chemistry, vol. 50, no. 12, pp. 3444-3452, 2002. https://doi.org/10.1021/jf011440s.

[14] Zaporozhets, O.A., Krushynska, O.A., Lipkovska, N.A., Barvinchenko, V.N., "A New Test Method for the Evaluation of Total Antioxidant Activity of Herbal Products", Journal of Agricultural Food Chemistry, vol. 52, no. 1, pp. 21-25, 2004. https://doi.org/10.1021/jf0343480.

[15] Yermakov, A., Arasimov, V., Yarosh, N., "Methods of Biochemical Analysis of Plants", Kolos, Agropromizdat, Leningrad, 1987.

[16] Karadag, A., Bozkurt, F., Bekiroglu, H., Sagdic, O., "Use of Principal Component Analysis and Cluster Aanalysis for Differentiation of Traditionally-Manufactured Vinegars Based on Phenolic and Volatile Profiles, and Antioxidant Activity", Polish Journal of Food and Nutrition Sciences, vol. 70, no. 4, 2020. https://doi.org/10.31883/pjfns/127399.

[17] Demiray, E., Tulek, Y., Yilmaz, Y., "Degradation Kinetics of Lycopene, B-Carotene and Ascorbic Acid

in Tomatoes During Hot Air Drying", LWT-Food Science Technology, vol. 50, no. 1, pp. 172-176, 2013. https://doi.org/10.1016/j.lwt.2012.06.001.

[18] Dorman, H., Peltoketo, A., Hiltunen, R., Tikkanen, M., "Characterisation of the Antioxidant Properties of De-Odourised Aqueous Extracts from Selected Lamiaceae Herbs", Food chemistry, vol. 83, no. 2, pp. 255-262, 2003. https://doi.org/10.1016/S0308-8146(03)00088-8.

[19] Re, R., Pellegrini, N., Proteggente, A., Pannala, A., Yang, M. Rice-Evans, C., "Antioxidant Activity Applying an Improved Abts Radical Cation Decolorization Assay. Free Radical", Biology and Medicine, vol. 26, no. 9-10, pp. 1231-1237, 1999. https://doi.org/10.1016/S0891-5849(98)00315-3.

[20] Hildreth, A.C., Brown, G.B., "Modification of Lane-Eynon Method for Sugar Determination", Journal of the Association of Official Agricultural Chemists, vol. 25, pp. 775-778, 1942. https://doi.org/10.5555/19421401811.

[21] Torres, L. G., Cadena, G., Carpinteyro-Urbán, S., & Corzo, L. J., "New galactomannans and mucilages with coagulant–flocculant activity for an environment-friendly treatment of wastewaters", Current Advances in Environmental Science, vol. 2, no. 2, pp. 52-58, 2014.

[22] El-Safy, F. S., "Evaluation and utilization of cladodes flour in formulating functional sponge cake", World Applied Sciences Journal, vol. 27, no. 4, pp. 512-523, 2013. https://doi.org/10.5829/idosi.wasj.2013.27.04.81117.

[23] Lee, Y. C., Hwang, K. H., Han, D. H., & Kim, S. D., "Compositions of Opuntia ficus-indica", Korean Journal of Food Science and Technology, vol. 29, no. 5, pp. 847-853, 1997.

[24] Ayadi, M. A., Abdelmaksoud, W., Ennouri, M., & Attia, H., "Cladodes from Opuntia ficus indica as a source of dietary fiber: Effect on dough characteristics and cake making", Industrial Crops and Products, vol. 30, no. 1, pp. 40-47, 2009. https://doi.org/10.1016/j.indcrop.2009.01.003.

[25] Chiteva, R., & Wairagu, N., "Chemical and nutritional content of Opuntia ficus-indica (L.)", African Journal of Biotechnology, vol. 12, no. 21, 2013.

[26] Shoukat, R., Cappai, M., Pia, G., & Pilia, L., "An updated review: Opuntia ficus indica (OFI) chemistry and its diverse applications", Applied Sciences, vol. 13, no. 13, 2023, Art no. 7724. https://doi.org/10.3390/app13137724.

[27] Aragona, M., Lauriano, E. R., Pergolizzi, S., & Faggio, C. J. N. P. R., "Opuntia ficus-indica (L.) Miller as a source of bioactivity compounds for health and nutrition", Natural product research, vol. 32, no. 17, pp. 2037-2049, 2018. https://doi.org/10.1080/14786419.2017.1365073.

[28] Chougui N, Louaileche H, Mohedeb S, Mouloudj Y, Hammoui Y, Tamendjari A., "Physico-chemical characterisation and antioxidant activity of some Opuntia ficus-indica varieties grown in North Algeria", Afr J Biotechnol., vol. 12, pp. 299–307, 2013. https://doi.org/10.5897/AJB12.1946.

[29] Benayad Z, Martinez-Villaluenga C, Frias J, Gomez-Cordoves C, Es-Safi NE., "Phenolic composition,antioxidant and anti-inflammatory activities of extracts from Moroccan Opuntia ficus-indica flowersobtained by different extraction methods", Ind Crop Prod., vol. 62, pp. 412–420, 2014. https://doi.org/10.1016/j.indcrop.2014.08.046.

Eurasian J. Sci. Eng. Tech., 2025; 6(1): 053-060

Eurasian Journal of Science Engineering and Technology

Review article

www.dergipark.org.tr/tr/pub/ejset / www.dergipark.org.tr/en/pub/ejset

A traditional food: *Köfter* (*Köftür*), A grape-based central Anatolian dessert

Ayşenur İnce [1,*], Hande Baltacıoğlu [2], Hasan Tangüler [3], Hasan Uslu [4]

[1,2,3,4] *Niğde Ömer Halisdemir University, Food Engineering Department, 51240, Niğde Türkiye*

Abstract

Grape (*Vitis vinifera*) is a widely cultivated and highly consumed agricultural product around the world. Owing to their high content of sugars, vitamins, minerals, and antioxidants, they hold an important place in human nutrition. In addition to being consumed raw or dried, due to their perishable nature, grapes are processed into various fruit-based products to extend their shelf life and make them available for consumption throughout the year. *Köfter (köftür)* is a traditional Turkish product prepared using grape juice, wheat flour, and starch. In Central Anatolia, particularly in provinces such as Nevşehir (Cappadocia) and Niğde, *köfter* is one of the most consumed snacks, especially during the winter months, and has a tradition of widespread production and consumption. *Köfter* is made by boiling grape juice obtained from high-yielding white grapes, adding wheat flour and starch, cooking the mixture to form a gel-like structure, and then spreading it onto trays to dry in the sun for several days. The dried *köfters* are stored in special containers produced from clay, allowing their surfaces to be coated with a thin layer of crystallized sugar. With its high nutritional value and energy-boosting properties, *köfter* offers a healthy snack alternative. Its unique texture and flavor make it an important product in Türkiye's cultural heritage. This review article was written to help conduct new research, preserve the traditional value of *köfter* in Turkish cuisine, and introduce it to more people.

Keywords: Grape, Snack, Traditional food, Köfter

1 Introduction

Grape (*Vitis vinifera)* is one of the oldest fruits in the World, an agricultural product which has a wide production area all over the World and has a high economic and nutritional value [1, 2]. Countries such as China, the USA, Chile, Iran, Iran, South Africa and Türkiye are among the leading countries in grape cultivation in recent years [3]. Türkiye ranked fourth among these countries in 2022 and agriculture of grape is very important for the Turkish economy [3]. Although grape production in Türkiye varies by year, it was 4,100,000 tons in 2019, 4,208,908 tons in 2020, 3,670,000 tons in 2021, 4,165,000 tons in 2022 and 3,400,000 tons in 2023 [4]. Grapes are composed of water, sugars, minerals, organic acids, nitrogenous compounds, aromatic substances, enzymes, vitamins, and phenolic compounds [5].

The primary sugars in grapes are glucose and fructose, which are important in human nutrition due to their ability to diffuse directly into the bloodstream. Additionally, grapes are rich in essential minerals such as potassium (K), calcium (Ca), phosphorus (P), sodium (Na), iron (Fe), and magnesium (Mg). Grapes predominantly contain two major acids: tartaric acid and malic acid, which together constitute 70-90% of the total acids in the fruit. Among the nitrogenous compounds present, glutamic acid, arginine, threonine, and proline collectively constitute 85% of the amino acids found in grapes. When examining the vitamin content of fresh grapes, it is seen that they are rich in inositol and thiamine (B_1). Additionally, it contains pantothenic acid (B_5), niacin, pyridoxine (B_6), biotin, folic acid, and small amounts of riboflavin (B_2) [5]. Grapes are rich in phenolic compounds such as catechins, gallic acid, myricetin, quercetin, kaempferol, and coumaric acid, along with anthocyanins and other flavonoids. These bioactive compounds contribute to various health benefits, including antioxidants, cardioprotective, anticancer, anti-inflammatory, and antiallergenic effects. The presence of these compounds highlights the potential of grapes to support human health and prevent chronic diseases, emphasizing their importance in a balanced diet [2]. Table, wine and dried grapes are produced according to the type of consumption [4]. Grape is a fruit that can be perishable quickly and its nutritional value decreases after storage, so its shelf life is extended by processing into different products [1]. For this purpose, in addition to being consumed fresh in season, it is processed into beverages such as wine, fruit juice, molasses and dried form. In addition, traditional foods such as pestil (bastık), kesme (tarhana), sausage (köme), saruç, hardaliye, ravanda, çullama, samsa, ilende, pepeçura, grape pickles and *köfter* are produced, which allow grapes to be consumed all year round [6].

Köfter is one of the grape-based traditional products produced especially in Central Anatolian provinces such as Nevşehir (Cappadocia) and Niğde [7]. This dessert, which has recently been consumed as a snack, is known by different names in different regions and districts and is generally called *köfter* in Niğde and its surroundings, and *köftür* in the Nevşehir Cappadocia region [8].

This dessert also transcends being merely a food item and serves as a significant symbol reflecting the region's agricultural efforts, social solidarity, and cultural identity. Shaped by geographical, religious, and national influences, *köfter* highlights the essence of Central Anatolian cuisine with its use of local ingredients and traditional preparation

* Corresponding author, e-mail: aysenurince@ohu.edu.tr. (A. İnce)
Recieved: 15.01.2025 Accepted: 20.01.2025 Published: 30.01.2025
doi: 10.55696/ejset.1620334

methods. *Köfter* is also presented as a cultural heritage product during festivals and special occasions, ensuring its transmission to future generations. Within the scope of gastronomy tourism, *köfter* attracts tourists' attention, contributing to the economic development of local communities while introducing the authentic culinary experience of Central Anatolia to the world. As such, it becomes an integral part of the intangible cultural heritage of the region [9].

In the production of *köfter*, grape juice obtained from high-yielding, light-coloured grapes is typically used as the raw material. Additionally, molasses soil (pekmez toprağı), flour, starch, and optionally eggs are used in the production of *köfter* [10].

Köfter production typically begins in the autumn season usually in September-October, which is the ripening period of grapesis consumed throughout the winter [1]. Due to its high nutritional value, significant caloric content, and unique flavor, this traditional product holds great importance for Türkiye [7]. For this reason, it has recently become a snack that can be eaten not only in winter but throughout the year. While there are a few small-scale factories producing throughout the country, it is generally a product produced in homes with traditional production [6].

The primary aim of this study is to review existing research on *köfter*, a traditional fruit-based product, and to highlight the unique characteristics and cultural significance of this product. By focusing on its production methods, nutritional value, and role in regional cuisine, this study seeks to draw attention to *köfter* as an important component of traditional food heritage.

2 Production process of *köfter*

Figure 1 presents the flowchart of *köfter* production. While the production steps are identical in both traditional and industrial methods, the processes are carried out differently in practice.

2.1 Industrial köfter production process

In the industrial production process of *köfter*, firstly the grapes are washed, and then destemming, crushing, and filtering are carried out using screw presses to obtain grape juice (must, şıra) (Figure 2). The resulting grape juice (must, şıra) is transferred to a tank for clarification and acidity reduction, where 5% grape molasses soil (pekmez soil) is added and it is left overnight (Figure 3). Pekmez soil is a type of soil with high calcium carbonate content, used to neutralize the acidity of grape juice. It is found in various regions with differing compositions and is characterized by its white or nearly white colour [11, 12].

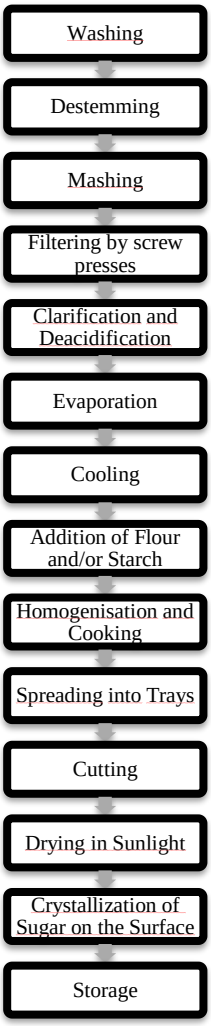

Figure 1. Production prosess of *köfter* [6]

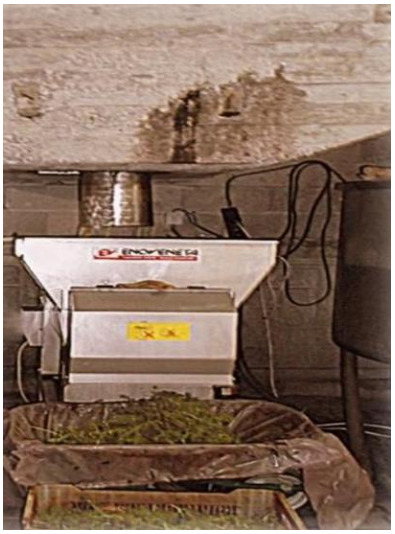

Figure 2. Pressing [6]

Figure 3. Clarification and deacidification tank [6]

Following clarification and acidity reduction, the juice is evaporated under vacuum conditions at 1 atm pressure and 65°C to 38 Brix. (Figure 4). After evaporation, the juice is cooled to 20–25°C to prepare for the addition of flour and/or starch (Figure 5). Flour and/or starch, amounting to 10% of the juice volume, are added, and the mixture is homogenized using a mixer. The mixture is strained to prevent lump formation. Sometimes flour can be used alone in production, sometimes it is used together. If *köfter* is made using only starch, it is softer than those made with flour alone. However, if *köfter* is made using equal amounts of both, a higher quality product can be obtained [6].

Figure 4. Evaporation with a bull-type evaporator [6]

Figure 5. Addition of flour and starch [6]

The homogenized mixture is transferred to containers in an open athmosphere and cooked at 90–93°C. After cooking, the mixture reaches a gel consistency and is spreaded manually onto trays moistened with grape juice (Figure 6). When the *köfter* have cooled and reached a suitable consistency, they are cut into square-shaped slices by hand using a knife (Figure 7). The shaped pieces are then spreaded evenly on racks to undergo the drying process, which lasts approximately four days (Figure 8). To ensure uniform drying, the pieces are flipped every two days.

Figure 6. Spreading into trays [6]

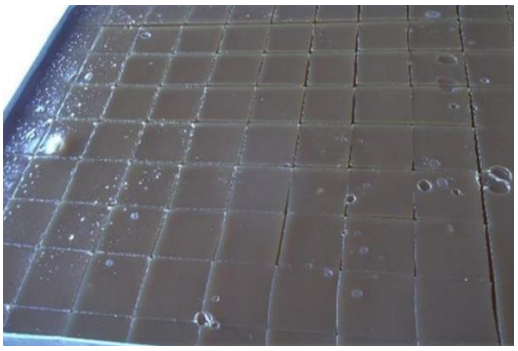

Figure 7. Cutting into squares [6]

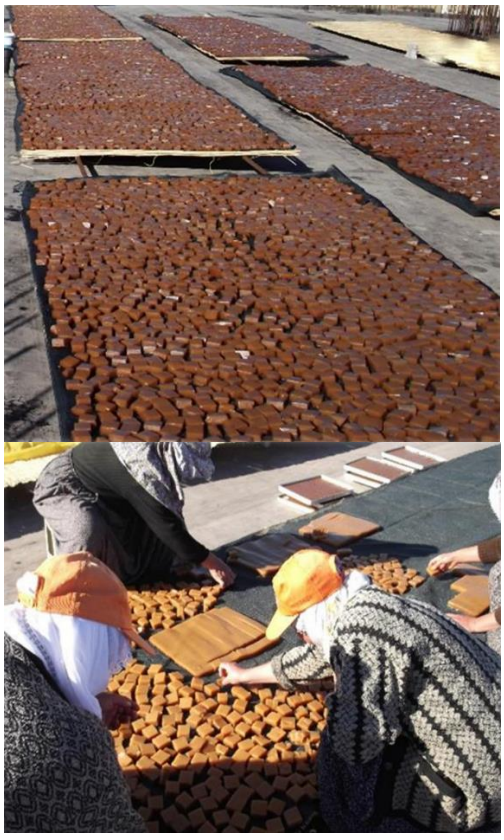

Figure 8. Drying [6]

At the end of the drying process, the surface of the *köfter* pieces is covered with breathable muslin cloth and left in the open air (Figure 9). This resting period allows a crystallized sugar layer on the surface of the *köfter* which gives its natural form, marking the final stage of production. Once this crystallization is complete, the *köfter* is ready for consumption (Figure 10) [6].

Figure 9. Storing for their surface is covered with a layer of crystalline sugar [6]

Figure 10. Final appearance [6]

2.2 Traditional köfter production method

In the traditional method of *köfter* production, the process begins with washing the grapes and separating them from their stems. The grapes are then crushed, and the juice is filtered through a muslin cloth to remove any residues.
To clarify and reduce acidity, 5% of grape molasses soil (pekmez soil) is added to the juice, which is left to settle for one day. After a day, the clear grape juice is collected and boiled in a container in the open air to evaporate the liquid (Figure 11). Once the juice reaches the consistency of molasses, a mixture of flour and starch is added at a ratio of one to nine. This addition is done gradually, with continuous mixing to achieve a homogeneous mixture. The cooking process continues until the raw flour taste is completely eliminated and the mixture is transformed into a gel-like structure [6].

The cooked mixture is spreaded into metal or wooden trays lined with a thin layer of juice, approximately 2 cm thick, and allowed to rest for a short time to facilitate cutting. As it cools, the *köfter* begins to solidify and begins to become suitable for slicing, it is cut into square-shaped or sometimes diamond shaped pieces. A thin muslin cloth is placed over the pieces, and they are dried in sunlight for about four days (Figure 12). After drying, the *köfter* is placed in special containers produced with clay (pots) and covered with breathable muslin cloths (Figure 13). Inside pots, the *köfter* develops a thin sugar film on its surface, which crystallizes over time, forming a protective sugar layer. The product is stored in these containers until it reaches its final form [6].

Figure 11. Boiling in containers in open air [13]

Figure 12. Drying in sunlight [13]

Figure 13. Storing into pots for their surface is covered with a layer of crystalline sugar [13]

3 General composition of *köfter*

In the literature, several studies have been conducted on the chemical composition of *köfter*, as reported in various sources. The data obtained from these studies provide comprehensive details on the maximum and minimum values of the components under different conditions. A summary of these values is presented in Table 1.

Table 1. Composition of *Köfter*

Compounds	Minimum	Maximum	References
Total solids (%)	79.17	82.17	[10]
Ash (%)	0.77	0.79	[1]
a_w	0.762	0.782	[1]
Moisture (%)	33.83	34,09	[1]
Titratable acidity (%)	0.04	0.08	[10]
Reducing sugar (%)	40.70	47.30	[10]
pH	5.37	6.09	[1], [14]
L*	23.93	38.60	[14], [15]
a*	1.12	14.22	[15]
b*	2.5	21.59	[15]
HMF (mg/kg)	2.42±0.09	11.67±0.20	[10]
Total phenolics (mg gallic acid equivalent/100g)	381.65±101.53	488.71±49.68	[10]
Antioxidant capacity (µmol trolox/g)	3268.38±42.05	3552.17±26.93	[6], [10]
Na (mg/kg)	243.00±49.52	1089.67±391.23	[10]
Mg (mg/kg)	278.67±61.07	393.33±63.62	[10]
Ca (mg/kg)	1116.00±258.92	1480.00±195.82	[10]
K (mg/kg)	7037±984,91	10247.67±344.28	[10]
Fe (mg/kg)	6.02±0.48	9.47±0.31	[10]

4 Studies on *köfter*

Traditionally, wheat flour and/or wheat starch are used as thickening agentin the production of *köfter* [6]. However, wheat, due to its gluten content, can cause intolerance and lead to celiac disease in many individuals [16]. The genetic condition triggered by the consumption of gluten-containing foods is defined as gluten intolerance or celiac disease [16]. This disease persists throughout an individual's lifetime and affects the autoimmune system [17]. In addition to causing gastrointestinal disorders by affecting the epithelial tissue of the small intestine, it can also lead to various systemic reactions throughout the body [17].

In recent years, the production of gluten-free foods using alternative components has gained attention. For this purpose, Alaşalvar and Erinç [15] used potato and corn starch as an alternative to wheat flour and wheat starch used in the production of *köfter* and examined the texture and colour properties of the products, which are important quality parameters for food products. For the study, *köfter* samples with different formulations were produced. The formulations included 100 g of grape molasses, 50 ml of pure water, and 15 g of one of the following: wheat flour, wheat starch, corn starch, or potato starch. The results of the colour analysis indicated that the use of different starches in *köfter* production significantly influenced the colour properties. Among the colour parameters, L* (lightness) value, which is the value expressing brightness, was highest in potato starch and lowest in corn starch. There was no statistically significant difference between the L* values of wheat flour and potato starch. The a* value shows the (redness-greenness) properties of the samples. The highest value was observed in wheat flour, followed by potato starch, wheat starch, and corn starch. The b* (yellowness-blueness) valuewas found to be highest for the sample produced with wheat flour, and lowest for the sample produced withcorn starch. According to the results of colour analysis, it was determined that usage of potato starch instead of wheat flour does not create a significant difference in colour quality.

In the study, the textural properties of *köfter* such as hardness, elasticity, stickiness, internal stickiness, gumminess, chewiness, and springiness were used to evaluate. The change in starch type in *köfter* formulations had a statistically significant impact on the textural properties of the samples. For the value of hardness, highest to lowest values were observed for the samples produced with wheat starch, corn starch, wheat flour, and potato starch, respectively. However, no statistically significant difference was found between the samples produced with wheat flour and potato starch. The elasticity values of *köfter* samples containing wheat starch and corn starch were found to be similar, while potato starch used in the sample reduced the elasticity. Gumminess values increased in the samples produced with wheat and corn starch, while that value decreased in the samples containing potato starch. Chewiness and elasticity parameters of the samples showed close responses for this parameter. It was observed that the use of potato starch increased the stickiness of the samples. Hardness, chewiness, and elasticity values were highest in *köfter* samples produced with wheat starch. This result is attributed to the interaction of other components in wheat flour forming complexes with starch or trapping the water required for gelatinization. Alaşalvar and Erinç [15] concluded that, in terms of colour properties, potato starch

provided brightness and redness levels similar to wheat flour. From a textural perspective, the parameters of hardness and elasticity for the samples produced with corn starch were found to be close to wheat flour.

Becerikli and Başoğlu [10] investigated the effects of starch and egg addition on the quality parameters, physicochemical and bioactive properties of *köfter* in their study. For this purpose, they used three different *köfter* samples: one containing only flour, one with a flour-starch mixture, and one with flour and egg. Becerikli and Başoğlu found no statistically significant differences in the dry matter content or pH values of the *köfter* samples. In the colour analysis, the L* value was highest in the sample containing flour-starch and lower in the sample containing flour-only. No statistically significant differences were observed for the a* and b* values. When titration acidity results were analyzed, the highest acidity was observed in the sample containing the flour-only, followed by the sample containing the flour-starch and the flour-egg, respectively. The highest reducing sugar content was observed in the sample containing the flour-starch, while the lowest value for that content was found in the sample containing the flour-only. This difference is believed to be related to the type and ripeness of the grapes used. HMF (hydroxymethylfurfural) analysis revealed the highest HMF content observed in the sample containing the flour-starch. However, despite variations in HMF levels among the samples, the differences were not statistically significant. In the total phenolic content analysis, the sample containing the flour-starch showed the highest total phenolic content, followed by the samples containing the flour-only and flour-egg. Conversely, the sample containing flour-only exhibited the highest antioxidant capacity, with no significant statistical differences observed between the other two samples. Mineral analysis revealed variations among the *köfter* samples, which were attributed to differences in raw materials and production conditions. The study highlights the nutritional importance of *köfter*, made from grape as its primary ingredient, due to its high mineral, antioxidant, and phenolic content. Additionally, its high sugar content makes it a calorie-dense and energy-rich food. As a traditional and unique product, further research on *köfter* is valuable for understanding its nutritional and cultural significance. Microbiological analyses (Total mesophilic aerobic bacteria, yeasts, and coliform bacteria) in *köfter* samples did not yield measurable results. The absence of microbial growth in the samples is believed to be due to the high sugar and dry matter content present in the *köfter* [10].

Gerçekaslan and Aktaş [8] investigated changes in *köfter* quality parameters over a 3-month storage period. They conducted various analyses on *köfter* samples after one, two, and three months of storage, respectively. During the storage period, increases in water activity and colour quality parameters, represented by L*, a*, and b* values, were found to be significant. In contrast, moisture content and pH values decreased during storage. A notable reduction in pH and moisture content occurred in the first month, but no significant changes were observed in subsequent months. The surface of *köfter* samples developed a thin, sugary film during the first month, which likely helped retain moisture content beyond this period. This film, formed by sugar crystallization, was also responsible for the increase in colour parameters and water activity during storage. To assess textural changes, Gerçekaslan and Aktaş performed shearing and penetration tests. The hardness values of *köfter* increased during storage but showed no significant changes after the first month. Adhesiveness values decreased throughout the storage period.

In texture profile analysis, small differences were observed among the measured parameters during storage. These differences were statistically significant for springiness, gumminess, and chewiness, while hardness showed a significant increase only in the third month. Cohesiveness and resilience values decreased over time. The textural changes during storage were related to the retrogradation of starch used in *köfter* production. Retrogradation led to an increase in hardness and a decrease in adhesiveness. Although cohesiveness (representing the internal strength of bonds) and resilience (indicating the ability to recover shape) decreased, the product remained intact and elastic. The minor changes in springiness further confirmed this stability. Gerçekaslan and Aktaş [8] concluded that *köfter* maintained its structural integrity during storage. Despite changes in some quality and textural properties, the product's overall characteristics were preserved, highlighting its durability and stability as a traditional food product.

In another study, Aktaş and Gerçekaslan [1] utilized Differential Scanning Calorimetry to determine the sorption properties and glass transition temperature (Tg) of *köfter*. They identified the Tg of *köfter* as 24.5°C [1]. Foods with high solid content transition to a glassy state when amorphous components lose their structural integrity upon rapid cooling at Tg. This temperature represents the point at which a glassy structure forms. Tg is critical for defining processing methods, storage conditions, and shelf-life criteria for food products [18]. Recent research has reported Tg data for numerous food components, including sugars, polysaccharides, and proteins [19]. Additionally, Aktaş and Gerçekaslan [1] used Iglesias-Chirife and Peleg models to classify the sorption type of *köfter* as Type-III. This finding underscores the importance of storing *köfter* under conditions below 24.5°C to maintain its quality and stability. In another study [20], the effect of molasses concentration on the textural, pasting, and sensory properties of *köfter* was investigated by preparing and analyzing *köfter* samples containing different formulations of molasses and water. The samples were prepared with different molasses-water mixtures in the following concentrations: 75%-25%, 70%-30%, 60%-40%, 50%-50%, 30%-70%, and 25%-75%. The analysis revealed that the amount of water significantly influenced the pasting properties. The swelling ability increased up to the 50%-50% molasses-water concentration, meaning that adding more than 50% molasses decreased the swelling capacity of the starch. Additionally, the interaction between sugar, starch, and water increased the peak viscosity (PV) of the samples. As the molasses concentration increased, the sugar content also increased, enhancing the

cohesion between starch granules. However, when the molasses content exceeded 50%, sugar penetration into starch granules hindered the interaction, leading to a decrease in viscosity. The interaction of sugar's hydroxyl groups with surrounding water molecules reduced and restricted the movement of water molecules. The trough viscosity (TV) of the starch paste was affected by the water concentration. As the water concentration decreased to 50%, the TV value increased, but when the water content surpassed 50%, the swelling capacity of starch granules increased, which led to a decrease in the TV value. As the molasses ratio increased, the high temperature and mechanical shear forces applied during Rapid Visco Analyzer (RVA) analysis caused the starch granules to lose their structure and integrity, resulting in a decrease in the breakdown viscosity (BV). The RVA is a device designed to simulate the cooking process of cereals by applying different temperature steps to the flour-water mixture and measuring the viscosity of the samples under controlled temperature and shear rate conditions [21, 22]. During RVA tests, the pasting process is observed in a starch or flour-water mixture subjected to heat and mixing [21, 22]. In this process, the starch granules swell, gelatinize and form a gel [22]. However, when the molasses ratio exceeded 50%, the BV value increased again. When the integrity of the granules weakened, starch showed less resistance. The blends with equal amounts of water and molasses demonstrated the ability to withstand more heat and stress [20].

During cooling, due to amylose retrogradation, the final viscosity (FV) increased as the molasses concentration increased. However, when the molasses concentration exceeded 60%, the FV value decreased because the sugar interacted with starch and prevented the alignment of starch chains. The setback viscosity (SV) decreased as the molasses concentration increased up to 50%. After exceeding 50% molasses, the SV value of the sample increased. High molasses concentrations accelerated retrogradation, and the increase in molasses concentration also extended the time required for starch granules to swell, which increased the pasting time and the stickiness temperature. The sensory properties of the samples were significantly influenced by the concentration of water and molasses. The most preferred sample was the one containing 60% water and 40% molasses, which also received the highest scores for colour, texture, taste, and odor. The sensory scores of samples with molasses concentrations between 75% and 40% were similar, while higher water concentrations (above 60%) negatively affected the sensory characteristics. This was likely due to the dilution of the sweet taste, which is undesirable in desserts. Therefore, the balance of water and molasses can be adjusted based on the desired sensory qualities, which directly affect consumer acceptance [20].

5 Conclusion

Grapes are one of the most widely cultivated fruits globally, holding substantial agricultural and economic importance. Due to their high sugar content, they are rich source of energy and calories. Additionally, their abundance in phenolic compounds, vitamins, and minerals makes them a highly nutritious food. These properties contribute positively to human health in various ways. Grapes are consumed extensively not only in fresh and dried forms but also as processed products. Besides their use in beverages such as wine, hardaliye, and molasses, grapes are transformed into numerous food items such as *köfter*, pestil, köme, and çullama, ensuring year-round consumption.

Köfter is a traditional product primarily produced in regions like Nevşehir (Cappadocia) and Niğde in Central Anatolia, Türkiye. It is made by boiling and evaporating grape juice with wheat flour and starch. The resulting mixture is spreaded into trays and dried. Once dried, the *köfter* is stored for a period to allow a thin layer of crystallized sugar to form on its surface, resulting in a long shelf-life. Due to its high caloric content, *köfter* serves as an energy-rich food, particularly consumed during the winter months. While traditionally made at home, *köfter* is also produced on an industrial scale. However, it is a unique Turkish taste, making it culturally significant for the country.

A review of the literature on *köfter* reveals a noticeable scarcity of studies on this product. Given its cultural heritage and unique value to Türkiye, there is a critical need to conduct more research on *köfter* and similar traditional products. Such efforts are essential to bringing these cultural significant taste into the global scientific and culinary literature. Therefore, further scientific studies on köfter are strongly encouraged to preserve and promote its cultural and nutritional importance.

Conflict of interest

The authors declare that there is no conflict of interest.

Similarity rate (iThenticate): 3 %

References

[1] N. Aktaş and K. E. Gerçekaslan, "Glass transition and sorption properties of köftür: A dehydrated fruit-based product," *Food Science and Technology (Brazil)*, vol. 40, pp. 503–511, Dec. 2020. https//doi.org/10.1590/fst.34419.

[2] S. Aktop, P. Şanlıbaba, and Y. Güçer, "Grape-based traditional foods produced in Turkey," *Italian Journal of Food Science*, vol. 35, no. 3, pp. 55–74, 2023. https://doi.org/10.15586/ijfs.v35i3.2339

[3] FAOSTAT, "Value of agricultural production." Accessed: Jan. 05, 2025. [Online]. Available: https://www.fao.org/faostat/en/#data/QI

[4] Turkish Statistical Institute, "Crop production statistics,". Accessed: Jan. 05, 2025. [Online]. Available: https://biruni.tuik.gov.tr/medas/?locale=en

[5] M. Gülcü, A. Şükrü Demirci, and K. Gürbüz Güner, "siyah üzüm; zengin besin içeriği ve sağlık açısından önemi," in *Türkiye 10. Gıda Kongresi*, Erzurum, May 2008, pp. 179–182.

[6] F. Becerikli, "Determination of physical, chemical and microbiologic properties of köftür is a traditional food in Turkey," M.S. thesis, Uludag University Graduate School of Natural and Applied Sciences, Bursa, 2015.

[7] E. Güneren and B. Yorgancı, "Highlighting local products in the context of sustainable gastronomy

tourism: a study on köftür," in *ITCC'22 I. International Tourism and Culinary Conference*, M. Daşkın, K. Pala, and M. Avşar, Eds., Amasya: Amasya University Press, Nov. 2022, pp. 45–57.

[8] K. E. Gerçekaslan and N. Aktaş, "Textural properties of Köftür, a fruit based dessert," *Food Science and Technology*, vol. 40, no. 2, pp. 718–721, Dec. 2020. https://doi.org/10.1590/fst.10819.

[9] M. Ölmez, "Yöresel yiyecek ve içeceklerin gastronomi turizmine etkileri: Niğde ili örneği," M. S. thesis, Nevşehir Hacı Bektaş Veli Üniversitesi Sosyal Bilimler Enstitüsü, Nevşehir, 2021.

[10] F. Becerikli and F. Başoğlu, "Some bioactive, physicochemical and chemical properies of köftür as a traditional food," *Gıda*, vol. 43, no. 2, pp. 356–363, Mar. 2018. https://doi.org/10.15237/gida.GD17085.

[11] T. B. Ekmekçiolu Erdoğan, "Characteristic properties of soils used ın traditionaly molasses production," M. S. thesis, Nevşehir Hacı Bektaş Veli University, Nevşehir, Türkiye, 2019.

[12] A. Batu and N. Aktan, "A study on the various quantities of acid remover applied to raisen vine ın pekmez making process," *Gıda*, vol. 17, no. 2, pp. 143–150, 1992.

[13] E. Keskin, "Köftür (Cappadocian jelly beans) as a sustainable regional delicacy," *Journal of Tourism and Gastronomy Studies*, vol. 12, no. 3, Sep. 2024. https://doi.org/10.21325/jotags.2024.1477.

[14] R. Cangi *et al.*, "Karaman Üzüm Köfterinin Bazı Özellikleri," in *1.Uluslararası Adriyatik'ten Kafkaslar'a Geleneksel Gıdalar Sempozyumu*, Tekirdağ, Apr. 2010, p. 1092.

[15] H. Alaşalvar and H. Erinç, "Investigation of color and texture properties of köfter produced with different starch sources," *Niğde Ömer Halisdemir University Journal of Engineering Sciences*, vol. 12, no. 4, pp. 1037–1041, 2023. https://doi.org/10.28948/ngumuh.934970.

[16] H. Gül and F. Hayıt, "Celiac disease and the quality characteristics of produced bread for celiac patients," *Journal of the Institute of Science and Technology*, vol. 7, no. 1, pp. 163–169, Apr. 2017. doi: 10.21597/jist.2017127429.

[17] F. Buriánek, C. Gege, and P. Marinković, "New developments in celiac disease treatments," *Drug Discov Today*, vol. 29, no. 9, Sep. 2024. https://doi.org/10.1016/j.drudis.2024.104113.

[18] D. Ikasari, V. D. Paramita, and S. Kasapis, "The effect of mechanical glass transition temperature on the oxidation rates of omega fatty acids in condensed biopolymer matrices," *Food Chem*, vol. 464, Feb. 2025. https://doi.org/10.1016/j.foodchem.2024.141613.

[19] F. Fan and Y. H. Roos, "Glass transition-associated structural relaxations and applications of relaxation times in amorphous food solids: a review," *Food Engineering Reviews*, vol. 9, no. 4, pp. 257–270, Dec. 2017. https://doi.org/10.1007/s12393-017-9166-6.

[20] O. Yildiz, B. Yurt, S. O. Toker, M. M. Ceylan, M. T. Yilmaz, and A. Basturk, "Pasting, textural and sensory characteristics of the kofter, a fruit-based dessert: effect of molasses and water concentration," *International Journal of Food Engineering*, vol. 11, no. 3, pp. 349–358, 2025. https://doi.org/10.1515/ijfe-2014-0313.

[21] T. H. Gamel, E. S. M. Abdel-Aal, P. J. Wood, N. P. Ames, and S. M. Tosh, "Application of the rapid Visco Analyzer (RVA) as an effective rheological tool for measurement of β-glucan viscosity," *Cereal Chem*, vol. 89, no. 1, pp. 52–58, 2012. https://doi.org/10.1094/CCHEM-07-11-008.

[22] S. Balet, A. Guelpa, G. Fox, and M. Manley, "Rapid Visco Analyser (RVA) as a Tool for Measuring Starch-Related Physiochemical Properties in Cereals: a Review," Oct. 01, 2019, *Springer Science and Business Media, LLC*. https://doi.org/10.1007/s12161-019-01581-w.